



HAL
open science

Insight into the control of nodule immunity and senescence during *Medicago truncatula* symbiosis

Fathi Berrabah, Gautier Bernal, Ait-Salem Elhosseyn, Cyrille El Kassis, Roxane l'Horset, Farouk Benaceur, Jiangqi Wen, Kirankumar S Mysore, Marie Garmier, Benjamin Gourion, et al.

► **To cite this version:**

Fathi Berrabah, Gautier Bernal, Ait-Salem Elhosseyn, Cyrille El Kassis, Roxane l'Horset, et al.. Insight into the control of nodule immunity and senescence during *Medicago truncatula* symbiosis. *Plant Physiology*, In press, 191 (1), pp.729-746. 10.1093/plphys/kiac505 . hal-03876300

HAL Id: hal-03876300

<https://cnrs.hal.science/hal-03876300>

Submitted on 28 Nov 2022

HAL is a multi-disciplinary open access archive for the deposit and dissemination of scientific research documents, whether they are published or not. The documents may come from teaching and research institutions in France or abroad, or from public or private research centers.

L'archive ouverte pluridisciplinaire **HAL**, est destinée au dépôt et à la diffusion de documents scientifiques de niveau recherche, publiés ou non, émanant des établissements d'enseignement et de recherche français ou étrangers, des laboratoires publics ou privés.

Copyright

1 **Insight into the control of nodule immunity and senescence during *Medicago***
2 ***truncatula* symbiosis**

3
4 Fathi Berrabah^{1,2*}, Gautier Bernal^{3,4}, Ait-Salem Elhosseyn^{3,4}, Cyrille El Kassis^{3,4}, Roxane
5 L'Horset⁵, Farouk Benaceur^{1,2}, Jiangqi Wen⁶, Kirankumar S. Mysore⁶, Marie Garmier^{3,4},
6 Benjamin Gourion⁷, Pascal Ratet^{3,4} and Véronique Gruber^{3,4*}

7 ¹ Department of Biology, Faculty of Sciences, Amar Telidji University, 03000 Laghouat, Algeria

8 ² Research Unit of Medicinal Plants (RUMP), National Center of Biotechnology Research, CRBt,
9 25000 Constantine, Algeria.

10 ³ Université Paris-Saclay, CNRS, INRAE, Université d'Évry, Institute of Plant Sciences Paris-
11 Saclay (IPS2), 91190 Gif-sur-Yvette, France.

12 ⁴ Université Paris Cité, CNRS, INRAE, Institute of Plant Sciences Paris-Saclay (IPS2), 91190
13 ²Gif-sur-Yvette, France.

14 ⁵ Pôle de Protection des Plantes, UMR PVBMT, 97410 Saint-Pierre, Réunion, France.

15 ⁶ The Institute of Agricultural Biosciences, Oklahoma State University, OK 73401 Ardmore,
16 USA.

17 ⁷ LIPME, Université de Toulouse, INRAE, CNRS, 31320 Castanet-Tolosan, France.

18
19
20
21 **Author contributions:** Fat.B, V.G: designed the experiments, supervised experiments, analyzed the data,
22 and wrote the paper. Fat.B, G.B, A-S.E, C.E.K, RLH: conducted the experiments. Fat.B, Far.B, M.G, B.G,
23 P.R and V.G: analyzed the data and discuss the paper. K.S.M. and J.W: contributed reagents and edited
24 the manuscript. Fat.B and V.G agree to serve as the authors responsible for contact and ensure
25 communication.

26 The authors responsible for distribution of materials integral to the findings presented in this article in
27 accordance with the policy described in the Instructions for Authors
28 (<https://academic.oup.com/plphys/pages/general-instructions>) are: Pr. Véronique Gruber
29 (veronique.gruber@u-paris.fr) and Dr. Fathi Berrabah (fa.berrabah@lagh-univ.dz).

30 **Corresponding authors:** Pr. Véronique Gruber (veronique.gruber@u-paris.fr) and Dr. Fathi Berrabah
31 (fa.berrabah@lagh-univ.dz).

32 **Short title:** Immunity and senescence in symbiotic nodules

33 **One-sentence summary:**

34 Analyses of *Medicago* mutants with non-functional nodules highlight the relationship and mechanisms
35 controlling the establishment of the immune and senescence programs during nodule organogenesis.

36

37 **Abstract**

38 Medicago (*Medicago truncatula*) establishes a symbiosis with the rhizobia *Sinorhizobium sp.*,
39 resulting in the formation of nodules where the bacteria fix atmospheric nitrogen. Loss of
40 immunity repression or early senescence activation compromises symbiont survival and leads to
41 the formation of non-functional nodules (fix-). Despite many studies exploring an overlap
42 between immunity and senescence responses outside the nodule context, the relationship between
43 these processes in the nodule remains poorly understood. To investigate this phenomenon we
44 selected and characterized three Medicago mutants developing fix- nodules and showing
45 senescence responses. Analysis of specific defense (*PATHOGENESIS-RELATED PROTEIN*) or
46 senescence (*CYSTEINE PROTEASE*) marker expression demonstrated that senescence and
47 immunity seem to be antagonistic in fix- nodules. Growth of senescence mutants on non-sterile
48 (sand/perlite) substrate instead of sterile *in vitro* conditions decreased nodule senescence and
49 enhanced defense, indicating that environment can affect the immunity/senescence balance.
50 Application of wounding stress on WT fix+ nodules led to the death of intracellular rhizobia and
51 associated with co-stimulation of defense and senescence markers, indicating that in fix+ nodules
52 the relationship between the two processes switches from opposite to synergistic to control
53 symbiont survival during response to the stress. Our data show that the immune response in
54 stressed WT nodules is linked to repression of *DEFECTIVE IN NITROGEN FIXATION 2*
55 (*DNF2*), *Symbiotic CYSTEINE-RICH RECEPTOR-LIKE KINASE (SymCRK)* and *REGULATOR*
56 *OF SYMBIOSOME DIFFERENTIATION (RSD)*, key genes involved in symbiotic immunity
57 suppression. This study provides insight to understand the links between senescence and
58 immunity in Medicago nodules.

59

60 **Introduction**

61 Under nitrogen starvation, the legume plant *Medicago* (*Medicago truncatula*) is able to perform a
62 symbiotic association with the soil nitrogen-fixing bacteria *Sinorhizobium* *sp.* During this
63 interaction a root organ, the nodule, is formed (Oldroyd, 2013). *Medicago* produces
64 indeterminate nodules characterized by the presence of a persistent meristem at the apex (zone I;
65 ZI) responsible for nodule growth. Below the ZI, in the infection zone (zone II; ZII), the rhizobia
66 infect the plant cells. Thanks to the action of the NODULE-SPECIFIC CYSTEINE-RICH (NCR)
67 antimicrobial peptides produced by the host plant, a differentiation process occurs in ZII leading
68 to an increase in size and genome endoreduplication of the bacteroids (Mergaert et al., 2006; Van
69 de Velde et al., 2010). In the fixation zone (zone III; ZIII) the differentiated bacteroids convert
70 atmospheric nitrogen into an organic form assimilated by the plant (Paau et al., 1980).

71 Despite the massive invasion of the rhizobia, the symbiotic nodule cells do not produce apparent
72 defense reactions (Gourion et al., 2015). Thanks to direct genetic studies of the *Medicago*-
73 *rhizobium* interaction, several genes that regulate defense responses in nodules have been isolated
74 (Kang et al., 2016; Berrabah et al., 2018b) including the *DEFECTIVE IN NITROGEN FIXATION*
75 *2* (*DNF2*, Bourcy et al., 2013), *Symbiotic CYSTEINE-RICH RECEPTOR-LIKE KINASE*
76 (*SymCRK*, Berrabah et al., 2014b), *REGULATOR OF SYMBIOSOME DIFFERENTIATION*
77 (*RSD*, Sinharoy et al., 2013) and *NODULES WITH ACTIVATED DEFENSE 1* (*NAD1*, Wang et
78 al., 2016; Yu et al., 2018) that encode respectively a PHOSPHATIDYL INOSITOL SPECIFIC
79 PHOSPHOLIPASE C-LIKE PROTEIN, a CYSTEINE-RICH RECEPTOR-LIKE KINASE, a
80 C₂H₂ TRANSCRIPTION FACTOR and a protein acting positively in the maintenance of the
81 bacteroids. *Medicago* mutants for these genes produce non-fixing nitrogen (fix-) nodules
82 exhibiting necrotic tissues with typical defense features like phenolic compounds accumulation
83 and stimulation of defense genes. Activation of this immune responses results in the death of the
84 undifferentiated bacteroids (Bourcy et al., 2013; Sinharoy et al., 2013; Berrabah et al., 2014b;
85 Wang et al., 2016). Historically, the first up-regulated defense gene was identified in *dnf2* and
86 correspond to the *PATHOGENESIS-RELATED PROTEIN 10* (*PR10*, *Medtr2g035150.1*, Bourcy
87 et al., 2013). This *PR10* belongs to the *PR* gene family linked to plant-pathogen responses (Ali et
88 al., 2018) and is stimulated in nodules of the necrotic mutants. Based on the diversity of their
89 biochemical activities, the *PR* proteins can be classified into 17 groups (van Loon et al., 2006;
90 Sels et al., 2008). Within each group, members share a specific protein domain used for the *PR*

91 classification. For example, the PR1, PR5, PR8 and PR10 members include respectively a
92 CYSTEINE-RICH SECRETORY PROTEIN (CAP; Schreiber et al., 1997), THAUMATIN-LIKE
93 (Wang et al., 2010), CHITINASE TYPE III (Métraux et al., 1988) and BET V1 DOMAIN
94 proteins (Liu and Ekramoddoullah, 2006).

95 During symbiosis, *DNF2*, *SymCRK*, *RSD* (Berrabah et al., 2015) and potentially *NADI*
96 (Domonkos et al., 2017) act sequentially to prevent the immune response in nodules. Different
97 factors can influence the stimulation of defenses in these mutants including the environment that
98 can change the defense response of nodules after rhizobium internalization. For example, the
99 Medicago *dnf2* mutant grown on agarose-based medium loses the immune responses and restores
100 nitrogen fixation (*fix+*). The addition of the plant defense elicitor ulvan (Jaulneau et al., 2010) to
101 this agarose-based medium primes defense responses and *dnf2* recovered the *fix-* phenotype
102 (Berrabah et al., 2014a).

103 Nodule senescence is also an important process that controls nodule functioning and bacteroid
104 survival. Early activation of the senescence results in bacteroid death (Berrabah et al., 2015) and
105 nitrogen-fixing inability of the nodules (Zimmerman et al., 1983). This phenomenon can be
106 triggered in WT nodules during developmental aging (Van de Velde et al., 2006), by addition of a
107 nitrogen source (e.g. nitrate) to the growth substrate (Chen and Phillips, 1977) or by treatment of
108 nodulated plants with the herbicide phosphinothricin that inhibits the glutamine synthase (Seabra
109 et al., 2012). Moreover, suppression of genes involved in essential nodule functions like iron
110 transport (Walton et al., 2020), sulfate transport (Krusell et al., 2005) or implicated in the
111 nitrogen fixation (Oke and Long, 1999; Maunoury et al., 2010) may also result in the formation
112 of *fix-* nodules with early senescence features. During the senescence, the formation of a
113 senescent zone (zone IV; ZIV) is observed at the base of the *M. truncatula* nodules in which
114 bacteria and host cells are degraded (Van de Velde et al., 2006). In the ZIV, cellular compounds
115 are recycled thanks to CYSTEINE PROTEASES (CPs, Wyk et al., 2014) such as CP2 to CP6
116 (Pérez Guerra et al., 2010) belonging to the papain cysteine protease family (Pierre et al., 2014).
117 These *CP* genes are specifically expressed in senescent nodules (Fedorova et al., 2002) and the
118 corresponding proteins are involved in proteolytic activities (Malik et al., 1981; Pladys and
119 Vance, 1993). CPs can be inhibited by PHYTOCYSTATINS, which are proteins involved in
120 control of the cellular proteolytic activities during various developmental processes (Martínez et
121 al., 2012; Díaz-Mendoza et al., 2014). Members of the *PHYTOCYSTATIN* gene family are indeed

122 induced during nodule senescence in soybean (*Glycine max*, Wyk et al., 2014) and *Medicago*
123 (Lambert et al., 2020).

124 The interconnection between immunity and senescence in legume nodules is poorly studied, in
125 contrast to leaves where a co-activation of these process is observed in many species (Zhang et
126 al., 2016; Patharkar et al., 2017; Lee et al., 2018; Ma X et al., 2018; Kusch et al., 2019; Zhang et
127 al., 2020) including soybean in which analysis of leaf senescence revealed the expression of
128 defense-related genes (Gupta et al., 2016).

129 Here we investigated the relationship between nodule immunity and senescence using different
130 substrates and *Medicago* mutants producing *fix*- nodules or in WT *fix*+ nodules exposed to
131 wounding stress. Our results show versatile behaviors of immunity and senescence relationship
132 between *fix*- and *fix*+ condition, opposite and co-activation of these processes are observed in
133 respectively *fix*- nodules and during *fix*+ stress responses and both correspond to bacteroids
134 suppression. Furthermore we observed that growth substrate composition also affects defenses
135 and senescence stimulation in *fix*- nodules.

136

137 **Results**

138 **Medicago fix⁻ mutants used to study the defense and senescence interaction in nodules**

139 To study the relationship between defense and senescence, we use three mutants (*nf583*, *nf2100*
140 and *nf2210*) developing fix⁻ nodules selected from a forward genetic screen of Medicago (*M.*
141 *truncatula*) *Tnt1* insertion mutant collection of the Noble Research Institute ([https://medicago-](https://medicago-mutant.dasnr.okstate.edu/mutant/index.php)
142 [mutant.dasnr.okstate.edu/mutant/index.php](https://medicago-mutant.dasnr.okstate.edu/mutant/index.php), Pislariu et al., 2012; Yarce et al., 2013). Nodule
143 nitrogenase activity was measured in plants cultivated *in vitro* on an agar-gelified medium
144 (Figure 1A) and in sand/perlite in a non-sterile growth chamber (Figure 1B) using the acetylene
145 reduction assay. Nitrogenase activity was not detected in these *Tnt1* mutant plants, confirming the
146 fix⁻ status of the nodules. To investigate the senescence feature of the symbiotic organ, 14 days
147 post inoculation (dpi) nodule sections were prepared from plant inoculated with the *S. medicae*
148 strain *WSM419* constitutively expressing *lacZ* (Figure 1C). Bacteroids are present above a large
149 senescence zone (ZIV) in the nodules of the mutants compared to the wild-type (WT). We will
150 refer to these fix⁻ mutants as senescence mutants in contrast to *dnf2-4* and *symCRK* mutants, also
151 used in this study and producing necrotic fix⁻ nodules (Berrabah et al., 2015).

152 To study the bacteroid differentiation state in the senescence mutants, we performed a DAPI
153 staining on bacteroids extracted from WT or fix⁻ mutant nodules (Figure 1D). Differentiated
154 bacteroids were detected in the nodules of these senescence mutants. Furthermore, the
155 intracellular survival of the endosymbionts was studied using the live/dead staining based on a
156 mixture of two fluorescent probes, SYTO9 and propidium iodide (PI). *nf583*, *nf2100* and *nf2210*
157 mutants displayed differentiated dead (red) bacteroids compared to the WT (Figure 1E). This
158 staining further confirms the differentiation of the bacteroids in the senescence mutants.
159 Altogether, our analyses indicated that *nf583*, *nf2100* and *nf2210* develop early senescent fix⁻
160 nodules eliciting premature death of the differentiated bacteroids.

161 ***nf583* and *nf2210* display *Tnt1* insertions in the sulfate transporter *MtSULTR3.5* that shows** 162 **high expression in nodules**

163 To identify the potential genes responsible for the *nf583*, *nf2100* and *nf2210* phenotypes, we
164 searched for their *Tnt1* Flanking Sequence Tags (FSTs) in the Medicago *Tnt1* mutant database
165 (<https://medicago-mutant.dasnr.okstate.edu/mutant/index.php>). In order to increase the

166 probability of selecting the genes responsible of the mutant phenotypes, we focused our analysis
167 on the FSTs with high confidence and located in the Open Reading Frames (ORF). Using this
168 approach, 52, 28 and 5 tagged-genes were respectively identified for *nf583*, *nf2210* and *nf2100*.
169 Interestingly, the gene *Medtr6g086170* (coding a SULFATE TRANSPORTER) is tagged with
170 *Tnt1* in lines *nf583* and *nf2210*. Similarly, the gene *Medtr4g005270* (coding a BETA-AMYRIN
171 SYNTHASE) is tagged with *Tnt1* in line *nf2210* and *nf2100* (Figure 1F, Supplemental Table S1).
172 These two genes represent potential candidates for the symbiotic genes tagged in these mutant
173 lines. Expression analysis using the Genevestigator database (<https://genevestigator.com/>, Hruz et
174 al., 2008 ; Supplemental Table S1) revealed that *Medtr6g086170* shows high expression in the
175 WT nodules (Figure 1G) and especially in the zone III (<https://medicago.toulouse.inrae.fr/GEA>).
176 By contrast all the other tagged-genes with available expression data (Supplemental Table S1)
177 including the *nf2100* tagged-genes, display low variations of their expression or reduced
178 expression in the nodule compared to the roots. *Medtr6g086170* corresponds to the *SULFATE*
179 *TRANSPORTER MtSULTR3.5* and the sequence analysis of the associated *Tnt1* insertions in the
180 *nf583* and *nf2210* backgrounds reveal insertions in the first exon (+36) and first intron (+892)
181 respectively (Figure 1H). The PCR genotyping confirms the *Tnt1* insertion in *nf583* and *nf2210*,
182 moreover the mutant plants are homozygous for the mutations in *MtSULTR3.5* (Supplemental
183 Figure S1). Our data suggest that the insertions in *MtSULTR3.5* are potentially responsible for the
184 *nf583* and *nf2210* phenotypes.

185 ***PATHOGENESIS-RELATED (PR) genes are key markers for the assessment of nodule*** 186 ***immunity***

187 In order to define appropriate defense markers for the evaluation of nodule immunity, we focused
188 our attention on the *PR* gene family associated with plant responses against pathogens. Genomic
189 data mining was done using key words and blast search on two databases: phytozome and *M.*
190 *truncatula* A17 r5.0 genome portal (see materials and methods). This analysis revealed the
191 presence of 106 *PR* genes in the *Medicago* genome of which *PR5*, *PR10* and *PR1* are the most
192 represented groups with 44, 35 and 16 members, respectively (Supplemental Table S2).

193 To select *PR* candidates for nodule defense studies, the expression of the identified *PR* genes was
194 analyzed using data from the *Medicago truncatula* Gene Expression Atlas (*MtGEA*) database
195 (<https://medicago.toulouse.inrae.fr/MtExpress>) after identification of the corresponding probe

196 sets (Supplemental Table S2). We noticed that genes showing hybridization signals (HS) values
197 lower than 100 are usually not reproducible in the qPCR analysis in our laboratory conditions.
198 Thus, in order to select *PR* genes with robust expression, a filtering step was applied and the
199 probesets displaying HS lower than 100 in both test and control conditions were excluded.

200 With the aim to identify *PR* genes potentially participating to the nodule physiology, we further
201 selected *PR* genes expressed in the symbiotic organ with or without senescence stimulation.
202 Based on the *Mt*GEA profiles, eight different probesets (Supplemental Table S3) were selected,
203 corresponding to *PR* genes induced at least two folds in the symbiotic context (WT nodules vs.
204 roots, Supplemental Figure S2A) and/or in nodules of WT plants treated with either nitrate
205 (KNO₃, Supplemental Figure S2A, Benedito et al., 2008) or phosphinothricin (Supplemental
206 Figure S2B, Seabra et al., 2012) compared to the controls. This resulted in the selection of twelve
207 *PR* genes belonging to the *PR5*, *PR8*, *PR10* and non-determined classes.

208 To check the expression of the selected *PR* genes in our conditions, we then examined their
209 expression by RT-qPCR analysis using cDNA of *Medicago* nodules. Expression was detected for
210 ten *PR* genes (Supplemental Table S3). The expression of these *PR* genes was then evaluated in
211 nodules collected from *dnf2-4* and *symCRK* mutants displaying exacerbated defense reactions in
212 the symbiotic organ (Supplemental Figure S3). Five *PR* genes (one *PR8*, two *PR5* and two *PR10*)
213 showed a significant induction in *dnf2-4* and *symCRK* compared to the WT and were finally
214 selected to study defense activation in nodules. *PR5.3*, *PR8* and *PR10* are stimulated in nodules
215 infected by the root pathogen *Ralstonia solanacearum* (Benezech et al., 2020), supporting the
216 choice of these markers for defense tracking in the nodules. It is also worth noting that the
217 sequence analysis of the identified *PR10* (*PR10.2* and *PR10.3*, Table S3) revealed the same
218 Coding Direct Sequence (CDS) despite different chromosome locations (chromosome 4 and 6,
219 Supplemental Figure S4). As we could not discriminate *PR10.2* and *PR10.3* expressions by RT-
220 qPCR, we commonly named these genes *PR10* in the manuscript.

221 ***PR* and *CP* genes show distinct expression patterns**

222 In addition to the selected *PR* genes used to assess immunity activation in the nodule, the
223 expression of four typical senescence markers (*CP2*, *3*, *4* and *5*) was monitored to follow nodule
224 senescence stimulation. To estimate the overlap between *PR* and *CP* gene expressions in

225 Medicago, the expression of corresponding genes was compared in different physiological
226 contexts using the Genevestigator software. Expression analysis at different developmental stages
227 revealed a high expression level of the *PR* genes in the whole plants until the beginning of the
228 flowering stage (Supplemental Figure S5). The initiation of flowering is associated with a
229 reduction in most of the *PR* gene expressions. By contrast the *CP* genes show low to medium
230 expression levels throughout the life cycle of the plants and they are less expressed than *PR*
231 genes.

232 In order to compare *PR* and *CP* gene expressions in response to different biotic and abiotic
233 elicitations ('perturbation set', Genevestigator), we used a scatter blot analysis (Figure 2).
234 Comparison of the *PR* or *CP* gene expression patterns revealed substantial number of conditions
235 showing co-expression of the genes in the same group (Figure 2, intragroup comparison). By
236 contrast, comparison of *PR* to *CP* expressions revealed low level of expression overlap (Figure 2,
237 intergroup comparison). Pearson analysis (Figure 2 and Supplemental Table S4) showed
238 correlation of 0.91 to 0.97 for *CPs* and 0.37 to 0.65 for *PR* genes, whereas a strong reduction of
239 the correlations (-0.06 to -0.11) was observed when *PR* and *CP* gene expressions were compared.
240 Together these results indicate that *PR* and *CP* genes display distinct expression patterns in
241 Medicago.

242 **Expression analysis of *PR* and *CP* genes reveals an opposite behavior between senescence** 243 **and immunity in nodules of *nf583* and *nf2210* mutants**

244 To evaluate the interconnection between immunity and senescence in nodules, the expression of
245 the selected *PRs* and *CP* 2 to 5 genes, was evaluated in mutants cultivated *in vitro* and producing
246 nodules with exacerbated defenses (*dnf2-4* and *symCRK*, Figure 3A) or displaying early
247 senescence (*nf583* and *nf2210*, Figure 3B). Due to a distinct behavior, *nf2100* is discussed in a
248 dedicated section. The *PR* genes were highly expressed in *symCRK* and *dnf2-4* nodules compared
249 to the WT (Figure 3A). In the nodules of the *nf583* and *nf2210* early senescence mutants, the *PR*
250 expressions remained low (Figure 3B). Unlike the defense markers, the *CP* genes were expressed
251 at low level in nodules of the necrotic mutants compared to the WT even if a slight but not
252 statistically significant induction of *CP* genes was observed in *dnf2-4* (Figure 3A). By contrast,

253 the expression of all *CP* genes was induced in *nf583* and *nf2210* compared to the control (Figure
254 3B).

255 Together these data indicate an opposite behavior between immunity and senescence markers in
256 nodules of *in vitro* cultured mutants. No overexpression of defense genes was observed during
257 senescence while no induction of senescence markers occurred in nodules showing defense
258 responses.

259 **The balance between defense and senescence is influenced by the environment**

260 To assess whether more complex conditions can have an impact on the immune and/or
261 senescence status of nodules, expressions of *PR* and *CP* genes were analyzed in fix- mutants
262 cultivated on sand/perlite (Figure 3, C and D). This non-sterile substrate displays more elicitors
263 than the cleaner agar-jellified medium used for *in vitro* culture (Berrabah et al., 2014a). *PR* gene
264 induction levels were similar in nodules of *symCRK* and *dnf2-4* cultivated in sand/perlite
265 compared to those observed during *in vitro* culture (Figure 3A vs. Figure 3C). Interestingly,
266 *nf583* and *nf2210* showed an increased expression of all *PR* genes in the sand/perlite contrary to
267 that of agar-jellified media (Figure 3B vs. Figure 3D). In contrast to *PR* gene induction, *CP* gene
268 expression levels were reduced in the nodules of the senescence mutants grown on sand/perlite
269 (Figure 3D) compared to *in vitro* conditions (Figure 3B). In addition, the analysis of *nf583* and
270 *nf2210* nodules inoculated with the *S. medicae LacZ* strain revealed some necrotic cells at 21-dpi
271 in the sand/perlite conditions whereas no necrosis was observed *in vitro* (Figure 3E).

272 Together these data suggest that, in contrast to *in vitro* conditions, when fix- mutants are
273 cultivated on a non-sterile sand/perlite substrate, plant defense responses are activated in the
274 nodules rather than senescence.

275 **Expression pattern of *MtPHYTOCYST32* supports the hypothesis of the opposite** 276 **relationship between defense and senescence in fix- nodules**

277 To test the hypothesis of a reduction of the senescence during defense activation in fix- nodules,
278 we identified potential *CP* inhibitors acting during nodule defense response. For this purpose, co-
279 expressed genes with *PR5.3*, *PR5.6*, *PR8* and *PR10* were isolated using the Phytomine tools of
280 the Phytozome database (<https://phytozome.jgi.doe.gov/phytomine/begin.do>) and the genes with

281 a Pearson correlation higher than 0.85 were selected. This analysis uncovered two
282 *PHYTOCYSTATINS* encoded by the *Medtr2g026040* (*MtPHYTOCYST5*) and *Medtr5g088770*
283 (*MtPHYTOCYST32*; *PHYTOCYST32*) genes co-expressed with *PR5.3/PR5.6/PR10* and
284 *PR5.3/PR10* respectively (Supplemental Table S5). Expression analysis of these
285 *PHYTOCYSTATINS* in the nodules of fix- mutants revealed that *MtPHYTOCYST5* was weakly
286 but significantly down-regulated in *symCRK* and *dnf2-4* *in vitro* (Supplemental Figure S6A) and
287 in sand/perlite (Supplemental Figure S6B). In addition, no significant variation in the senescence
288 mutants was observed *in vitro* and in sand/perlite, except for *nf2210* showing a small repression
289 of *MtPHYTOCYST5* expression *in vitro* (Supplemental Figure S6A). By contrast,
290 *MtPHYTOCYST32* was induced in *symCRK* and *dnf2-4* cultivated *in vitro*, whereas low or no
291 induction was detected in *nf583* and *nf2210*, respectively, compared to the reference (Figure 3F).
292 Nodule *MtPHYTOCYST32* expression increased in all fix- mutants compared to the WT (Figure
293 3F) when plants were grown on sand/perlite. The *MtPHYTOCYST32* expression pattern agrees
294 with the hypothesis of a reduction of senescence during the defense activation in fix- nodules.
295 Furthermore, the behaviors of *MtPHYTOCYST5* suggest that only some members of the
296 *PHYTOCYSTATINS* family are stimulated during the nodule immunity.

297 ***nf2100* displays a complex phenotype contrasting with the other senescence mutants**

298 The expression of defense and senescence markers was studied on *nf2100* nodules of plants
299 cultivated *in vitro* (Figure 4A). Surprisingly, despite the formation of nodules with typical
300 senescence features, *nf2100* exhibits a much higher expression of defense than senescence
301 markers. The increased expression of all *PR* genes together with the *MtPHYTOCYSTATIN32* was
302 observed in this mutant (Figure 4A). By contrast *CP* genes showed low level of expression
303 compared to those observed in *nf583* and *nf2210* (Figure 4A vs. Figure 3B) with only two *CP*
304 genes (*CP2* and *CP5*) showing significant up-regulation compared to WT (Figure 4A).
305 Cultivation of *nf2100* in sand/perlite strongly increased all *PRs* expression in nodules (Figure 4B)
306 with levels similar to those observed in *dnf2-4* and *symCRK* (Figure 4B vs. Figure 3C).
307 Moreover, *nf2100* displays slight induction of *CP3* and repression of *CP4* (Figure 4B) in
308 sand/perlite substrate. Analysis of the necrosis in 21-dpi nodules of *nf2100* grown *in vitro* reveals
309 the presence of reduced necrotic zones (Figure 4C), which are greatly enlarged in sand/perlite
310 (Figure 4D).

311 Together these data indicate that *nf2100* produces senescent nodules with more stimulation of
312 defenses associated with reduction of the *CP* expression and that the growth substrate has a
313 higher impact on *nf2100* immunity than on the other senescence mutants.

314 **Defense and senescence display simultaneous activation in nitrogen-fixing nodules under** 315 **stress**

316 In contrast to the opposite relationship observed between immunity and senescence in the fix-
317 mutants described above, expression data from nodules treated with nitrate (Supplemental Figure
318 S7A) or phosphinothricin (Supplemental Figure S7B) showed concomitant induction of *CP* and
319 *PR* genes (<https://medicago.toulouse.inrae.fr/MtExpress>, Benedito et al., 2008; Seabra et al.,
320 2012) suggesting simultaneous activation of the two processes in the WT nodule upon certain
321 circumstances. Among the main differences between the fix- mutants and the senescence
322 induction experiments is the state of nodule development; in the former the nodules do not fix
323 nitrogen whereas in the latter the chemical treatments were carried out on fix+ nodules. To check
324 if co-activation of the immunity and the senescence can occur once nitrogen fixation takes place
325 in nodule, we evaluated defense and senescence response of WT nodules during stress response.
326 Wounding was previously shown to stimulate defense and stress responses in various plants and
327 organs (van Loon et al., 2006; Sinha et al., 2014; Shen et al., 2018). To trigger a mechanical
328 stress on WT nodules, we cut the nodules from the roots (Figure 5A) and we vacuum infiltrated
329 them in liquid BNM (see materials and methods).

330 The *PR* and *CP* gene expressions were evaluated on dissected WT nodules at 0, 1, 3, 5 or 24
331 hours of incubation (Figure 5, B and C). Induction of all *PR* (except *PR5.3*) occurred 1h after
332 treatment. *PR8* and *PR5.6* were stimulated in all the incubation times, while *PR5.3* was induced
333 at 5 and 24h after treatment (Figure 5B). Interestingly all *CPs* are stimulated at 3h and expression
334 increased over time (Figure 5C). Altogether, these results indicate that wounding stimulates
335 defense and senescence processes in WT mature nodules with defense stimulation taking place
336 earlier than senescence.

337 **Stimulation of defense and senescence in fix+ nodule is associated with the death of** 338 **differentiated bacteroids**

339 To determine if the activation of defense and senescence in fix⁺ nodules can trigger bacteroids
340 death, live and dead staining was performed on WT nodules at 0 (Ctr), 1, 3, 5 and 24h after
341 wounding (Figure 5D and Supplemental Figure S8). After 1h, differentiated bacteroids exhibiting
342 red staining were observed in zone III. The abundance of these dead differentiated bacteroids
343 increased with time. At 24h the number of dead bacteroids was increased compared to alive
344 bacteroids. Quantification of the green/red ratio in zone III from the nodules sections was
345 evaluated using the Corrected Total Fluorescence Cell (CTFC). It revealed a significant
346 accumulation of red staining in wounded nodules 1, 3, 5 and 24h after treatment compared to the
347 control (Figure 5E). To check if infected host cells accumulated preferentially dead bacteroids
348 during the treatment, a counting of host cells showing High Density of Live Bacteroids (HDLB)
349 versus High Density of Dead Bacteroids (HDDB) was realized in zone III (Figure 5F). After 1h,
350 the proportion of the cells with HDDB raised compared to the control. The proportion of HDDB
351 cells increased with time and reached 70% of infected cells at 24h. Altogether these observations
352 indicate that the stimulation of defense and senescence following wounding is associated with
353 death of the differentiated bacteroids.

354 **Connection of the nodules to their roots reduces wounding effects and delays defense and** 355 **senescence stimulation**

356 To test the effect of wounding on defense and senescence responses in a less destructive context,
357 nodulated WT plants were used instead of detached nodules. To this end, the wounding treatment
358 was applied to root-attached WT nodules (Figure 5G), which were then incubated 0 (Ctr), 1, 3, 5,
359 24 and 72h. Bacteroids started to die 5h after the incubation at the cutting site and the death
360 increased around the treated zone upon the time of incubation (Figure 5H and Supplemental
361 Figure S9). In this context, most *PR* (Figure 5I) and *CP* (Figure 5J) are induced after 24h of
362 treatment. These observations contrast with the behavior of detached nodules where a strong
363 induction of *PRs* and *CPs* was observed already after 1h (Figure 5, B and C). Altogether, these
364 data confirm the observations realized on detached nodules and, reveal a delay of defense and
365 senescence responses and moderate amplitude of bacteroid death when the wounded nodules
366 remain attached to the plants.

367 **Stimulation of defense in the fix+ nodules is accompanied by down-regulation of symbiotic**
368 **genes repressing defense reactions**

369 In order to investigate the mechanism controlling the activation of defense in fix+ nodules during
370 stress response, expression of the symbiotic genes *DNF2*, *SymCRK* and *RSD* was assessed in
371 wounded detached nodules at different time points (Supplemental Figure S10). *DNF2* expression
372 was not affected by nodule dissection (Supplemental Figure S10A), while the expressions of
373 *SymCRK* and *RSD* were drastically reduced (Supplemental Figure S10B). Likewise, expression of
374 *SymCRK*, *RSD* and *DNF2* was also reduced in fix+ nodules treated with nitrate (Supplemental
375 Figure S11A, Benedito et al., 2008) or in the nodules of plants exposed to phosphinothricin
376 (Supplemental Figure S11B, Seabra et al., 2012), two conditions in which *PR* genes are up-
377 regulated (Supplemental Figure S7). These data suggest an antagonistic behavior between the
378 genes involved in the defense repression (*SymCRK*, *RSD*, *DNF2*) and the *PRs* in fix+ nodules
379 under stress response or senescence stimulation.

380 **Discussion**

381 To investigate the relationship between immunity and senescence in the nodules, we analyzed the
382 expression of *PR* and *CP* genes in *Medicago (M. truncatula)* mutants forming fix- nodules with
383 senescence or exacerbated defense. Five *PR* genes were identified as stimulated during nodule
384 defense responses and were used for the tracking of defense activation. Among them, *PR10* is
385 involved in the control of the programmed cell death during plant response to pathogens (Ma H et
386 al., 2018) and the PR5 homolog of THAUMATIN-LIKE proteins from *Arabidopsis* (*Arabidopsis*
387 *thaliana*) displays an antimicrobial activity (Hu and Reddy, 1997). The soybean line displaying
388 the loci *Rj4* which carried a PR5-like gene, *THAUMATIN-LIKE PROTEIN* shows an arrest of the
389 roots infection with its symbiont *Bradyrhizobium elkanii* strain *USDA61* (Hayashi et al., 2014;
390 Tang et al., 2016; Yasuda et al., 2016). It is proposed that *Rj4* restricts nodulation of the soybean
391 through activation of defense signaling (Yasuda et al., 2016). PR8 is the last identified class and
392 corresponds to a class III CHITINASE (Sels et al., 2008) showing homology with lysozyme, an
393 enzyme well known for its antibacterial effect (Stintzi et al., 1993). Altogether, these
394 observations suggest the recruitment of a wide range of defense genes by the legume probably for
395 the control of the bacteroid persistence. Moreover, the up-regulation of *PRs* genes (*PR5.3*, *PR8*,

396 and *PR10*) in nodules infected by *Ralstonia solanacearum* (Benezech et al., 2020) indicates that
397 at least a part of the described defense genes participate in nodule protection against pathogens.

398 Our data revealed an opposite behavior between *PR* and *CP* expressions in mutants showing
399 nodules with early senescence or exacerbated defenses. In mutant nodules displaying typical
400 defense responses (*dnf2* or *symCRK*), *PR* genes are strongly induced in contrast to the majority of
401 the *CPs* that show no stimulation. The opposite was observed in the mutants producing senescent
402 nodules and cultivated *in vitro*, in which *PR* genes are not (*nf583*, *nf2210*) or moderately (*nf2100*)
403 induced, while *CP* expressions are significantly increased. The defense gene induction is
404 associated with nodule necrosis, which is absent and occasionally observed *in vitro* in
405 *nf583/nf2210* and *nf2100* respectively. These data indicate that in the fix- mutants studied here,
406 when the defenses are increased, generally the *CPs* expression is reduced. This led us to propose
407 an opposite behavior between defense and senescence in fix- nodules and to hypothesize that
408 these processes are preferentially stimulated in necrotic and senescent nodules, respectively.

409 Interestingly, the defense genes are expressed at similar levels in the *nf2100*, *dnf2* and *symCRK*
410 mutants when grown in sand/perlite and this is linked to a large necrotic zone. Likewise, the other
411 senescence mutants also show enhanced *PR* expressions and reduced *CP* expressions with the
412 apparition of few and disparate necrotic cells in sand/perlite compared to the *in vitro* growth
413 conditions. Agar-jellified media are sufficient to induce expression of *PR10* (*Medtr2g035150.1*)
414 in nodules (Berrabah et al., 2014a). As agar contains agaropectin and impurities in addition to
415 agarose, it was proposed that it displays defense elicitors that are able to prime defense reactions
416 in the nodules. According to this hypothesis, Fukui *et al.*, (1983) showed that agaropectin
417 contained in the agar can stimulate defenses in *Lithospermum erythrorhizon*. Based on these
418 observations, we postulate that sand/perlite contain potentially more defense elicitors than agar,
419 enhancing the immune response and reducing senescence in nodules. In agreement with this, the
420 behavior of the *nf2100* mutant could be explained by a greater sensitivity to environmental
421 elicitors. Its cultivation on agar-jellified media is sufficient to initiate the low level of defenses, in
422 contrast to the behavior of the *nf2210* and *nf583* mutants. The CP-inhibitor
423 *MtPHYTOCYSTATIN32* shows an expression pattern similar to the *PR* ones in the fix- mutants, *in*
424 *vitro* and in sand/perlite conditions, suggesting a reduction of CP activities during defense
425 activation in fix- nodules. The contrasted results obtained in our study for fix- mutants grown *in*

426 *in vitro* or in sand/perlite suggest that *in vitro* studies, convenient for the control of the microbial
427 and chemical plant environment, are clearly different from the natural situations mimicked by the
428 sand/perlite substrate, in which plants face a more complex environment that can strongly impact
429 their responses.

430 *nf583* and *nf2210* share FSTs in *MtSULTR3.5*, a sulfate transporter gene whose expression is
431 stimulated in *Medicago* nodules. Both mutants display similar phenotype characteristics and
432 defense vs. senescence responses, supporting the hypothesis of a common target gene
433 corresponding to two mutated alleles. Interestingly, inactivation in *Lotus japonicus* of
434 *SYMBIOTIC SULFATE TRANSPORTER1 (SST1)*, a homolog of *MtSULTR3.5*, also leads to the
435 formation of fix- nodules and early senescence (Krusell et al., 2005), thereby reinforcing
436 *MtSULTR3.5* as candidate responsible for *nf583* and *nf2100* phenotypes. However, a potential
437 combined effect of other mutations with *MtSULTR3.5* cannot be excluded without isolation of
438 additional alleles or complementation of the mutation. For *nf2100*, based on the expression
439 pattern of the five identified tagged-genes, we failed to isolate the gene responsible for *nf2100*
440 dysfunction. Thus, the gene involved in the mutant remains to be identified.

441 Surprisingly, during nodule senescence induced by phosphinothricin, a co-stimulation of *CP* and
442 *PR* genes was observed (Seabra et al., 2012). This behavior is supported by an RNAseq analysis
443 of *Glycine max* nodules which revealed the presence of *PR* transcripts in these organs during
444 natural senescence (Chen et al., 2017), suggesting activation of defense in determinate as well as
445 indeterminate nodules during induced and natural senescence. These results contrast with our
446 observations in the fix- mutants that show an opposite pattern between expressions of defense
447 and senescence markers in the nodules. In these previous studies, transcriptomic analyses were
448 performed on mature fix+ nodules (Seabra et al., 2012; Chen et al., 2017), whereas in our work,
449 the nodules of the fix- mutants are characterized by an incomplete organogenesis and early
450 senescence. These observations prompt us to study the role of nodule development and/or the
451 state of nitrogen fixation on the immunity and senescence relationship. To this end, we have
452 induced a defense-like stimulation on fix+ nodules by two wounding approaches: i) cutting of
453 isolated nodules separated from the roots and ii) cutting the root-attached nodules. Both
454 treatments result in bacteroid death and co-induction of *PR* and *CP* genes. Remarkably, the delay
455 of gene induction is accompanied by a reduction of bacteroids death when the nodules remain

456 connected to the roots. These observations support the hypothesis that a co-occurrence between
457 immunity and senescence activation is operating in functional nodules. In addition to the
458 differences in nodule development between our study and previous transcriptomic analyses
459 (Seabra et al., 2012; Chen et al., 2017), the plant genotype and the type of treatment also
460 represent important changes. Despite these differences, the co-activation of *PRs* and *CPs*
461 observed in all these situations indicates that the co-occurrence between immunity and
462 senescence activations is probably an ubiquitous process rather than a specific response.
463 Similarly, accumulation of *PR* transcripts takes place during leaf senescence in different plants
464 species (Azumi and Watanabe, 1991; Hanfrey et al., 1996; Walter et al., 1996; John et al., 1997;
465 Wingler et al., 2005). The high degree of overlap of transcriptional responses between nodule-
466 and leaf-senescence in *Medicago* (Van de Velde et al., 2006) may suggest that activation of some
467 of the *PR* defense genes is a common feature between leaf and nodule senescence. We show that
468 nodule wounding similar to nitrate or phosphinothricin treatments reduced the expression of
469 genes that repress defense reactions in the nodule (*SymCRK*, *RSD* and *DNF2*) and enhanced *PR*
470 expression. These data allow us to propose that defense activation in the nitrogen-fixing nodules
471 may result from down-regulation of *SymCRK*, *RSD* and *DNF2*, that may act before and during
472 nitrogen fixation by various ways (Sinharoy et al., 2013, Berrabah et al., 2018a).

473

474 **Conclusion**

475 This work deciphers the relationship between immunity and senescence. The use of mutants
476 producing non-fixing nitrogen (fix-) nodules uncovers the mechanisms controlling the dynamic
477 of the establishment of the immune and the senescence programs during nodule organogenesis. In
478 *symCRK* and *dnf2* nodules, which display symbiotic arrest prior to bacteroid differentiation,
479 defense is stimulated more than the senescence (Figure 6). By contrast, under *in vitro* growth
480 conditions, senescence is more promoted than defense in the senescence mutants *nf583* and
481 *nf2210* containing differentiated fix- bacteroids. The senescence mutant *nf2100* in the same
482 growth substrates shows a greater defense than senescence response. The growth of the fix-
483 mutants in sand/perlite enhances greatly defenses and reduces senescence, pointing out the
484 influence of the environment in the defense/senescence balance. Finally, when the nodule
485 becomes functional (fix+), a co-activation of defense and senescence in response to stresses
486 (wounding, phosphinothricin) or induced senescence (nitrate) is observed and is associated with
487 suppression of the fixing-nitrogen bacteroids at least during nodule responses to wounding.

488

489 **Materials and methods**

490 **Bacterial material and growth conditions**

491 *Sinorhizobium medicae* strains *WSM419* (Ma and Ewing, 1986) and *WSM419* expressing *lacZ*
492 provided by G. Endre (Horvátha et al., 2015) were used. The bacteria were cultivated in yeast
493 extract broth (YEB) medium (Krall et al., 2002) supplemented with the appropriate antibiotics for
494 24-48h at 30°C. The following antibiotics were added to the media: chloramphenicol at 12.5
495 $\mu\text{g.mL}^{-1}$ for *WSM419*, chloramphenicol at 12.5 $\mu\text{g.mL}^{-1}$ and tetracycline at 5 $\mu\text{g.mL}^{-1}$ for
496 *WSM419* expressing *lacZ*.

497 **Plant material**

498 *Medicago (Medicago truncatula)* ecotype R108 (Hoffmann et al., 1997) and the derived *Tnt1*
499 transposon tagged-lines (provided by the Noble Research Institute) *nf583*, *nf2100* and *nf2210*
500 isolated in a community screen (Tadege et al., 2008; Pislariu et al., 2012; Cheng et al., 2014) as
501 well as *nf737 (symCRK)*, Berrabah et al., 2014b) were used in this study. In addition, the *MERE1*
502 insertion mutant line *ms240 (dnf2-4)* corresponding to a somaclonal variant obtained by
503 regeneration of a T-DNA-tagged *Medicago* line was used (Bourcy et al., 2013).

504 **Growth conditions and plant inoculation**

505 *Medicago* seeds were surface sterilized as previously described by Berrabah et al. (2015) and
506 vernalized for at least 48h at 4°C in the dark on solid medium (Bacto-agar 1% w/v). Seeds were
507 then germinated for 24h in the dark at 24°C before transfer to Buffered Nodulation Medium
508 (BNM, Ehrhardt et al., 1992) solidified with 1.5% (w/v) bacto-agar for plants cultivated *in vitro*
509 or in a mixture of sand/perlite (2/1, v/v). The plants are cultivated into a growth chamber
510 conditions at 24°C and 60% humidity under a photoperiod of 16h light /8h dark (150 μE
511 intensity).

512 Overnight cultures of the bacterial strains were pelleted and washed twice in sterile water. OD600
513 nm was adjusted to 0.1 in water. Roots of eight seedlings per plate (*in vitro* culture) or five
514 seedlings per pot (growth in sand/perlite) were inoculated with 1 mL or 10 mL of bacterial cell
515 suspension, respectively.

516 **Plant treatments**

517 ***Wounding treatment***

518 Twenty-one days post-inoculation (dpi) nodules from WT plant inoculated with *S. medicae*
519 *WSM419* were collected using forceps and scalpel or wounded with one wound on the nodule
520 attached to the plant and incubated in 5 mL of liquid BNM. Immediately after harvesting, to
521 enhance the mechanical stress with nodules integrity preservation, the collected nodules or
522 nodulated plants were vacuum-infiltrated for 15 min and collected (control) or incubated for 1, 3,
523 5, 24 and 72h (hours) under checking in multiwell plates filled with BNM.

524 **Nitrogenase activity**

525 Acetylene Reduction Assays (ARA) were conducted on individual plants with a modified
526 protocol from Koch and Evans (1966). Plants were harvested after *in vitro* growth at 21-dpi or in
527 a growth chamber at 24-dpi. Individual whole plants (*in vitro*) or nodulated roots (growth
528 chamber) were incubated with 500 μ L of acetylene for 2h at room temperature in a 21 mL air-
529 tight glass vials sealed with rubber septa. After incubation, 200 μ L of gas samples was removed
530 from the vial and was injected into a gas chromatography system (7820A; Agilent Technology)
531 to determine the ethylene production. For each test 14 plants were used for ARA analysis (See
532 “Replicates and statistical tests” part).

533 **Histological analysis**

534 ***LacZ staining***

535 Nodules were embedded into agarose 6% (w/v, Bourcy et al., 2013) and 60 μ m sections were
536 prepared using the vibratome VT1200S (Leica Biosystems GmbH, Germany). For LacZ activity
537 detection, the slices were incubated for 15 min in Z' buffer (phosphate buffer pH 7 [100 mM],
538 MgCl₂ [1 mM] and KCl [10 mM]). The slices were then incubated for 2h under darkness, at
539 28°C in reaction buffer (Z' buffer, potassium ferricyanide [5 mM], potassium ferrocyanide [5
540 mM], 45 μ m filtrated 5-bromo-4-chloro-3-indolyl- β -D-galactopyranoside [X-gal, 2,4 mM]). The
541 samples were observed using AZ10 microscope (Nikon).

542 ***DAPI staining***

543 The bacteroids were purified from 17-dpi aged nodules cultivated *in vitro* and stained with DAPI
544 as described in Mergaert et al. 2006. Free-living bacteria or bacteroids were incubated for 10 min
545 in 50 μ g.mL⁻¹ of DAPI at 60°C and then observed using an epifluorescent microscope

546 (AxioImager Z2, Zeiss) with the following setup: 365 nm and 420 nm – 470 nm respectively for
547 filter excitation and emission wavelengths, 47.89% for light source intensity. The contrast and the
548 brightness are equally adjusted between the test and the control in each experiment.

549 ***Live and dead staining***

550 The nodules were embedded in 6% (w/v) agarose and sliced into 70 µm sections using the
551 vibratome VT1200S. Live and dead stainings were carried out as previously described by Haag *et*
552 *al.* (2011). Nodule sections were incubated in a 50 mM Tris-HCl buffer (pH 7.2) containing 30
553 µM Propidium Iodide (PI) and 5 µM SYTO9 (Life Technology) for 20 min. Stained sections
554 were then mounted between slide and slip cover with a few Tris-HCl buffer drops and observed
555 using the confocal microscope LSM880 (Zeiss) with the following setup: 561 nm and 488 nm for
556 laser wavelengths, 594 nm - 687 nm and 508 nm – 553 nm for detection wavelengths, 550 V and
557 600 V for detector gains. The images were not subjected to erasure; the contrast and the
558 brightness are equally adjusted between the test and the control in each experiment.

559 Quantification of PI and SYTO9 fluorescence in nodule sections was carried out using the
560 Corrected Total Fluorescence Cell (CTCF) as described by Jakic *et al.*, (2017) in the ImageJ
561 software (<https://imagej.net/Bio7>). The following equation was used for CTCF calculation:
562 $CTCF = \text{Integrated Density} - (\text{Area of selected cell} \times \text{Mean fluorescence of background readings})$

563 **RNA extraction, cDNA synthesis and expression analysis**

564 RNA extraction, cDNA synthesis and RT-qPCR were performed as previously described
565 (Berrabah *et al.*, 2018a). After freezing in liquid nitrogen, the nodules collected from 16 plants (*in*
566 *vitro* growth) or 5 plants (sand/perlite growth) per experiment were ground in a 2 mL tube with
567 beads and the total RNA was extracted using a TRI Reagent® procedure recommended by the
568 manufacturer (Molecular Research Center). DNA was removed from the samples using the
569 DNase I kit (Invitrogen) as recommended by the manufacturer. The concentration and the RNA
570 quality were checked using the NanoDrop ND-1000 (Thermo Scientific).

571 Reverse transcription was performed on 0.5 or 1 µg of total RNA (DNA free) using oligo dT and
572 SuperScript II (Life Technology) according to the supplier in a final volume of 20 µL.

573 For each tested genes, the primers amplified 200 to 300 nucleotides of the cDNA sequence and
574 the quantification was made using quantitative PCR on a LightCycler® 480 (Roche Life Science)
575 with the LightCycler® FastStart DNA Master SYBR green I kit according to manufacturer's
576 instructions (Roche). The temperatures of 94°C, 58 to 62 °C and 72°C were used respectively for
577 the denaturation, annealing and extension steps. In all analyzed samples, expression levels were
578 normalized using the housekeeping gene *MtACT* (*Actin 11*, Supplemental Table S6, Plet et al.,
579 2011).

580 **Identification of *PATHOGENESIS-RELATED* genes and sequence analyses**

581 Identification of *PR* genes was realized using two genome databases: phytozome
582 (<https://phytozome.jgi.doe.gov/pz/portal.html>) and Medicago A17 r5.0 genome portal
583 (<https://medicago.toulouse.inra.fr/MtrunA17r5.0-ANR/>). Key word search was done on the used
584 databases with the term "Pathogenesis". The genes corresponding to *PRs* were then isolated. A
585 complementary approach of identification was realized by blasting the coding DNA sequence
586 (CDS) of identified *PR*. To confirm the classification of the *PRs*, functional domains were
587 detected on full-length protein sequences using the NCBI prediction domain tool
588 (<https://www.ncbi.nlm.nih.gov/Structure/cdd/wrpsb.cgi>). The identified *PR*, their corresponding
589 groups and their domains used for the classification are reported in Supplemental Table S1.
590 Sequence comparison between *PR10.2* and *PR10.3* was performed on the Coding Direct
591 Sequence (CDS) using ClustalW method in the BioEdit software
592 (<https://bioedit.software.informer.com>).

593 **Replicates, statistical tests and data representation**

594 ARA tests were analyzed using three independent experiments with 14 plants per experiment. For
595 all microscopic analyses, at least two independent replicates with at least 10 samples were
596 observed. Expression analyses were carried out on two to three independent experiments with
597 two technical replicates, for each experiment 16 and 5 plants were analyzed for respectively *in*
598 *vitro* and sand/perlite condition. In all RT-qPCR data, mean expression is represented with
599 standard error. For RT-qPCR data a Mann-Whitney statistical test was performed and only
600 experiments with a p-value <2.5% were considered as statistically significant. Student's t-tests
601 were realized for ARA experiments, SYTO9 and PI fluorescence quantification and the
602 evaluation of bacteroids death, and only variations with p-value <5% were considered as

603 significant. All graphics were generated using the Prism8 software
604 (<https://www.graphpad.com/scientific-software/prism/>), with the exception of graphics in Figures
605 5E and 5F for which an Excel software was used ([https://www.microsoft.com/fr-fr/microsoft-
606 365/excel](https://www.microsoft.com/fr-fr/microsoft-365/excel)).

607

608 **Accession Numbers**

609 Sequence data from this article can be found in the GenBank/EMBL data libraries under accession
610 numbers:

611 *Medtr4g107930: CP3; Medtr4g079770: CP4; Medtr5g022560: CP2; Medtr4g079470: CP5; TC106667:*
612 *Actine; Medtr1g099310.1: PR8; Medtr4g120970.1/ Medtr6g033450.1: PR10; Medtr5g010640.1: PR5.3;*
613 *Medtr8g096910.1: PR5.6; Medtr5g088770.1: PHYTOCYSTATIN32; Medtr2g026040.1:*
614 *PHYTOCYSTATIN5; Medt4g0044681: DNF2; Medt3g0119041: SymCRK; Medt7g0239441: RSD.*

615

616 **Supplemental Data**

617 **Supplemental Figure S1.** PCR genotyping of the *Tnt1* insertion in *nf583* and *nf2210*.

618 **Supplemental Figure S2.** Expression patterns of *PR* candidate genes in wild-type nodules in
619 response to nitrate and phosphinothricin.

620 **Supplemental Figure S3.** Validation by RT-qPCR analysis of 10 *PR* genes selected for defense
621 monitoring in the *Medicago* nodules.

622 **Supplemental Figure S4.** Comparison of CDS sequences between *PR10.2* (*Medtr4g120970.1*)
623 and *PR10.3* (*Medtr6g033450.1*).

624 **Supplemental Figure S5.** Expression analyses of *PRs* and *CPs* during the development of
625 *Medicago*.

626 **Supplemental Figure S6.** Expression pattern of *PHYCYST5* in *Medicago* fix- nodules mutants in
627 response to different environmental conditions.

628 **Supplemental Figure S7.** Expression pattern of senescence and defense markers in *Medicago*
629 wild-type nodules in response to nitrate and phosphinothricin treatments.

630 **Supplemental Figure S8.** Live and dead staining of wild-type inoculated nodules separated from
631 the roots.

632 **Supplemental Figure S9.** Live and dead staining of *Medicago* wild-type inoculated nodules
633 attached to the roots.

634 **Supplemental Figure S10.** Expression patterns of *DNF2*, *SymCRK* and *RSD* in *Medicago* wild-
635 type nodules in response to wounding.

636 **Supplemental Figure S11.** Expression pattern of *DNF2*, *SymCRK* and *RSD* in *Medicago* wild-
637 type nodules in response to nitrate and phosphinothricin treatments.

638 **Supplemental Table S1.** List of *nf583*, *nf2210* and *nf2100* genes with FSTs.

639 **Supplemental Table S2.** List of the identified *PR* genes in the *M. truncatula* genome.

640 **Supplemental Table S3.** List of *PR* genes validated by RT-qPCR for the study.

641 **Supplemental Table S4.** Pearson correlation analysis of the *PRs*, *CPs* and *PRs* vs. *CPs*
642 expression.

643 **Supplemental Table S5.** Co-expressed *PHYTOCYSTATIN* genes with the studied *PR*.

644 **Supplemental Table S6.** List of primers used in this study.

645

646 **Funding Information:** This work was supported by the grant ANR-15-CE20 0005 (STAYPINK) and
647 funding obtained from the invitation programs for foreign researchers from Paris Cité University and Paris
648 Saclay University. This study contributes to the IdEX Université de Paris ANR-18-IDEX-0001. *M.*
649 *truncatula Tnt1* mutants were created through research funded, in part, by grants from the National
650 Science Foundation, USA (DBI 0703285 and IOS-1127155).

651 **Acknowledgments**

652 Thanks to Hossein Khademian and Peter Mergaert for preliminary characterization of line NF583
653 and to Messaoudi Hala Selma and Souaiaia Nour El Houda for their help during PR
654 identification.

655

656 **Figure legends**

657 **Figure 1. New *M. truncatula* fix- mutants producing early senescent nodules**

658 (A) Nodules of three *M. truncatula Tnt1* lines (*nf583*, *nf2100* and *nf2210*) show no nitrogenase
659 activity *in vitro* at 21-dpi and (B) in sand/perlite at 24-dpi growing conditions. The results are
660 represented by boxplots showing the mean nitrogenase activity of three independent experiments
661 with 14 plants per experiment. The central line of the box shows the median, the box limits
662 display the upper and the lower quartiles, the whiskers show the minimum and the maximum
663 values. The letters show statistical groups between genotypes using Student tests (p-value < 5%).
664 (C) Analysis of 17-dpi *in vitro* nodules infected with *S. medicae* WSM419 strain expressing *lacZ*
665 reveals a senescent zone in the nodules of the three *fix-* mutants (*nf583*, *nf2100*, *nf2210*). The
666 asterisk indicates the senescent zone and the scale bars represent 500 μ m. (D) Exploration of the
667 bacterial differentiation with the DAPI staining of bacteroids extracted from 17-dpi *in vitro*
668 nodules of WT or the isolated *fix-* mutants reveals an increase of the bacteroids size
669 (corresponding to bacteroids differentiation) in *nf2100*, *nf2210*, *nf583* and WT nodules compared
670 to free living bacteria. The white arrows show the bacteroids, the scale bars indicate 5 μ m. (E)
671 The differentiation state is confirmed by the live and dead staining of 18-dpi *in vitro* nodules
672 sections of the WT and the mutants. In this staining method, living rhizobia are stained in green
673 with SYTO9 whereas dying cells are stained in red with Propidium Iodide (PI). Death of
674 differentiated bacteroids is observed in *nf2100*, *nf2210* and *nf583*. The images were taken in the
675 fixation zone (WT) or the putative ZIII (mutants). The scale bars indicate 10 μ m. The
676 observations in D and E are realized on plants of three independent experiments (8 plants per
677 experiments). (F) The identification of the FSTs reveals the presence of 52, 28 and 5 genes
678 showing a *Tnt1* insertion in an ORF for *nf583*, *nf2210* and *nf2100* respectively. One gene is
679 shared between *nf583* - *nf2210* (*Medtr6g086170*, blue) and one between *nf583*- *nf2100*
680 (*Medtr4g005257*, red). (G) The expression analysis of the common genes in roots and nodules of
681 *M. truncatula* shows that *Medtr6g086170* is induced, while *Medtr4g005257* is down regulated in
682 the nodules compared to the roots. Expressions were determined from three independent
683 experiments and the data are downloaded from Genevestigator. (H) *Medtr6g086170* encodes the
684 sulfate transporter MtSULTR3.5 and displays *Tnt1* insertions in first exon (+36) and intron
685 (+892) in *nf2210* and *nf583* mutant lines, respectively.

686 **Figure 2. Selected *PR* and *CP* display distinct pattern expressions**

687 Scatterplot analysis of *PR* or *CP* (intragroup comparison) and *PR* vs. *CP* (intergroup comparison)
688 expression. The results display the average of the gene expressions in log2 of ratio between the
689 test and the control obtained for 290 conditions of perturbations (response to abiotic and biotic
690 stress, symbiosis, elicitors, defense hormones, seeds development, effect of the nutrients and the
691 genotypes). The data are downloaded and analyzed using the Genevestigator database. The r
692 numbers show the Pearson correlation values between the genes. *PRs* are represented in black.
693 *CP2*, *CP3* and *CP4/5* are represented in blue, red and black.

694 **Figure 3. Senescence and immunity activation in *fix-* mutants**

695 (A) Analyses of 21-dpi nodules of plant cultivated *in vitro* reveal induction of all selected *PRs* in
696 *dnf2-4* and *symCRK* compared to the WT. By contrast no significant variation of *CP* expressions
697 is observed in the same condition. (B) In the opposite to *dnf2-4* and *symCRK*, *PR* expression is
698 largely reduced in the nodules of the *nf583* and *nf2210* senescence mutants, while expression of
699 used *CPs* increased in these mutants compared to the WT. (C) Analysis of 24-dpi nodules from
700 *fix-* plants cultivated in sand/perlite revealed the stimulation of *PRs* and reduction of *CPs*
701 expression in *dnf2-4*, *symCRK*. (D) In the same way *nf583* show up-regulation of all *PRs* and
702 *nf2210* display significant stimulation of *PR8*, *PR5.3*, *PR5.6*. *CPs* expression is reduced in the
703 senescence mutants, *nf583* and *nf2210*, which show stimulation of *CP2/CP3* and *CP4/CP5*
704 respectively. (E) Analysis of 21-dpi *in vitro* and sand/perlite nodules induced by *S. medicae*
705 *WSM419 lacZ* reveals that *nf583* and *nf2210* produce senescent nodules without necrosis *in vitro*.
706 By contrast in sand/perlite a slight necrosis is observed and the arrows show necrotic cells. The
707 scale bars represent 500 μ m. (F) Expression analysis of the *PHYTOCYSTATIN32*
708 (*MtPHYTOCYSTATIN32*) *CP* inhibitor in *fix-* mutant nodules compared to the WT cultivated
709 respectively *in vitro* (21-dpi) or in sand/perlite (24-dpi) reveal induction of *PHYTOCYSTATIN32*
710 in *dnf2-4* and *symCRK* *in vitro*, whereas cultivation of plants in sand/perlite shows up-regulation
711 of *PHYTOCYSTATIN32* in the necrotic mutants as well as in *nf583* and *nf2210*. Values represent
712 the mean of induction folds in the tested mutants compared to the WT, dashed line represent the
713 value of gene expression in the WT. The RT-qPCR analyses in A-D and F were made on three
714 biological repetitions with two technical replicates. For each experiment, 16 and 5 plants were
715 analyzed for *in vitro* and sand/perlite conditions, respectively. The actin housekeeping gene was

716 used for expression normalization. Error bars indicate SE and the asterisks represent significant
717 variations compared to the WT using Mann-Whitney statistical test (p-value < 2.5%).

718 **Figure 4. *nf2100* produces senescent nodules with higher immunity stimulation than the**
719 **other senescence mutants**

720 (A) Expression analysis of *PRs* and *CPs* in 21-dpi nodules of WT or *nf2100* cultivated *in vitro*
721 show up-regulation of these genes in *nf2100*. (B) Cultivation of *nf2100* or the WT on sand/perlite
722 led to increase of *PR* expression and reduction of *CP* expression in 24-dpi nodules of *nf2100*
723 compared to the WT. Values in A and B represent the mean of induction folds in the tested
724 mutants compared to the WT. The RT-qPCR analyses in A and B were made on three biological
725 repetitions with two technical replicates. For each experiment 16 and 5 plants were analyzed for
726 respectively *in vitro* and sand/perlite conditions. The actin housekeeping gene is used for the
727 expression normalization. Error bars indicate SE and the asterisks represent significant variations
728 (p-value < 2.5%) compared to the WT using Mann-Whitney statistical test. (C) Analysis of 21-
729 dpi *in vitro* nodules induced by *S. medicae* WSM419 *lacZ* reveals that *nf2100* produce nodules
730 with few necrotic cells. (D) By contrast sand/perlite cultivation leads to the apparition of a large
731 necrotic areas. The arrow shows necrotic cells and the scale bars in C and D represent 500 μ m

732 **Figure 5. Wounding triggers defense and senescence activation in fix+ nodules associated**
733 **with the death of the differentiated bacteroids**

734 (A) In the first wounding treatment the WT nodules at 21-dpi inoculated with *S. medicae*
735 WSM419, nodules were separated from the roots. Expression analysis of (B) *PR* and (C) *CP*
736 genes after incubation of 0 (Ctr), 1, 3, 5 and 24h (hours) revealed that *PRs* and *CPs* are
737 respectively induced after 1 and 3h. (D) Observation of bacteroid survival using live (green
738 (SYTO9)) and dead (red (Propidium Iodide)) staining in wounded 21-dpi nodules after 0 (Ctr), 1,
739 3, 5 and 24h of incubations reveals a death of the differentiated bacteroids 1h after incubation
740 which increases with time. Top panel displays the nodule sections (scale bars are 200 μ m) and
741 bottom panel shows the bacteroids in the fixation zone III (scale bars are 20 μ m). Asterisks
742 indicate the nitrogen-fixation zone and the arrows show dead bacteroids. (E) The Corrected Total
743 Fluorescence Cell (CTFC) of SYTO9 and Propidium Iodide (PI) staining calculated from nodule
744 section of wounded nodules reveals more PI than SYTO9 staining in 1, 3, 5 and 24h compared to
745 the reference (Ctr). The CTFC were calculated for each time of incubation on five to seven

746 sections of independent nodules and error bars show the SE. Asterisks show significant variation
747 between SYTO9 and PI fluorescence and the letters show statistical groups between incubations
748 times using Student tests (p-value < 5%). (F) The percentage of nodule infected cells with High
749 Density of Dead Bacteroids (HDDB) or High Density of Live Bacteroids (HDLB) is calculated in
750 the ZIII of sections from wounded nodules at 0 (Ctr), 1, 3, 5 and 24h. Augmentation of HDDB
751 cell proportion is observed as early as 1h and increases during the time of incubation. The
752 proportions of HDDB and HDLB were calculated on the nodules section used in the CTFC
753 determination. The analysis was performed on five to seven sections collected from nodules of
754 independent plants. The letters show statistical groups between incubations times using Student
755 tests (p-value < 5%). (G) The second wounding treatment consists of cutting WT nodules
756 attached to the roots at 21-dpi with *S. medicae* WSM419. (H) Observation of bacteroid survival
757 using live (green) and dead (red) staining in wounded 21-dpi nodules after 0 (Ctr), 1, 3, 5, 24 and
758 72h of incubation reveals that bacteroid death starts at 5 h after incubation and is located around
759 the wounded zones. The arrows show the wounded zones and the scale bars represent 250 μ m.
760 Expression analysis of the *PRs* (I) and the *CPs* (J) shows up-regulation of most of these genes
761 after 24 h of incubation. The expression analysis in B, C, I, and J corresponds to the mean
762 expression of three independent experiments (8 plants per experiment) with two to three technical
763 replicates. The actin housekeeping gene was used for expression normalization. Error bars
764 indicate SE and asterisks represent significant variation (p-value < 2.5%) compared to the WT
765 using the Man-Whitney statistical test.

766 **Figure 6. Defense and senescence activation in Medicago nodules**

767 After rhizobia internalization, failure in defense repression can lead to death of undifferentiated
768 bacteroids in *dnf2* and *symCRK* producing non-fixing nitrogen (fix-) nodules showing necrosis
769 and low stimulation of senescence. By contrast the senescence mutants show degradation of
770 differentiated bacteroids in a fix- senescent nodule associated with senescence marker expression
771 and low defense responses in *nf583* and *nf2210*, two potential mutated alleles of *MtSULTR3.5*.
772 Interestingly *nf2100* displays more defense stimulation than the other senescence mutants. The
773 environment (as sand/perlite substrate) can stimulate immunity and reduce senescence
774 stimulation in the senescence mutants. In the sand/perlite conditions, *nf2100* show *PR* stimulation
775 similar to that observed in *dnf2* and *symCRK* with accumulation of necrotic tissues. Finally, in
776 nitrogen-fixing (fix+) nodules, stress conditions (wounding, phosphinothricin) or induction of

777 senescence with addition of nitrate to the growth medium, lead to a co-activation of defense and
778 senescence and suppression of nitrogen-fixing bacteroids.

779

780 **References**

- 781 **Ali S, Ahmad B, Kamili AN, Ali A, Ahmad Z, Akhter J, Tyagi A, Tajamul S, Mushtaq M,**
782 **Yadav P, et al** (2018) Pathogenesis-related proteins and peptides as promising tools for
783 engineering plants with multiple stress tolerance. *Microbiol Res* **212–213**: 29–37
- 784 **Azumi Y, Watanabe A** (1991) Evidence for a senescence-associated gene induced by darkness.
785 *Plant Physiol* **95**: 577–583
- 786 **Benedito VA, Torres-jerez I, Murray JD, Andriankaja A, Allen S, Kakar K, Ott T, Moreau**
787 **S, Niebel A, Frickey T** (2008) A gene expression atlas of the model legume *Medicago*
788 *truncatula*. *Plant J* **55**: 504–513
- 789 **Benezech C, Berrabah F, Jardinaud MF, Le Scornet A, Milhes M, Jiang G, George J, Ratet**
790 **P, Vaillau F, Gourion B** (2020) Medicago-Sinorhizobium-Ralstonia Co-infection Reveals
791 Legume Nodules as Pathogen Confined Infection Sites Developing Weak Defenses. *Curr*
792 *Biol* **30**: 351-358
- 793 **Berrabah F, Balliau T, A EH, George J, Zivy M, Ratet P, Gourion B** (2018a) Control of the
794 ethylene signaling pathway prevents plant defenses during intracellular accommodation of
795 the rhizobia. *New Phytol* **219**: 310–323
- 796 **Berrabah F, Bourcy M, Cayrel A, Eschstruth A, Mondy S, Ratet P, Gourion B** (2014a)
797 Growth conditions determine the *DNF2* requirement for symbiosis. *PLoS One* **9**: 1–10
- 798 **Berrabah F, Bourcy M, Eschstruth A, Cayrel A, Guefrachi I, Mergaert P, Wen J, Jean V,**
799 **Mysore KS, Gourion B, et al** (2014b) A nonRD receptor-like kinase prevents nodule early
800 senescence and defense-like reactions during symbiosis. *New Phytol* **203**: 1305–1314
- 801 **Berrabah F, Hosseyn E, Salem A, Garmier M, Ratet P** (2018b) The multiple Faces of the
802 Medicago-Sinorhizobium Symbiosis. *Funct. genomics Medicago truncatula Methods*
803 *Protoc. Methods Mol. Biol.* **1822**: 241–260
- 804 **Berrabah F, Ratet P, Gourion B** (2015) Multiple steps control immunity during the intracellular
805 accommodation of rhizobia. *J Exp Bot* **66**: 1977–1985
- 806 **Bourcy M, Brocard L, Pislariu CI, Cosson V, Mergaert P, Tadege M, Mysore KS, Mickael**

807 **K U, Benjamin G, Ratet P** (2013) *Medicago truncatula* DNF2 is a PI-PLC-XD-containing
808 protein required for bacteroid persistence and prevention of nodule early senescence and
809 defense-like reactions. *New Phytol* **197**: 1250–1261

810 **Chen P-C, Phillips DA** (1977) Induction of root nodule senescence by combined nitrogen in
811 *Pisum sativum L.* *Plant Physiol* **59**: 440–442

812 **Chen SL, Shan ZH, Yang ZL, Zhang XJ, Qiu DZ, Zhou XA** (2017) RNA-Seq analysis of
813 nodule development at five different developmental stages of soybean (*Glycine max*)
814 inoculated with *Bradyrhizobium japonicum* strain 113-2. *Scientific Reports* **7**: 42248

815 **Cheng X, Wang M, Lee HK, Tadege M, Ratet P, Udvardi M, Mysore KS, Wen J** (2014) An
816 efficient reverse genetics platform in the model legume *Medicago truncatula*. *New Phytol*
817 **201**: 1065–1076

818 **Díaz-Mendoza M, Velasco-Arroyo B, González-Melendi P, Martínez M, Díaz I** (2014) C1A
819 cysteine protease-cystatin interactions in leaf senescence. *J Exp Bot* **65**: 3825–3833

820 **Domonkos A, Szilard K, Aniko G, Erno K, Horváth B, Gyongyi ZK, Attila F, Monika TT,**
821 **Ferhan A, Karoly B, et al** (2017) *NAD1* Controls defense-like responses in *Medicago*
822 *truncatula* symbiotic nitrogen fixing nodules following rhizobial colonization in a BacA-
823 independent Manner. *Genes (Basel)* **8**: 387

824 **Ehrhardt DW, Morrey Atkinson E, Long SR** (1992) Depolarization of alfalfa root hair
825 membrane potential by *Rhizobium meliloti* nod factors. *Science* **256**: 998–1000

826 **Fedorova M, Van de Mortel J, Matsumoto PA, Cho J, Town CD, VandenBosch KA, Gantt**
827 **JS, Vance CP** (2002) Genome-wide identification of nodule-specific transcripts in the
828 model legume *Medicago truncatula*. *Plant Physiol* **130**: 519–537

829 **Fukui H, Yoshikawa N, Tabata M** (1983) Induction of shikonin formation by agar in
830 *Lithospermum erythrorhizon* cell suspension cultures. *Phytochemistry* **22**: 2451–2453

831 **Gourion B, Berrabah F, Ratet P, Stacey G** (2015) Rhizobium – legume symbioses : the crucial
832 role of plant immunity. *Trends Plant Sci* **20**: 186–194

833 **Gupta R, Lee SJ, Min CW, Kim SW, Park KH, Bae DW, Lee BW, Agrawal GK, Rakwal R,**

834 **Kim ST** (2016) Coupling of gel-based 2-DE and 1-DE shotgun proteomics approaches to
835 dig deep into the leaf senescence proteome of *Glycine max*. *J Proteomics* **148**: 65–74

836 **Haag AF, Baloban M, Sani M, Kerscher B, Pierre O, Angelo SD, Kondorosi E, Longhi R,**
837 **Boncompagni E, He D, et al** (2011) Protection of Sinorhizobium against host Cysteine-
838 Rich Antimicrobial Peptides is critical for symbiosis. *Plos Biol* **9**: e1001169

839 **Hanfrey C, Fife M, Buchanan-Wollaston V** (1996) Leaf senescence in *Brassica napus*:
840 expression of genes encoding pathogenesis-related proteins. *Plant Mol Biol* **30**: 597–609

841 **Hayashi M, Shiro S, Kanamori H, Mori-Hosokawa S, Sasaki-Yamagata H, Sayama T,**
842 **Nishioka M, Takahashi M, Ishimoto M, Katayose Y, et al** (2014) A thaumatin-like
843 protein, Rj4, controls nodule symbiotic specificity in soybean. *Plant Cell Physiol* **55**: 1679–
844 1689

845 **Hoffmann B, Trinh TH, Leung J, Kondorosi A, Kondorosi E** (1997) A new *Medicago*
846 *truncatula* line with superior *in vitro* regeneration, transformation, and symbiotic properties
847 isolated through cell culture selection. *Mol Plant-Microbe Interact* **10**: 307–315

848 **Horváth B, Domonkos Á, Kereszt A, Szűcs A, Ábrahám E, Ayaydin F, Bóka K, Chen Y,**
849 **Chen R, et al** (2015) Loss of the nodule-specific cysteine rich peptide, NCR169, abolishes
850 symbiotic nitrogen fixation in the *Medicago truncatula dnf7* mutant. *Proc Natl Acad Sci*
851 **112(49)**: 15232–15237

852 **Hruz T, Laule O, Szabo G, Wessendorp F, Bleuler S, Oertle L, Widmayer P, Gruissem W,**
853 **Zimmermann P** (2008) Genevestigator V3: A Reference Expression Database for the Meta-
854 Analysis of Transcriptomes. *Adv Bioinformatics* **2008**: 420747

855 **Hu X, Reddy ASN** (1997) Cloning and expression of a PR5-like protein from Arabidopsis:
856 inhibition of fungal growth by bacterially expressed protein. *Plant Mol Biol* **34**: 949–959

857 **Jakic B, Buszko M, Cappellano G, Wick G** (2017) Elevated sodium leads to the increased
858 expression of *HSP60* and induces apoptosis in HUVECs. *PloS One* **12(6)**: e0179383.

859 **Jaulneau V, Lafitte C, Jacquet C, Fournier S, Salamagne S, Briand X, Esquerré-Tugayé M-**
860 **T, Dumas B** (2010) Ulvan, a sulfated polysaccharide from green algae, activates plant
861 immunity through the jasmonic acid signaling pathway. *J Biomed Biotechnol* **2010**: 525291

- 862 **John I, Hackett R, Cooper W, Drake R, Farrell A, Grierson D** (1997) Cloning and
863 characterization of tomato leaf senescence-related cDNAs. *Plant Mol Biol* **33**: 641–651
- 864 **Kang Y, Li M, Sinharoy S, Verdier J** (2016) A Snapshot of Functional Genetic Studies in
865 *Medicago truncatula*. *Front Plant Sci* **7**: 1175
- 866 **Koch B, Evans HJ** (1966) Reduction of Acetylene to Ethylene by Soybean Root Nodules. *Plant*
867 *Physiol* **41**: 1748–1750
- 868 **Krall L, Wiedemann U, Unsin G, Weiss S, Domke N, Baron C** (2002) Detergent extraction
869 identifies different VirB protein subassemblies of the type IV secretion machinery in the
870 membranes of *Agrobacterium tumefaciens*. *Proc Natl Acad Sci USA* **99**: 11405–11410
- 871 **Kusch S, Thiery S, Reinstädler A, Gruner K, Zienkiewicz K, Feussner I, Panstruga R**
872 (2019) Arabidopsis *mlo3* mutant plants exhibit spontaneous callose deposition and signs of
873 early leaf senescence. *Plant Mol Biol* **101(12)**: 21-40
- 874 **Krusell L, Krause K, Ott T, Desbrosses G, Krämer U, Sato S, Nakamura Y, Tabata S, K.**
875 **James E, Sandal N et al.,** (2005) The sulfate transporter SST1 is crucial for symbiotic
876 nitrogen fixation in *Lotus japonicus* root nodules. *Plant Cell* **17(5)**: 1625–1636.
- 877 **Lambert I, Pervent M, Le Queré A, Clément G, Tausin M, Severac D, Benezech C, Tillard**
878 **P, Martin-Magniette M-L, Colella S, et al** (2020) Responses of mature symbiotic nodules
879 to the whole-plant systemic nitrogen signaling. *J Exp Bot* **71**: 5039–5052
- 880 **Lee D, Lee G, Kim B, Jang S, Lee Y, Yu Y, Seo J, Kim S, Lee YH, Lee J, et al** (2018)
881 Identification of a spotted leaf sheath gene involved in early senescence and defense
882 response in rice. *Front Plant Sci* **9**: 1274
- 883 **Liu JJ, Ekramoddoullah AKM** (2006) The family 10 of plant pathogenesis-related proteins:
884 their structure, regulation, and function in response to biotic and abiotic stresses. *Physiol*
885 *Mol Plant Pathol* **68**: 3–13
- 886 **MA H, Ewing J** (1986) Acid tolerance in the *Rhizobium meliloti* – *Medicago* symbiosis. *Aust J*
887 *Agric. Res* **37**: 55–64
- 888 **Ma H, Xiang G, Li Z, Wang Y, Dou M, Su L, Yin X, Liu R, Wang Y, Xu Y** (2018) Grapevine

889 904 VpPR10.1 functions in resistance to *Plasmopara viticola* through triggering a cell
890 death-like defence response by interacting with VpVDAC3. *Plant Biotechnol J* **16**: 1488–
891 1501

892 **Ma X, Keller B, McDonald BA, Palma-Guerrero J, Wicker T** (2018) Comparative
893 transcriptomics reveals how wheat responds to infection by *Zymoseptoria tritici*. *Mol Plant-*
894 *Microbe Interact* **31**: 420–431

895 **Malik NSA, Pfeiffer NE, Williams DR, Wagner FW** (1981) Peptidohydrolases of soybean root
896 nodules. *Plant Physiol* **68**: 386–392

897 **Martínez M, Cambra I, González-Melendi P, Santamaría ME, Díaz I** (2012) C1A cysteine-
898 proteases and their inhibitors in plants. *Physiol Plant* **145**: 85–94

899 **Maunoury N, Redondo-nieto M, Bourcy M, Velde W Van De, Alunni B, Ratet P, Aggerbeck**
900 **L, Kondorosi E, Mergaert P** (2010) Differentiation of symbiotic cells and endosymbionts
901 in *Medicago truncatula* nodulation are coupled to two transcriptome-switches. *PLoS One*
902 **5(3)**: e9519

903 **Mergaert P, Uchiumi T, Alunni B, Evanno G, Cheron A, Catrice O, Mausset A-E, Barloy-**
904 **Hubler F, Galibert F, Kondorosi A, et al** (2006) Eukaryotic control on bacterial cell cycle
905 and differentiation in the Rhizobium – legume symbiosis. *Proc Natl Acad Sci USA* **103**:
906 5230–5235

907 **Métraux JP, Streit L, Staub T** (1988) A pathogenesis-related protein in cucumber is a chitinase.
908 *Physiol Mol Plant Pathol* **33**: 1–9

909 **Oke V, Long SR** (1999) Bacteroid formation in the Rhizobium-legume symbiosis. *Curr Opin*
910 *Microbiol* **2**: 641–646

911 **Oldroyd GED** (2013) Speak , friend , and enter : signalling systems that promote beneficial
912 symbiotic associations in plants. *Nature* **11**: 252–263

913 **Paau AS, Bloch CB, Brill WJ** (1980) Developmental fate of *Rhizobium meliloti* bacteroids in
914 alfalfa nodules. *J Bacteriol* **143**: 1480–1490

915 **Patharkar OR, Gassmann W, Walker JC** (2017) Leaf shedding as an anti-bacterial defense in

916 Arabidopsis cauline leaves. PLoS Genet **13**(12): 849-1584

917 **Pérez Guerra JC, Coussens G, De Keyser A, De Rycke R, De Bodt S, Van De Velde W,**
918 **Goormachtig S, Holsters M** (2010) Comparison of developmental and stress-induced
919 nodule senescence in *Medicago truncatula*. Plant Physiol **152**: 1574–1584

920 **Pierre O, Hopkins J, Combiér M, Baldacci F, Engler G, Brouquisse R, Hérouart D,**
921 **Boncompagni E** (2014) Involvement of papain and legumain proteinase in the senescence
922 process of *Medicago truncatula* nodules. New Phytol **202**: 849–863

923 **Pislariu CI, D. Murray J, Wen J, Cosson V, Muni RRD, Wang M, A. Benedito V,**
924 **Andriankaja A, Cheng X, Jerez IT, et al** (2012) A *Medicago truncatula* tobacco
925 retrotransposon insertion mutant collection with defects in nodule development and
926 symbiotic nitrogen fixation. Plant Physiol **159**: 1686–1699

927 **Pladys D, Vance CP** (1993) Proteolysis during development and senescence of effective and
928 plant gene-controlled ineffective alfalfa nodules. Plant Physiol **103**: 379–384

929 **Plet J, Wasson A, Ariel F, Le Signor C, Baker D, Mathesius U, Crespi M, Frugier F** (2011)
930 MtCRE1-dependent cytokinin signaling integrates bacterial and plant cues to coordinate
931 symbiotic nodule organogenesis in *Medicago truncatula*. Plant J **65**: 622–633

932 **Schreiber MC, Karlo JC, Kovalick GE** (1997) A novel cDNA from Drosophila encoding a
933 protein with similarity to mammalian cysteine-rich secretory proteins, wasp venom antigen
934 5, and plant group 1 pathogenesis-related proteins. Gene **191**: 135–141

935 **Seabra AR, Pereira PA, Becker JD, Carvalho HG** (2012) Inhibition of glutamine synthetase
936 by phosphinothricin leads to transcriptome reprogramming in root nodules of *Medicago*
937 *truncatula*. Mol Plant-Microbe Interact **25**: 976–992

938 **Sels J, Mathys J, De Coninck BMA a, Cammue BPA a, De Bolle MFCC** (2008) Plant
939 pathogenesis-related (PR) proteins: a focus on PR peptides. Plant Physiol Biochem **46**: 941–
940 50

941 **Shen Q, Liu L, Wang L, Wang Q** (2018) Indole primes plant defense against necrotrophic
942 fungal pathogen infection. PLoS One **13**: e0207607

943 **Sinha M, Singh RP, Kushwaha GS, Iqbal N, Singh A, Kaushik S, Kaur P, Sharma S, Singh**
944 **TP** (2014) Current overview of allergens of plant pathogenesis related protein families. *Sci*
945 *World J* **2014**: 543195

946 **Sinharoy S, Torres-Jerez I, Bandyopadhyay K, Kereszt A, Pislariu CI, Nakashima J,**
947 **Benedito VA, Kondorosi E, Udvardi MK** (2013) The C₂H₂ transcription factor regulator
948 of symbiosome differentiation represses transcription of the secretory pathway gene
949 *VAMP721a* and promotes symbiosome development in *Medicago truncatula*. *Plant Cell* **25**:
950 3584–3601

951 **Stintzi A, Heitz T, Prasad V, Wiedemann-Merdinoglu S, Kauffmann S, Geoffroy P,**
952 **Legrand M, Fritig B** (1993) Plant “pathogenesis-related” proteins and their role in defense
953 against pathogens. *Biochimie* **75**: 687–706

954 **Tadege M, Wen J, He J, Tu H, Kwak Y, Eschstruth A, Cayrel A, Endre G, Zhao PX,**
955 **Chabaud M, et al** (2008) Large-scale insertional mutagenesis using the *Tnt1*
956 retrotransposon in the model legume *Medicago truncatula*. *Plant J* **54**: 335–347

957 **Tang F, Yang S, Liu J, Zhu H** (2016) *Rj4*, a gene controlling nodulation specificity in soybeans,
958 encodes a thaumatin-like protein but not the one previously reported. *Plant Physiol* **170**: 26–
959 32

960 **Van de Velde W, Guerra JCP, De Keyser A, De Rycke R, Rombauts S, Maunoury N,**
961 **Mergaert P, Kondorosi E, Holsters M, Goormachtig S** (2006) Aging in legume
962 symbiosis. A molecular view on nodule senescence in *Medicago truncatula*. *Plant Physiol*
963 **141**: 711–720

964 **Van de Velde W, Zehirov G, Szatmari A, Debreczeny M, Ishihara H, Kevei Z, Farkas A,**
965 **Mikulass K, Nagy A, Tiricz H, et al** (2010) Plant peptides govern terminal differentiation
966 of bacteria in symbiosis. *Science* **327**: 1122–1126

967 **van Loon LC, Rep M, Pieterse CMJ** (2006) Significance of inducible defense-related proteins
968 in infected plants. *Annu Rev Phytopathol* **44**: 135–162

969 **Walter MH, Liu JW, Wünn J, Hess D** (1996) Bean ribonuclease-like pathogenesis-related
970 protein genes (*Ypr10*) display complex patterns of developmental, dark-induced and

971 exogenous-stimulus-dependent expression. *Eur J Biochem* **239**: 281–293

972 **Walton JH, Kontra-Kováts G, Green RT, Domonkos Á, Horváth B, Brear EM,**
973 **Franceschetti M, Kaló P, Balk J** (2020) The *Medicago truncatula* vacuolar iron
974 transporter-like proteins VTL4 and VTL8 deliver iron to symbiotic bacteria at different
975 stages of the infection process. *New Phytol* **228**: 651–666

976 **Wang C, Yu H, Luo L, Duan L, Cai L, He X, Wen J, Mysore KS, Li G, Xiao A, et al** (2016)
977 *NODULES WITH ACTIVATED DEFENSE 1* is required for maintenance of rhizobial
978 endosymbiosis in *Medicago truncatula*. *New Phytol* **212**: 176–191

979 **Wang X, Tang C, Deng L, Cai G, Liu X, Liu B, Han Q** (2010) Characterization of a
980 pathogenesis-related thaumatin-like protein gene *TaPR5* from wheat induced by stripe rust.
981 *Physiol Plant* **139**: 27–38

982 **Wingler A, Brownhill E, Pourtau N** (2005) Mechanisms of the light-dependent induction of
983 cell death in tobacco plants with delayed senescence. *J Exp Bot* **56**: 2897–2905

984 **Wyk SG Van, Plessis M Du, Cullis CA, Kunert KJ, Vorster BJ** (2014) Cysteine protease and
985 cystatin expression and activity during soybean nodule development and senescence. *BMC*
986 *Plant Biol* **14**: 1–13

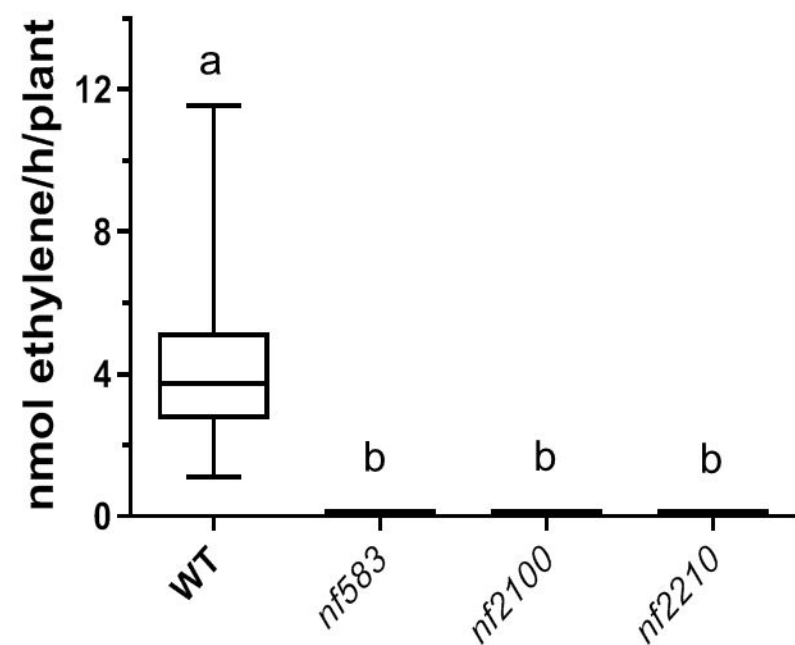
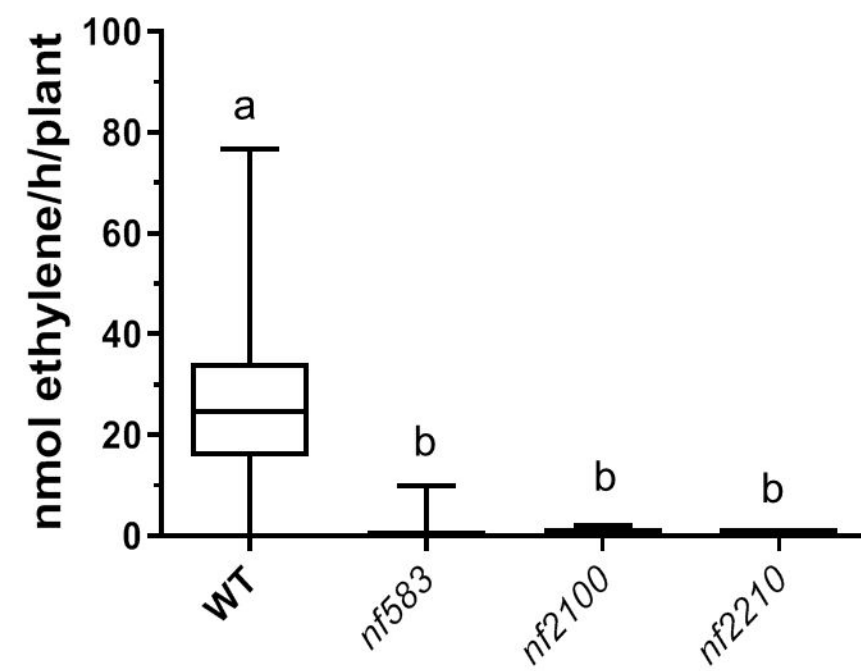
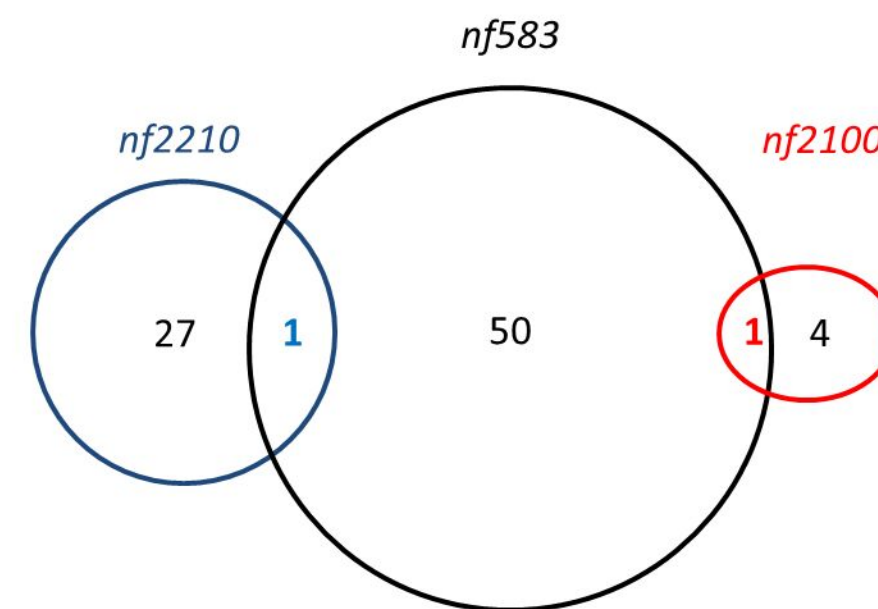
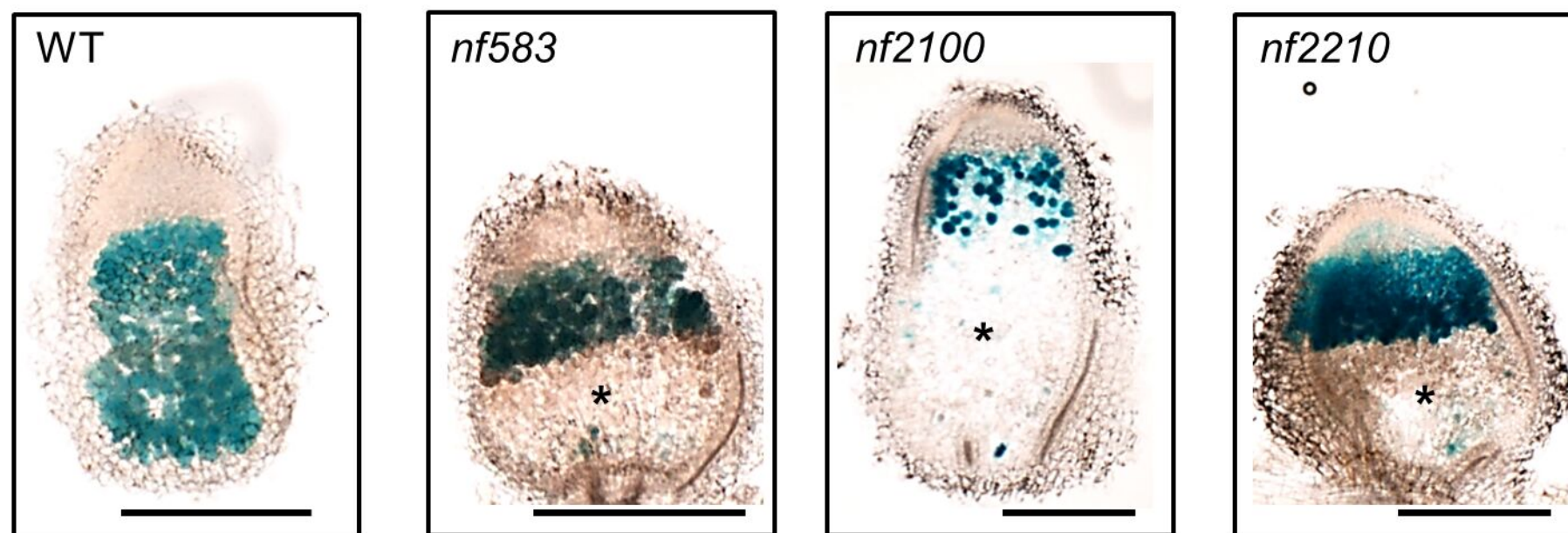
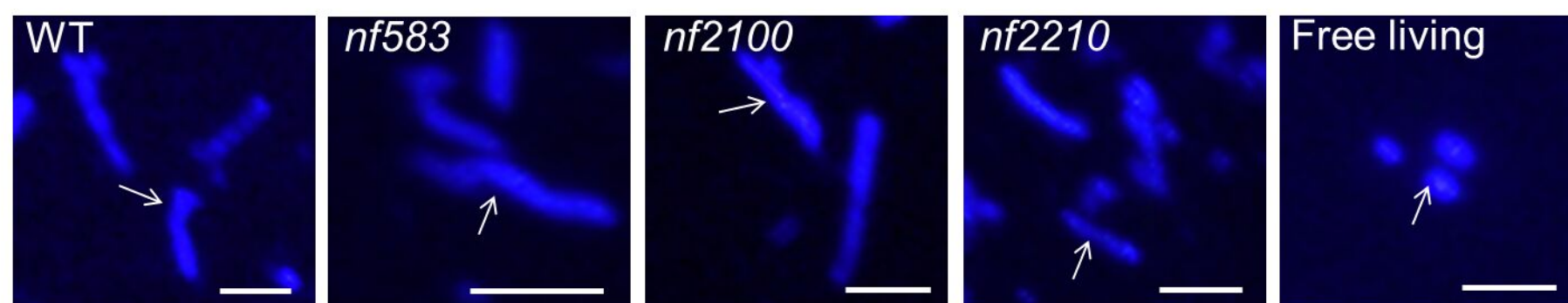
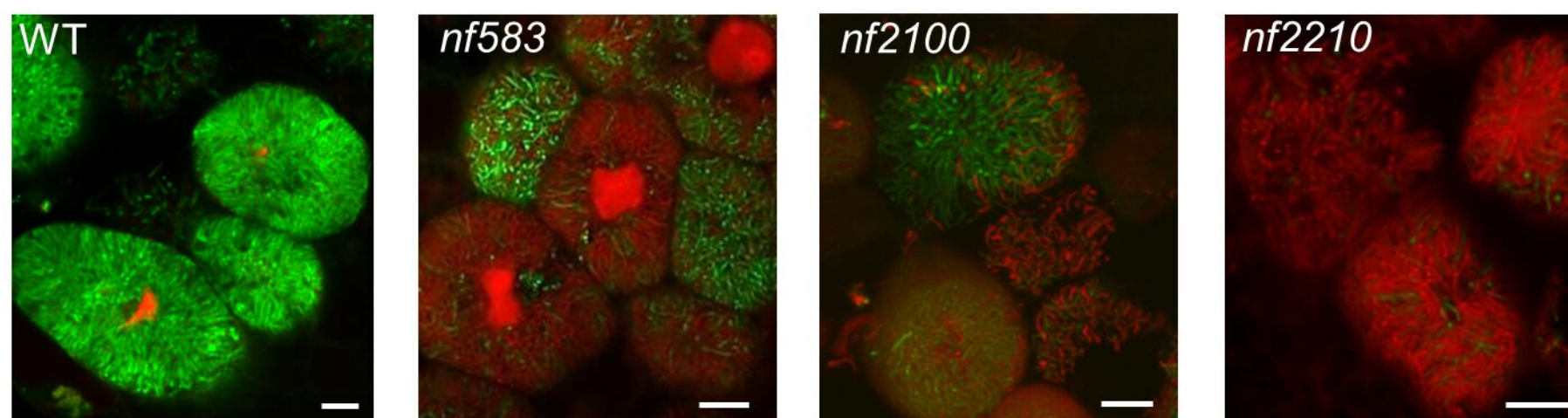
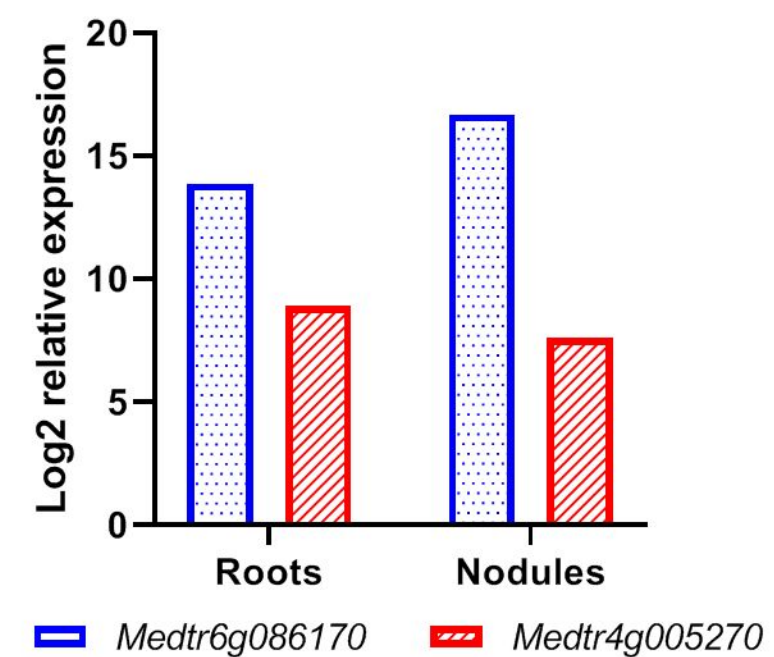
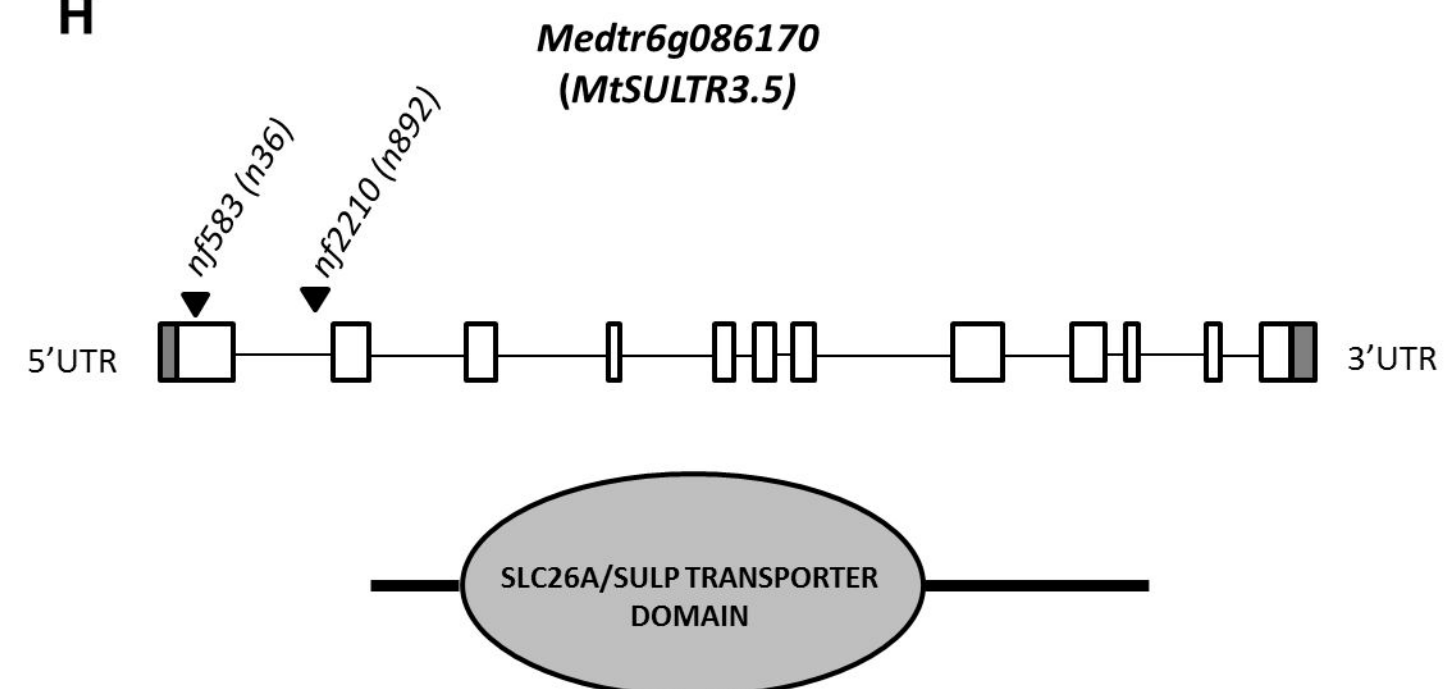
987 **Yarce JCS, Lee HK, Tadege M, Ratet P, Mysore KS** (2013) Forward genetics screening of
988 *Medicago truncatula Tnt1* insertion lines. *Methods Mol Biol* **1069**: 93–100

989 **Yasuda M, Miwa H, Masuda S, Takebayashi Y, Sakakibara H, Okazaki S** (2016) Effector-
990 triggered immunity determines host genotype-specific incompatibility in legume-rhizobium
991 symbiosis. *Plant Cell Physiol* **57**: 1791–1800

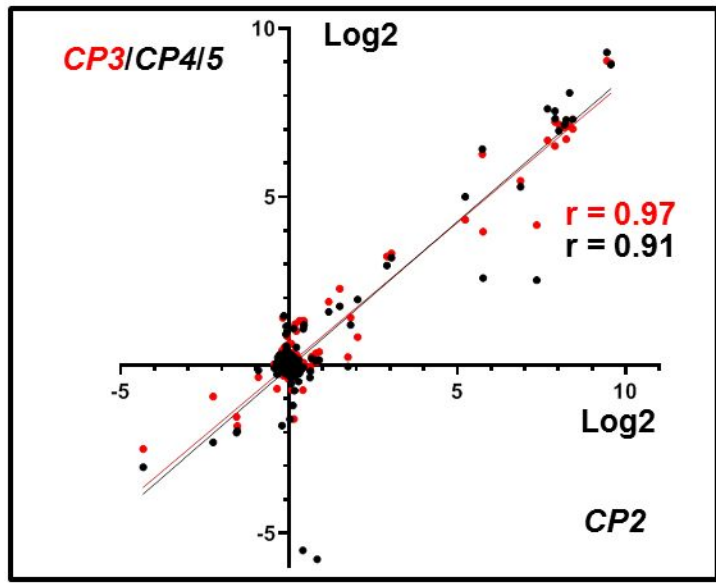
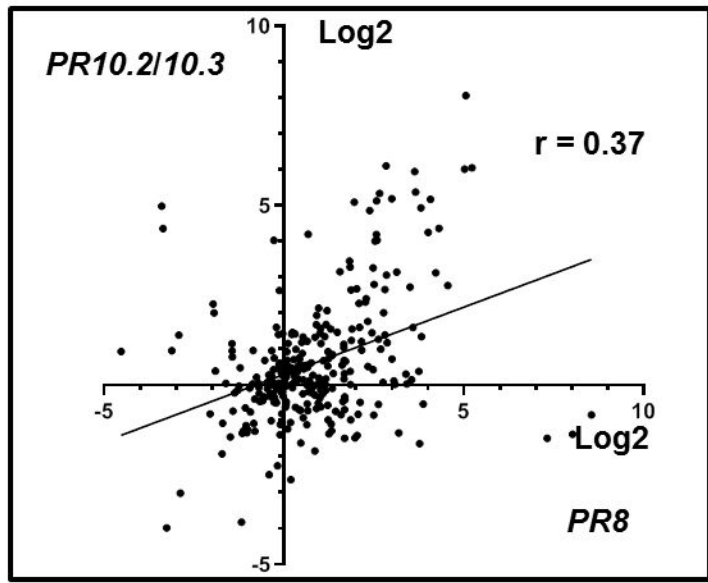
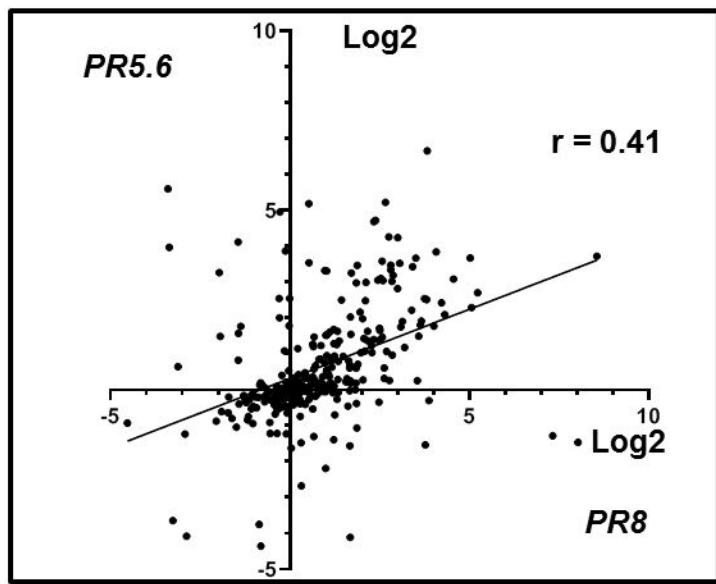
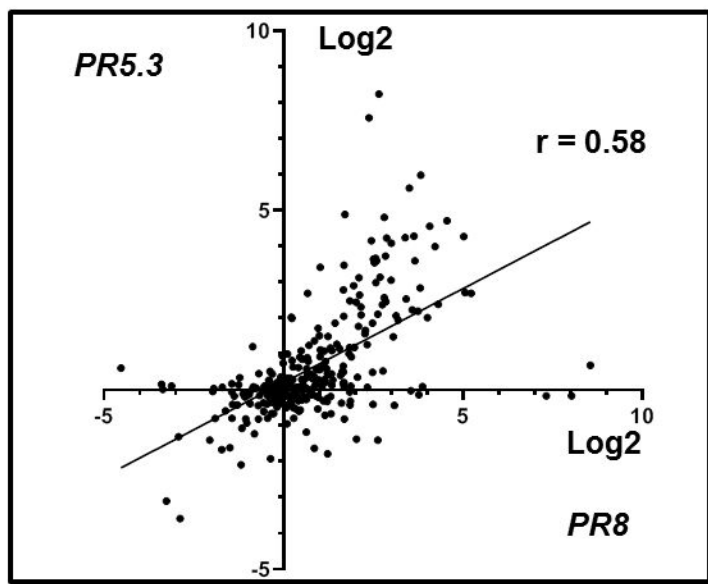
992 **Yu H, Xiao A, Dong R, Fan Y, Zhang X, Liu C, Wang C, Zhu H, Duanmu D, Cao Y, et al**
993 (2018) Suppression of innate immunity mediated by the CDPK-Rboh complex is required
994 for rhizobial colonization in *Medicago truncatula* nodules. *New Phytol* **220**: 425–434

995 **Zhang H, Dugé de Bernonville T, Body M, Glevarec G, Reichelt M, Unsicker S, Bruneau M,**
996 **Renou JP, Huguet E, Dubreuil G, et al** (2016) Leaf-mining by *Phyllonorycter*
997 *blancardella* reprograms the host-leaf transcriptome to modulate phytohormones associated
998 with nutrient mobilization and plant defense. *J Insect Physiol* **84**: 114–127

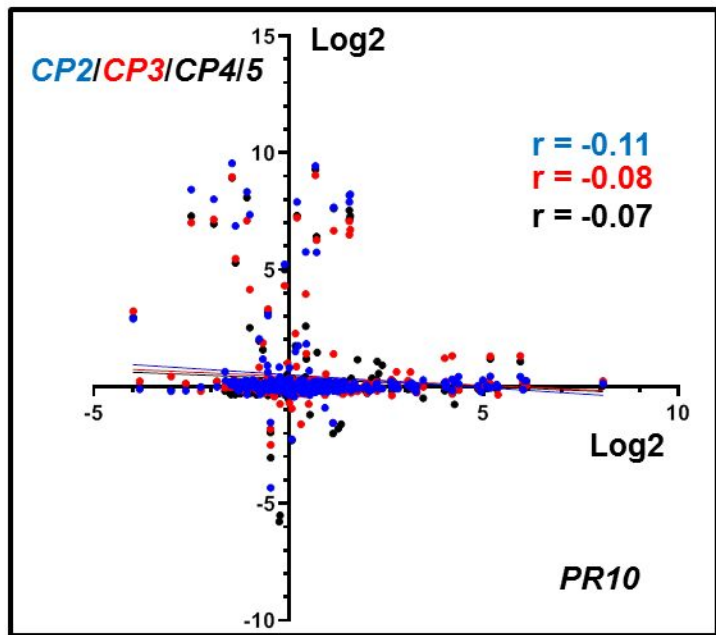
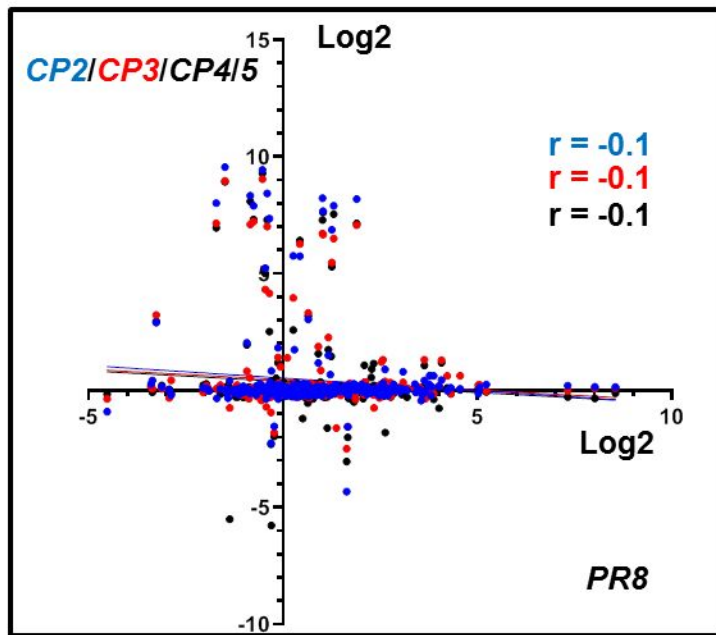
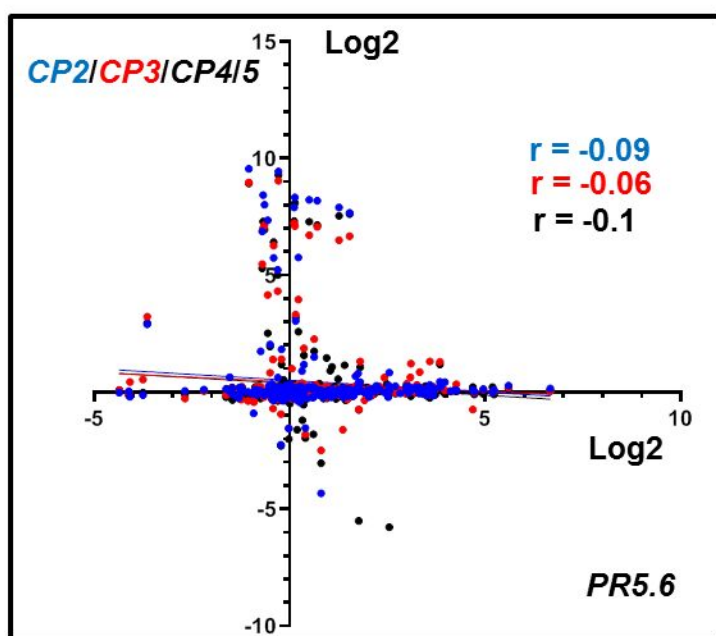
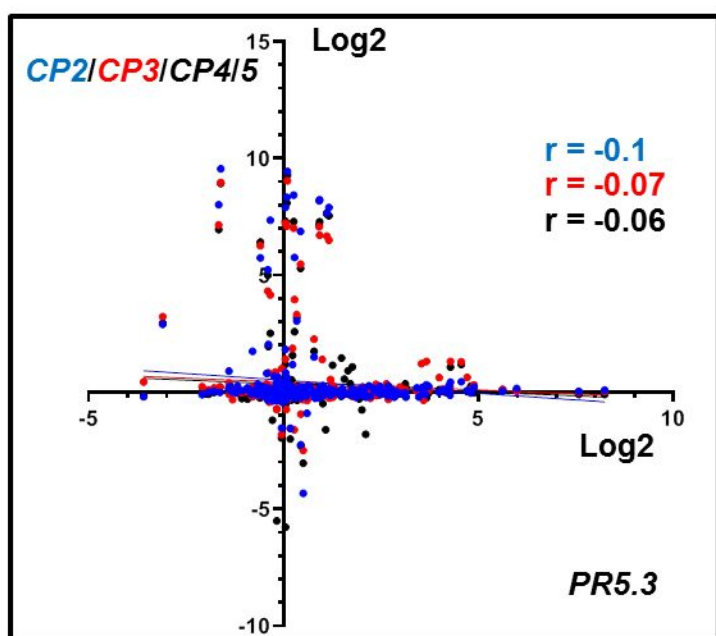
- 999 **Zhang Y, Wang H-L, Li Z, Guo H** (2020) Genetic Network between leaf senescence and plant
1000 immunity : crucial regulatory nodes and new insights. *Plants(Basel)* **9(4)**: 495
- 1001 **Zimmerman JL, Szeto WW, Ausubel FM** (1983) Molecular characterization of *Tn5*-induced
1002 symbiotic (Fix-) mutants of *Rhizobium meliloti*. *J Bacteriol* **156**: 1025–1034
- 1003

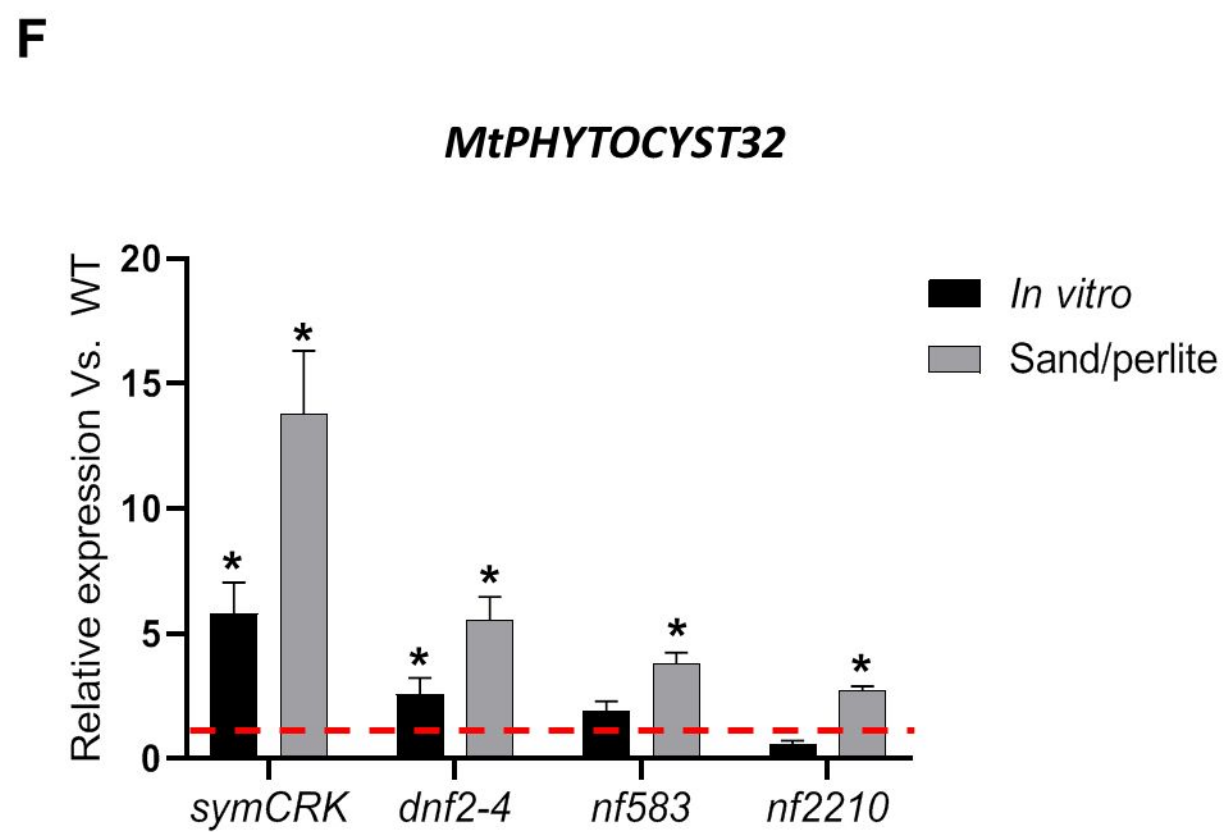
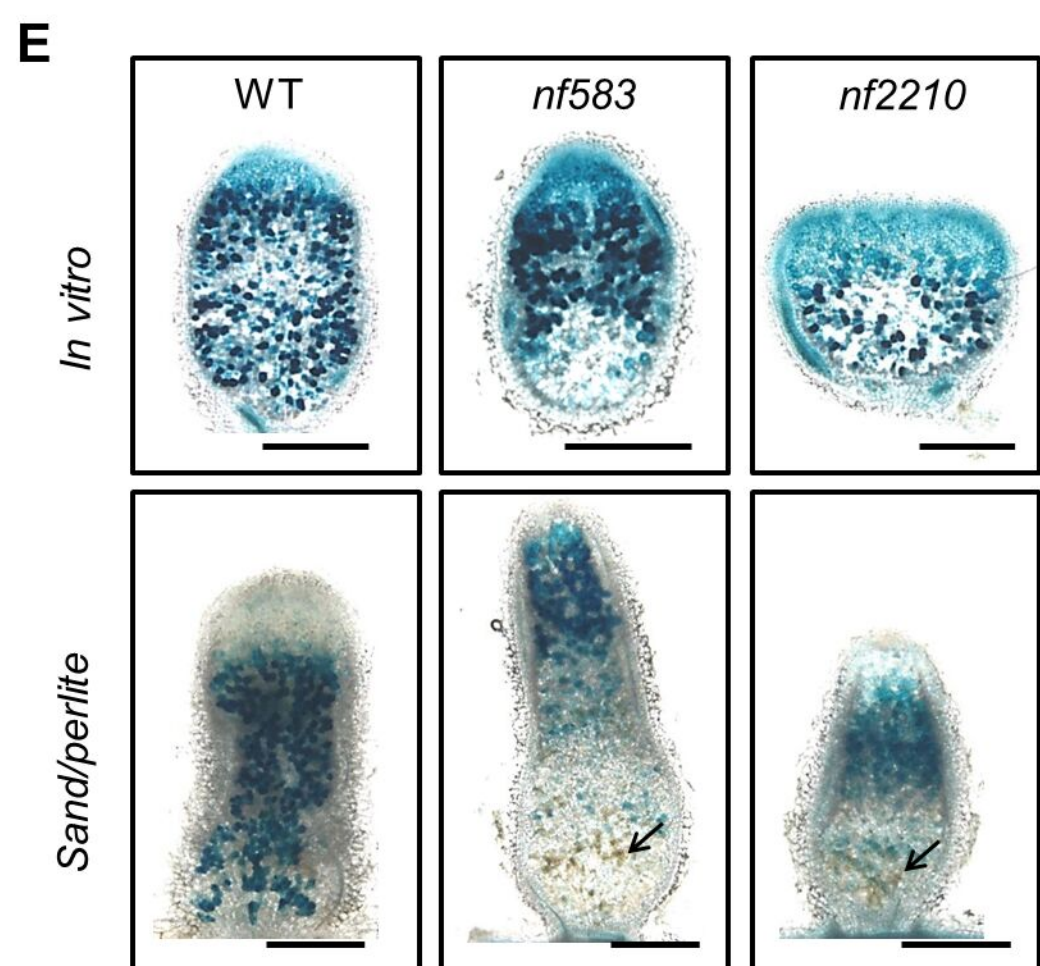
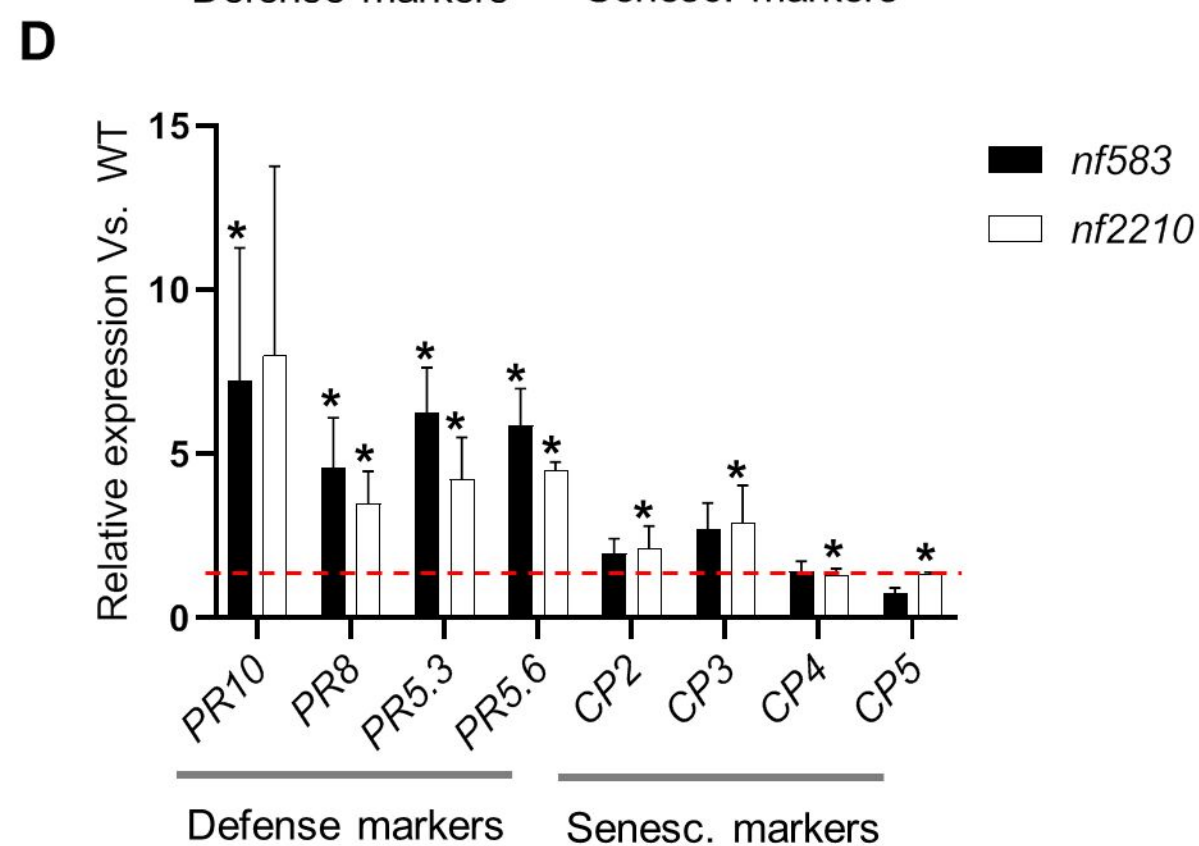
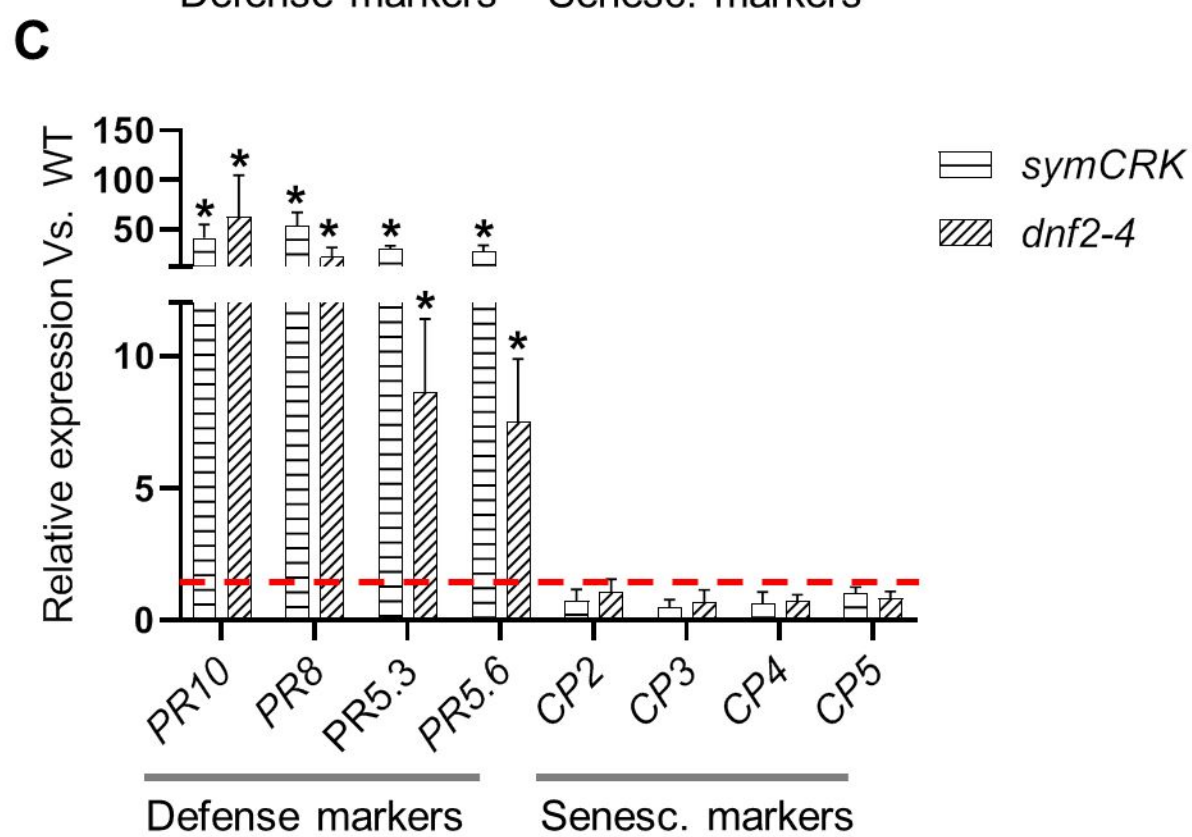
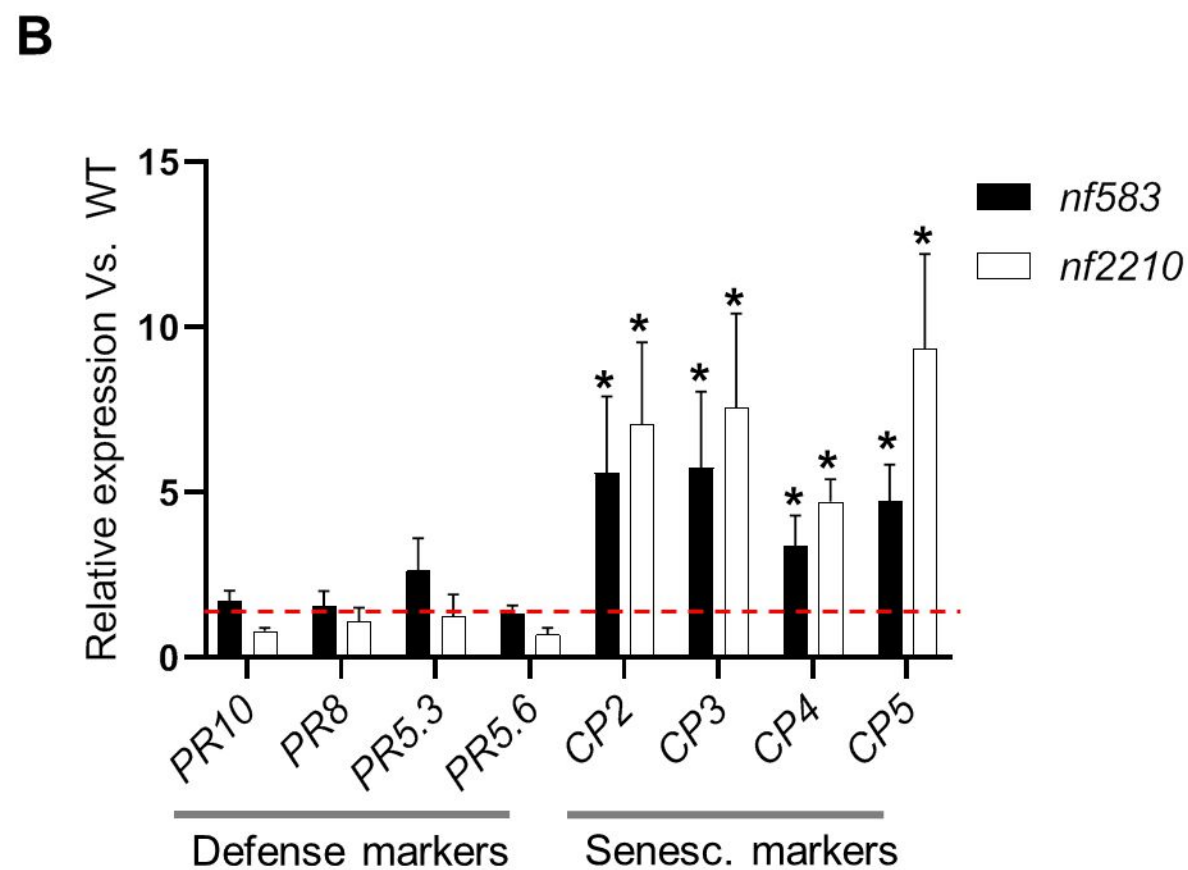
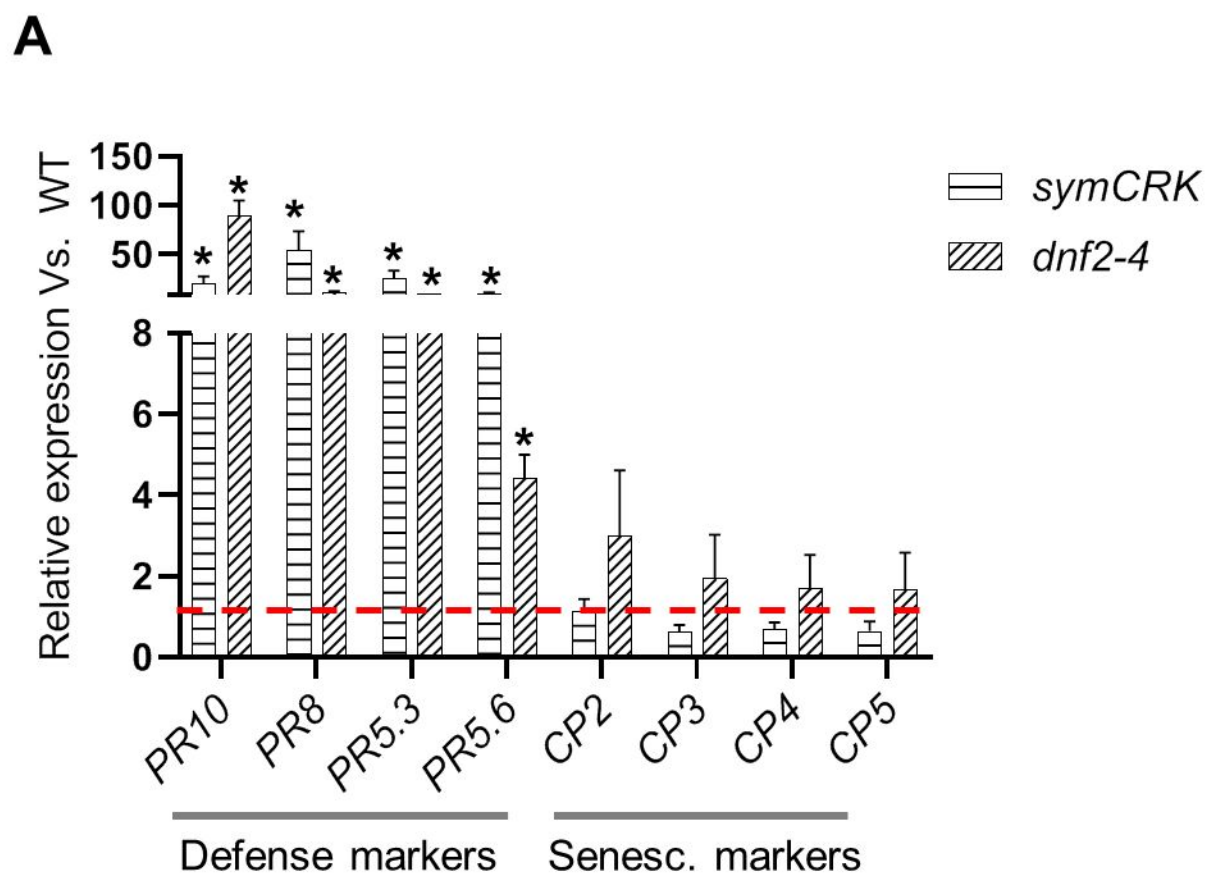
A**B****F****C****D****E****G****H**

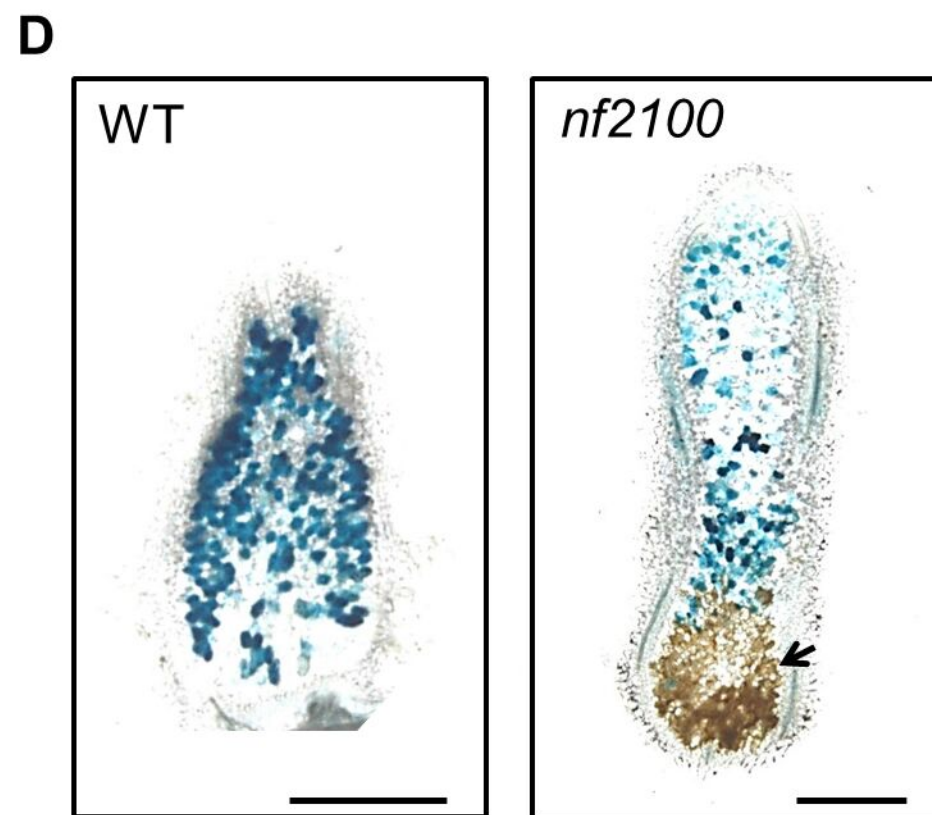
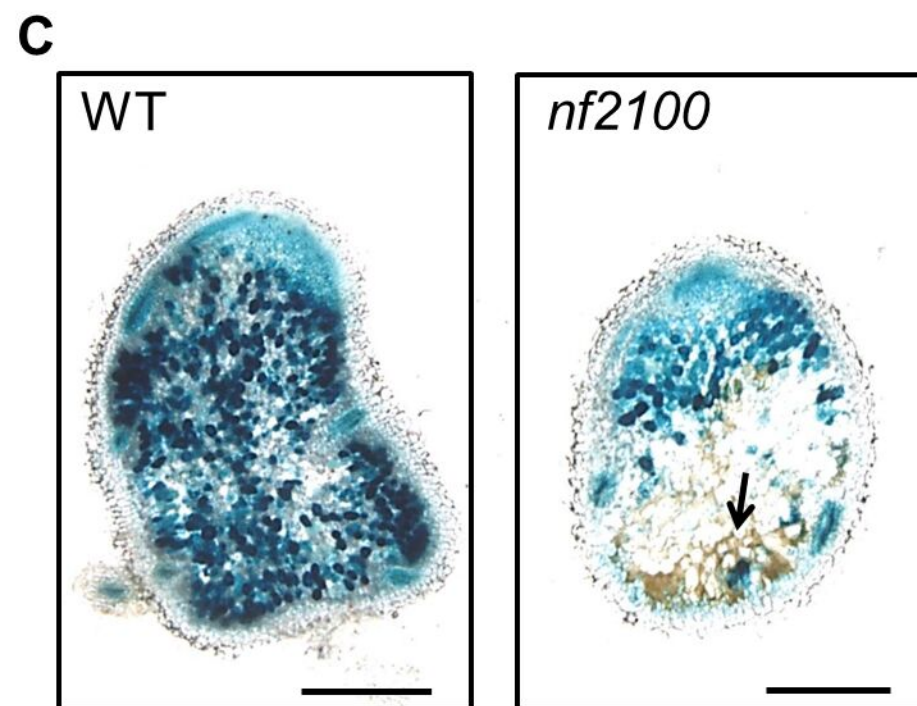
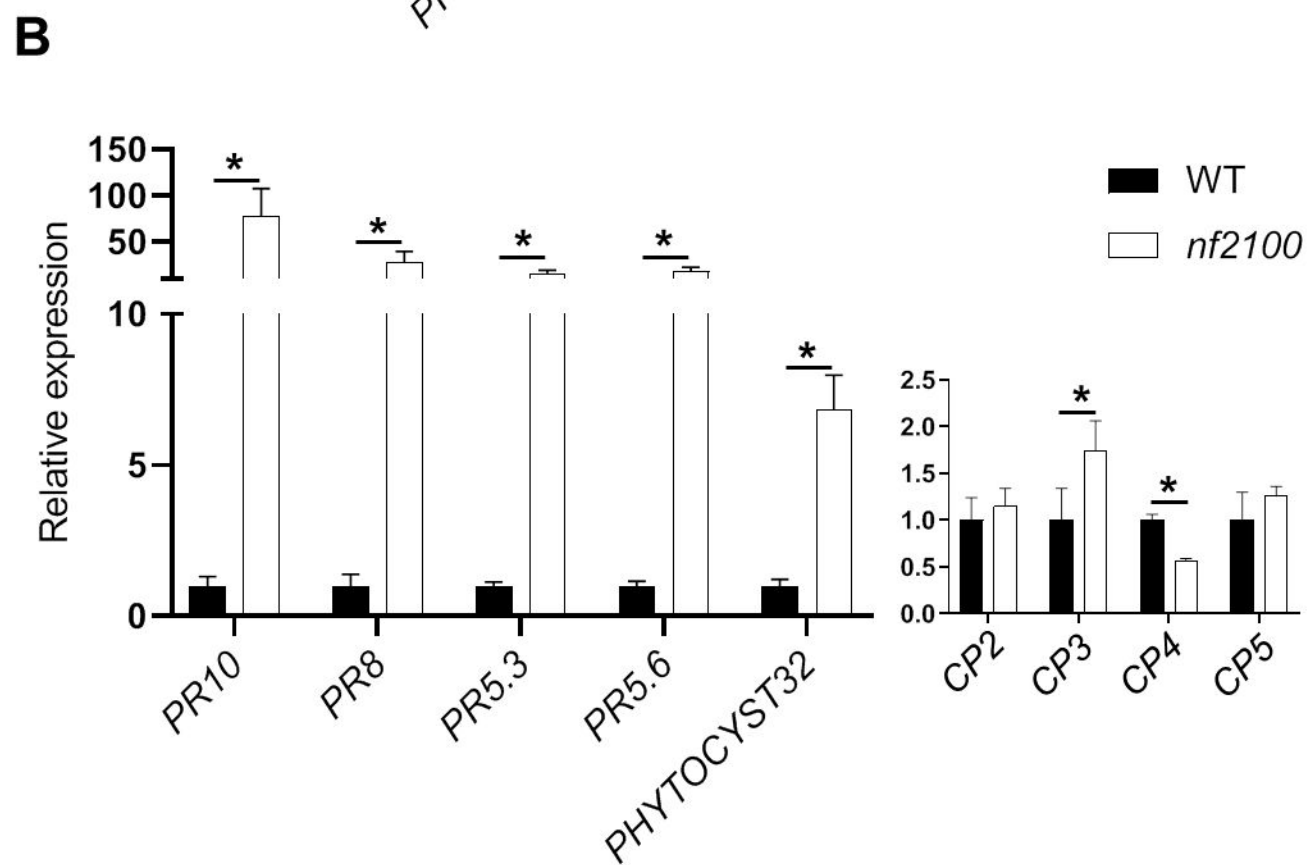
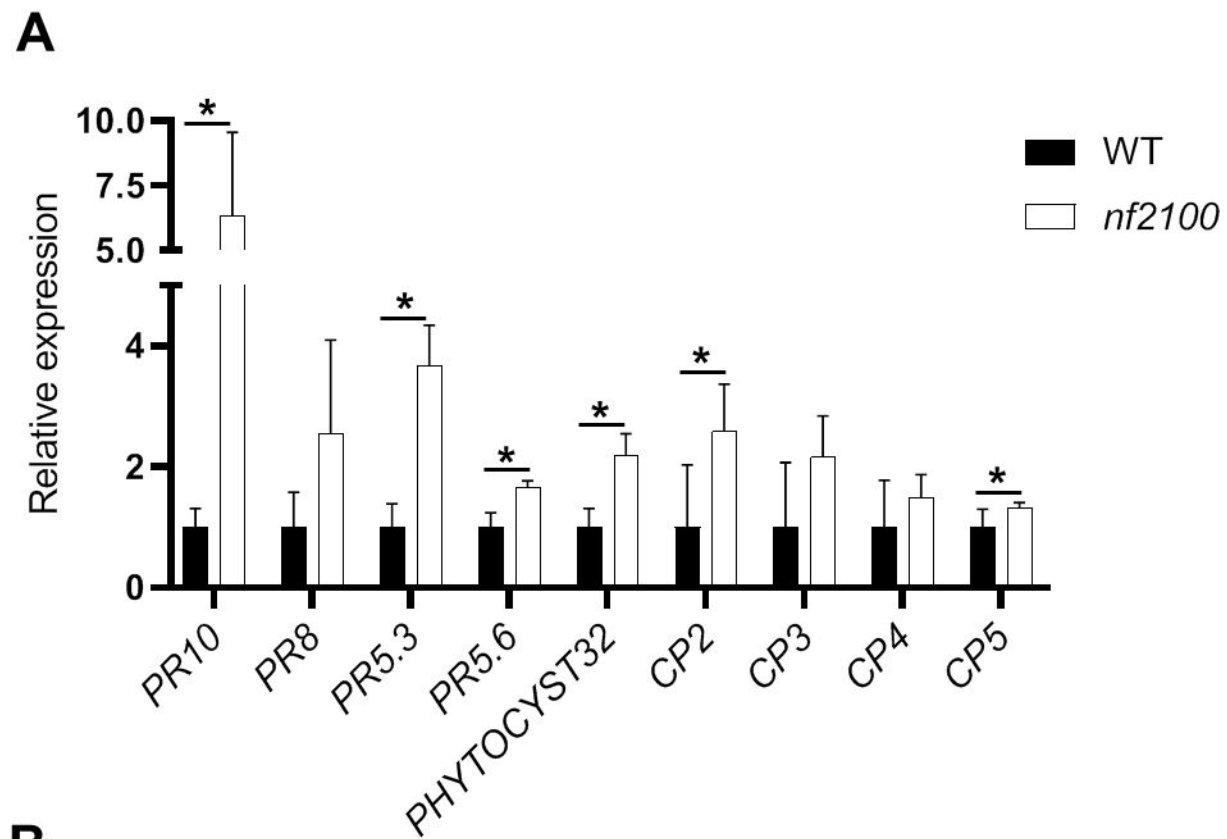
Intragroup comparison

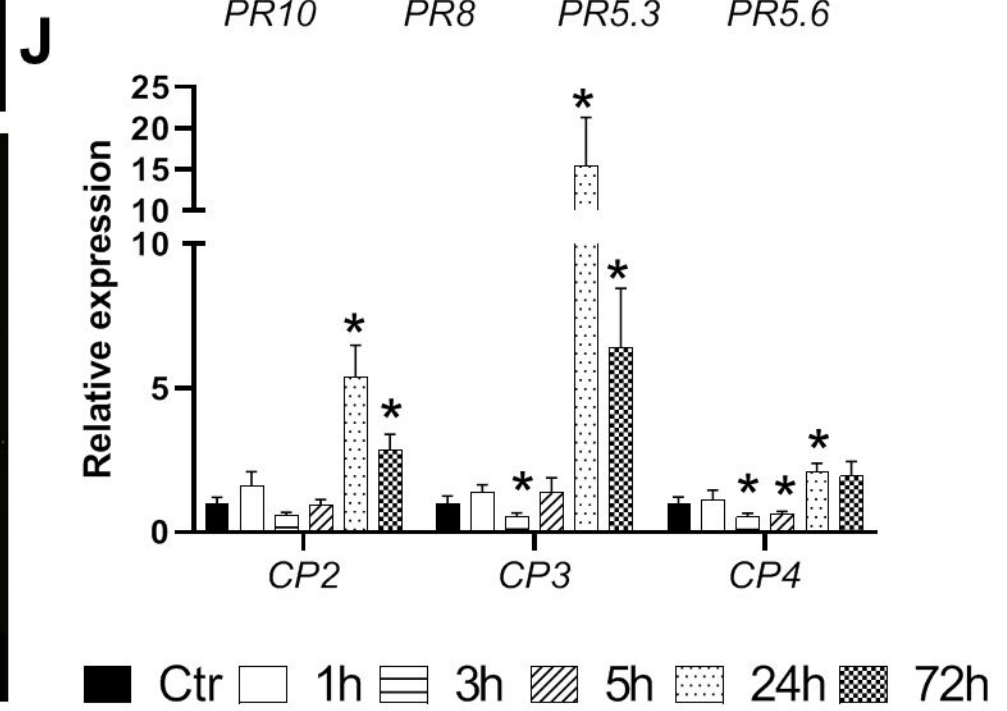
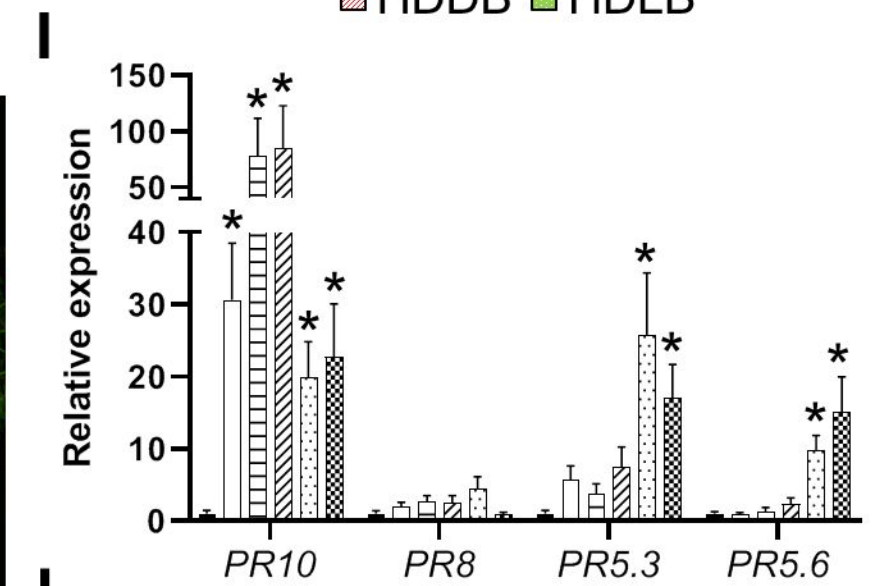
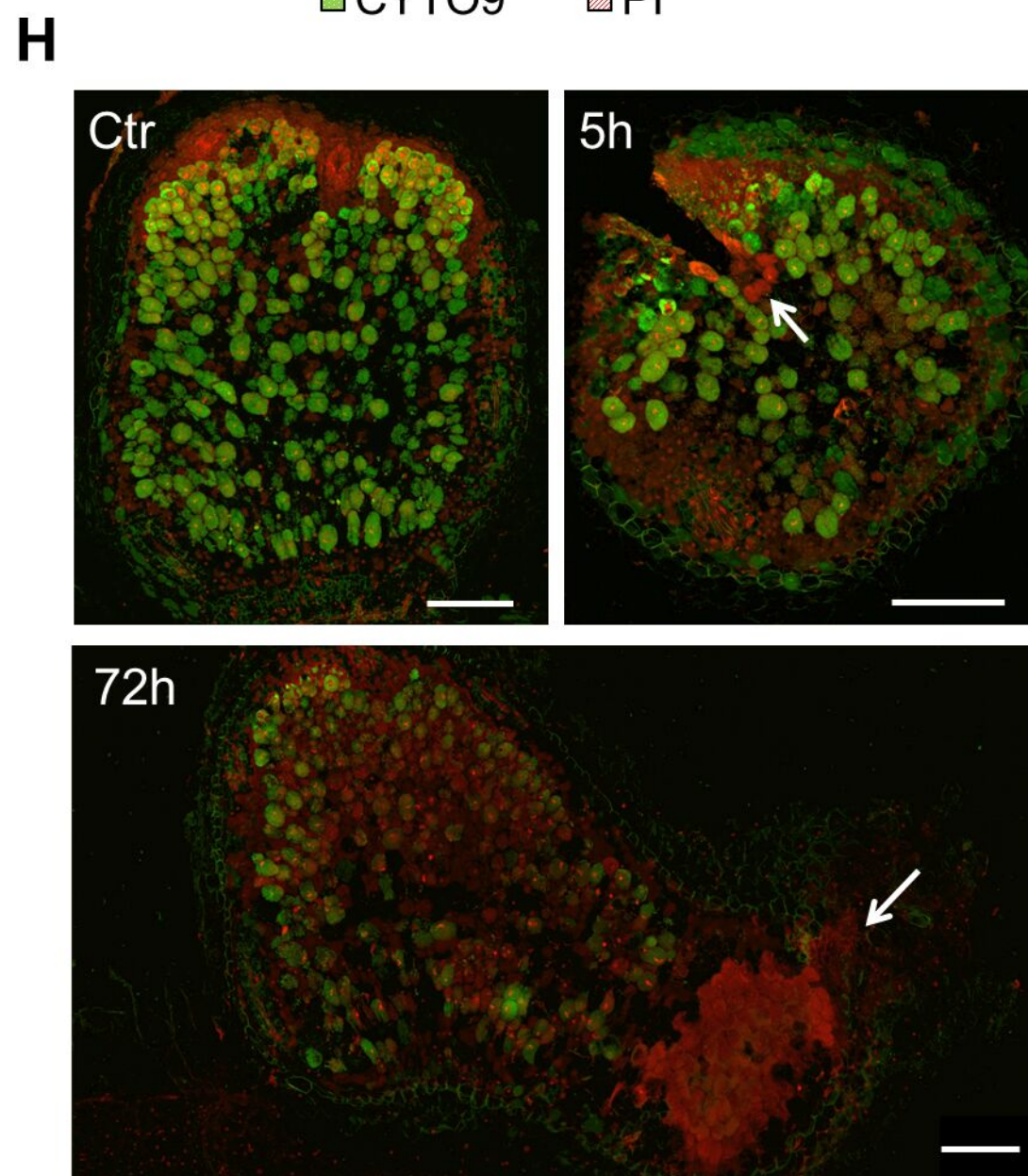
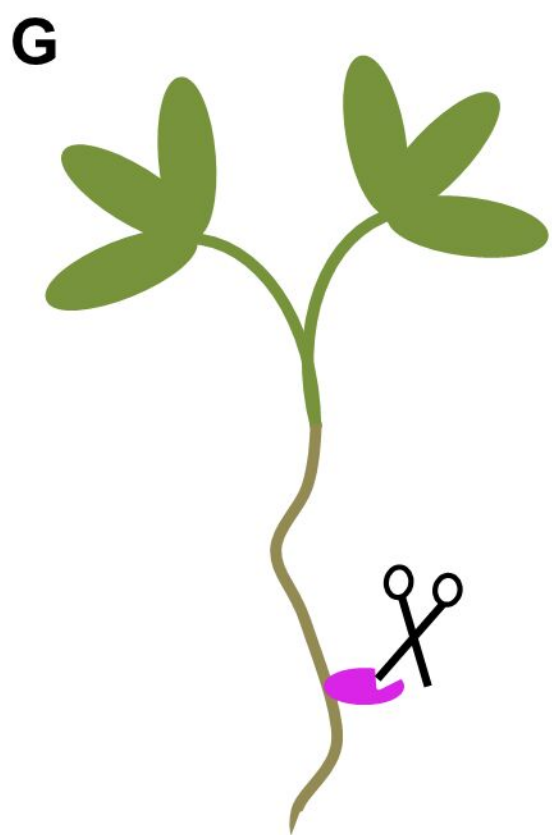
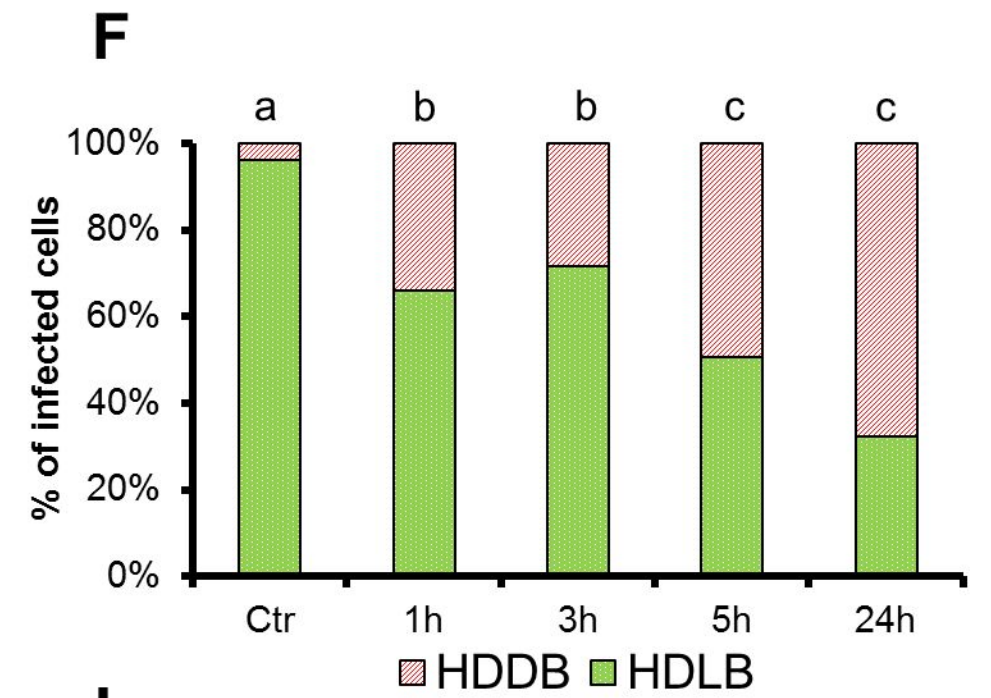
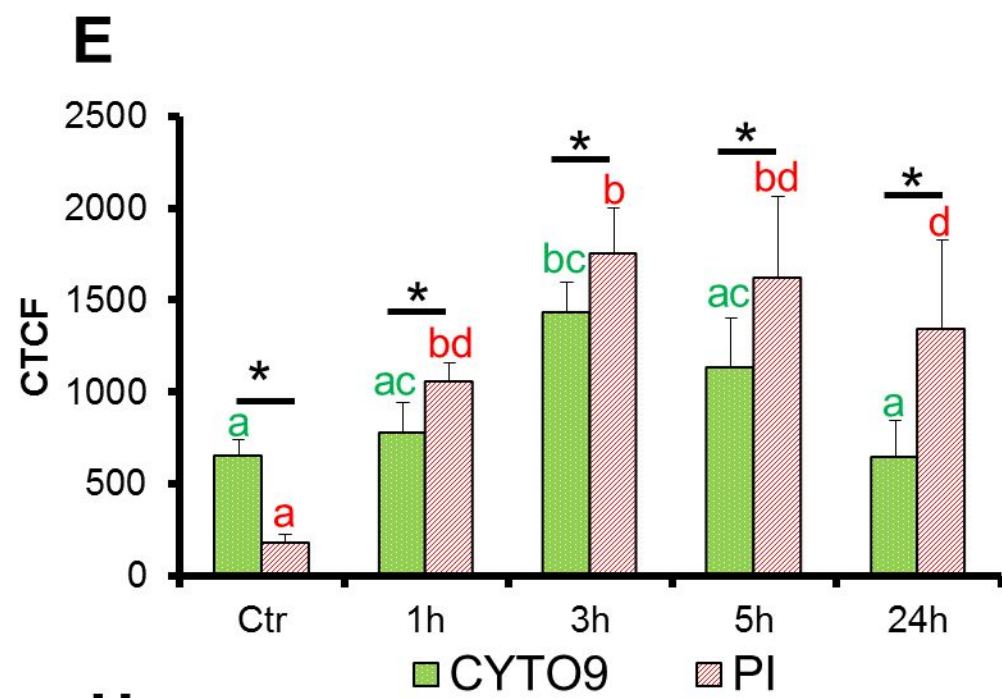
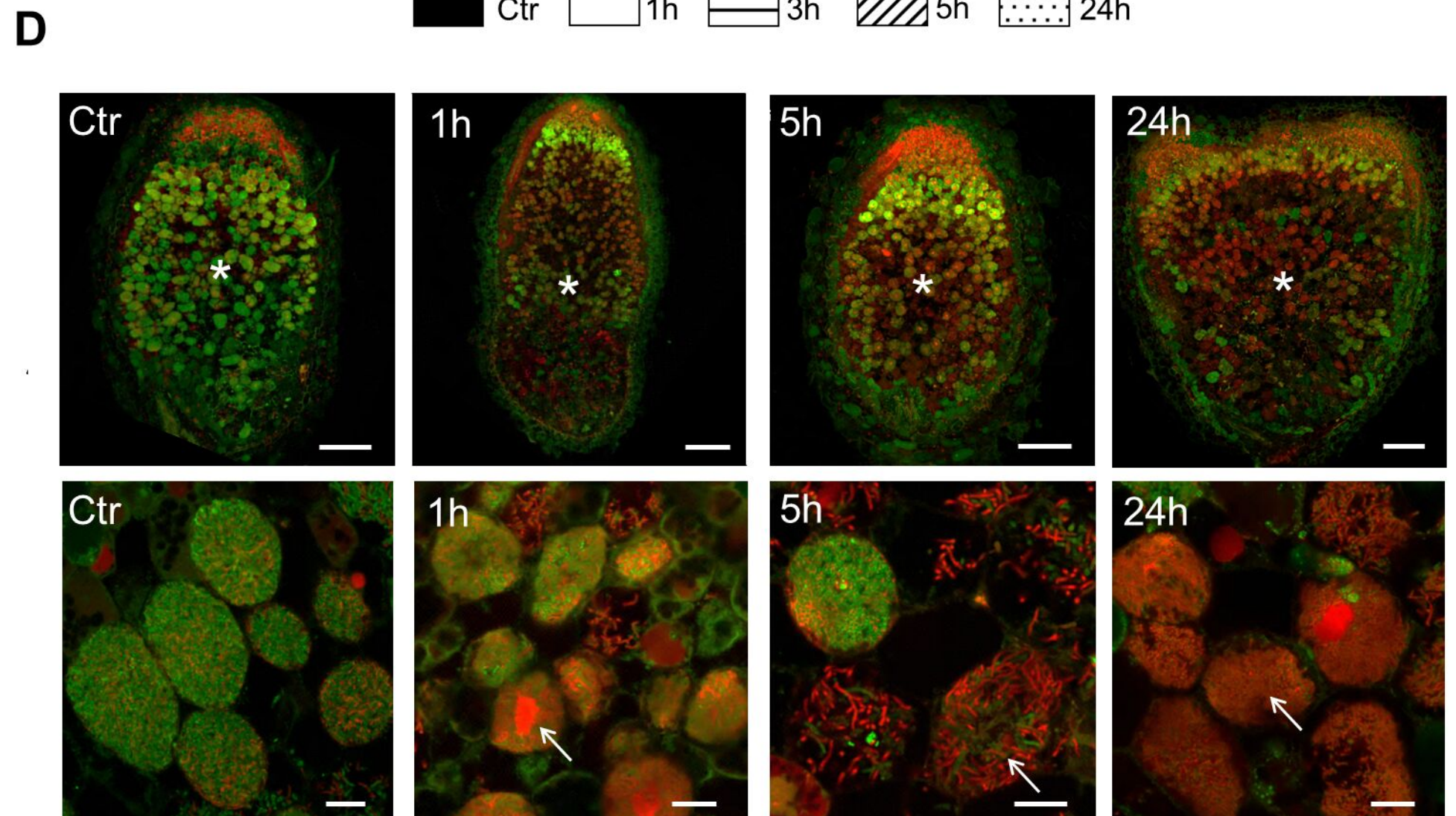
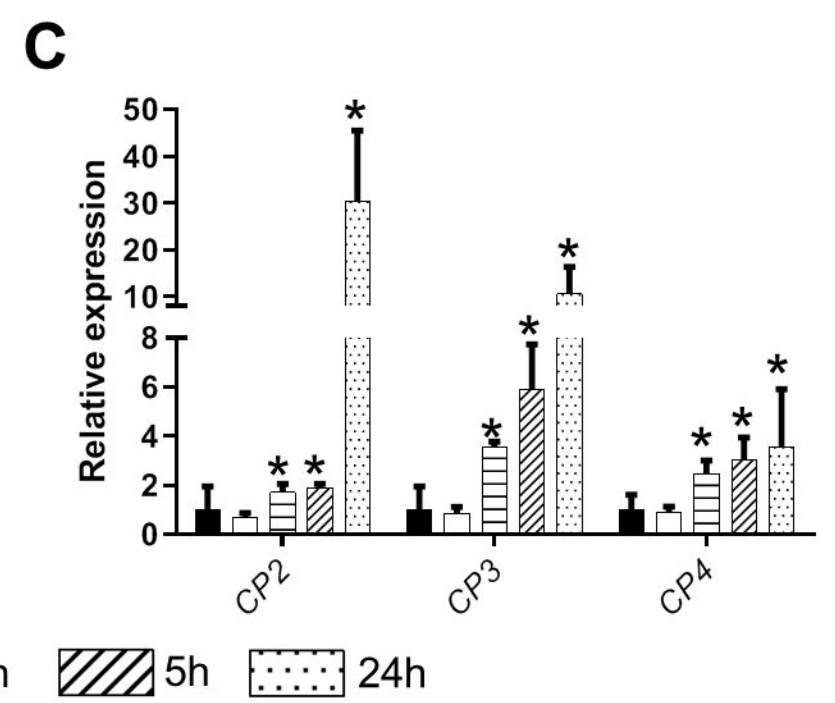
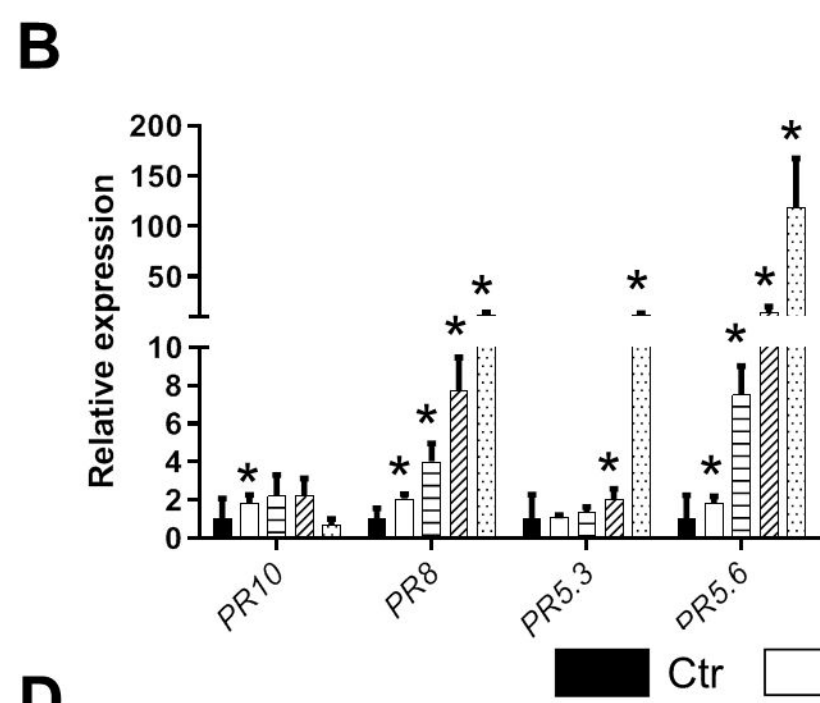
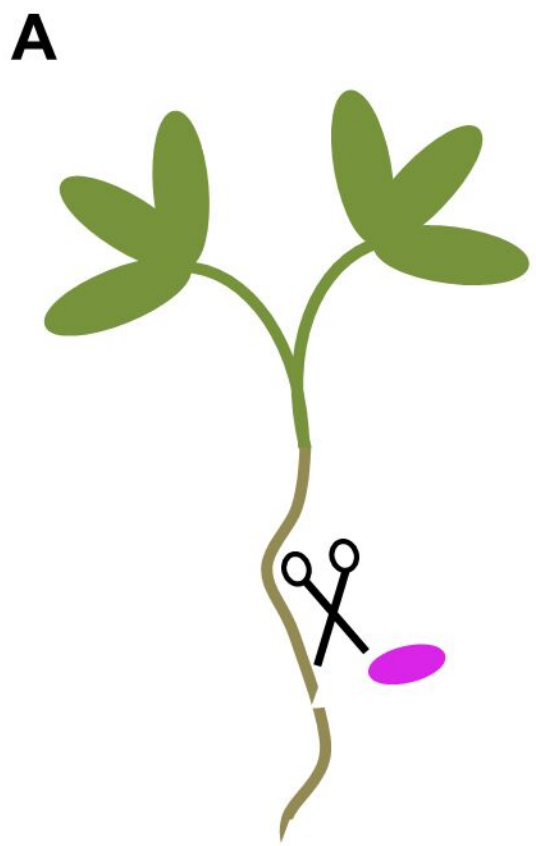


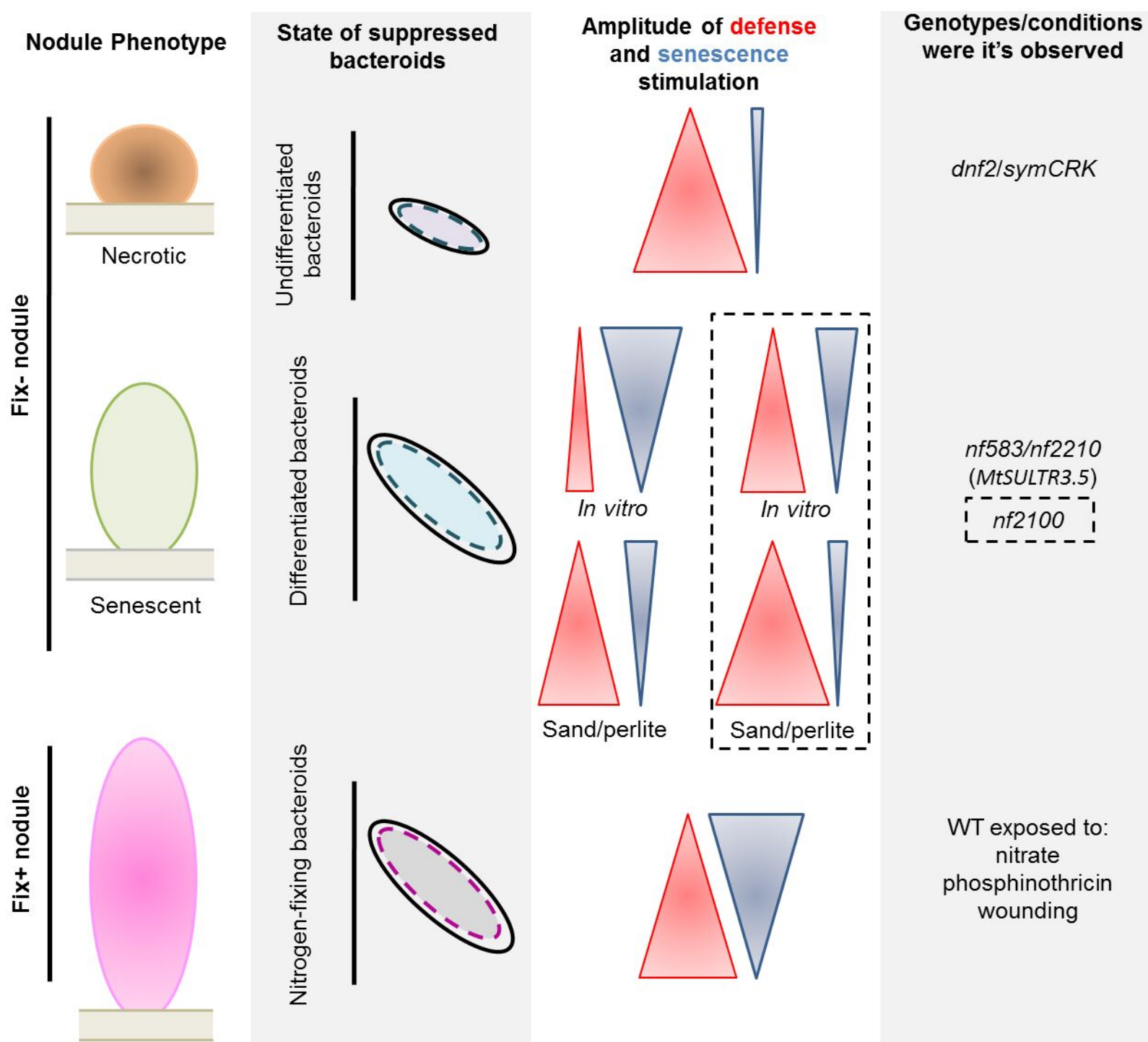
Intergroup comparison











Parsed Citations

- Ali S, Ahmad B, Kamili AN, Ali A, Ahmad Z, Akhter J, Tyagi A, Tajamul S, Mushtaq M, Yadav P, et al (2018) Pathogenesis-related proteins and peptides as promising tools for engineering plants with multiple stress tolerance. *Microbiol Res* 212–213: 29–37
Google Scholar: [Author Only](#) [Title Only](#) [Author and Title](#)
- Azumi Y, Watanabe A (1991) Evidence for a senescence-associated gene induced by darkness. *Plant Physiol* 95: 577–583
Google Scholar: [Author Only](#) [Title Only](#) [Author and Title](#)
- Benedito VA, Torres-jerez I, Murray JD, Andriankaja A, Allen S, Kakar K, Ott T, Moreau S, Niebel A, Frickey T (2008) A gene expression atlas of the model legume *Medicago truncatula*. *Plant J* 55: 504–513
Google Scholar: [Author Only](#) [Title Only](#) [Author and Title](#)
- Benezech C, Berrabah F, Jardinaud MF, Le Scornet A, Milhes M, Jiang G, George J, Ratet P, Vaillau F, Gourion B (2020) *Medicago-Sinorhizobium-Ralstonia* Co-infection Reveals Legume Nodules as Pathogen Confined Infection Sites Developing Weak Defenses. *Curr Biol* 30: 351-358
Google Scholar: [Author Only](#) [Title Only](#) [Author and Title](#)
- Berrabah F, Balliau T, AEH, George J, Zivy M, Ratet P, Gourion B (2018a) Control of the ethylene signaling pathway prevents plant defenses during intracellular accommodation of the rhizobia. *New Phytol* 219: 310–323
Google Scholar: [Author Only](#) [Title Only](#) [Author and Title](#)
- Berrabah F, Bourcy M, Cayrel A, Eschstruth A, Mondy S, Ratet P, Gourion B (2014a) Growth conditions determine the DNF2 requirement for symbiosis. *PLoS One* 9: 1–10
Google Scholar: [Author Only](#) [Title Only](#) [Author and Title](#)
- Berrabah F, Bourcy M, Eschstruth A, Cayrel A, Guefrachi I, Mergaert P, Wen J, Jean V, Mysore KS, Gourion B, et al (2014b) A nonRD receptor-like kinase prevents nodule early senescence and defense-like reactions during symbiosis. *New Phytol* 203: 1305–1314
Google Scholar: [Author Only](#) [Title Only](#) [Author and Title](#)
- Berrabah F, Hosseyn E, Salem A, Garmier M, Ratet P (2018b) The multiple Faces of the *Medicago-Sinorhizobium* Symbiosis. *Funct. genomics Medicago truncatula Methods Protoc. Methods Mol. Biol.* 1822: 241–260
Google Scholar: [Author Only](#) [Title Only](#) [Author and Title](#)
- Berrabah F, Ratet P, Gourion B (2015) Multiple steps control immunity during the intracellular accommodation of rhizobia. *J Exp Bot* 66: 1977–1985
Google Scholar: [Author Only](#) [Title Only](#) [Author and Title](#)
- Bourcy M, Brocard L, Pislariu CI, Cosson V, Mergaert P, Tadege M, Mysore KS, Mickael K U, Benjamin G, Ratet P (2013) *Medicago truncatula* DNF2 is a PI-PLC-XD-containing protein required for bacteroid persistence and prevention of nodule early senescence and defense-like reactions. *New Phytol* 197: 1250–1261
Google Scholar: [Author Only](#) [Title Only](#) [Author and Title](#)
- Chen P-C, Phillips DA (1977) Induction of root nodule senescence by combined nitrogen in *Pisum sativum* L. *Plant Physiol* 59: 440–442
Google Scholar: [Author Only](#) [Title Only](#) [Author and Title](#)
- Chen SL, Shan ZH, Yang ZL, Zhang XJ, Qiu DZ, Zhou XA (2017) RNA-Seq analysis of nodule development at five different developmental stages of soybean (*Glycine max*) inoculated with *Bradyrhizobium japonicum* strain 113-2. *Scientific Reports* 7: 42248
Google Scholar: [Author Only](#) [Title Only](#) [Author and Title](#)
- Cheng X, Wang M, Lee HK, Tadege M, Ratet P, Udvardi M, Mysore KS, Wen J (2014) An efficient reverse genetics platform in the model legume *Medicago truncatula*. *New Phytol* 201: 1065–1076
Google Scholar: [Author Only](#) [Title Only](#) [Author and Title](#)
- Díaz-Mendoza M, Velasco-Arroyo B, González-Melendi P, Martínez M, Díaz I (2014) C1A cysteine protease-cystatin interactions in leaf senescence. *J Exp Bot* 65: 3825–3833
Google Scholar: [Author Only](#) [Title Only](#) [Author and Title](#)
- Domonkos A, Szilard K, Aniko G, Erno K, Horváth B, Gyongyi ZK, Attila F, Monika TT, Ferhan A, Karoly B, et al (2017) NAD1 Controls defense-like responses in *Medicago truncatula* symbiotic nitrogen fixing nodules following rhizobial colonization in a *BacA*-independent Manner. *Genes (Basel)* 8: 387
Google Scholar: [Author Only](#) [Title Only](#) [Author and Title](#)
- Ehrhardt DW, Morrey Atkinson E, Long SR (1992) Depolarization of alfalfa root hair membrane potential by *Rhizobium meliloti* nod factors. *Science* 256: 998–1000
Google Scholar: [Author Only](#) [Title Only](#) [Author and Title](#)

- Fedorova M, Van de Mortel J, Matsumoto PA, Cho J, Town CD, VandenBosch KA, Gantt JS, Vance CP (2002) Genome-wide identification of nodule-specific transcripts in the model legume *Medicago truncatula*. *Plant Physiol* 130: 519–537
Google Scholar: [Author Only](#) [Title Only](#) [Author and Title](#)
- Fukui H, Yoshikawa N, Tabata M (1983) Induction of shikonin formation by agar in *Lithospermum erythrorhizon* cell suspension cultures. *Phytochemistry* 22: 2451–2453
Google Scholar: [Author Only](#) [Title Only](#) [Author and Title](#)
- Gourion B, Berrabah F, Ratet P, Stacey G (2015) Rhizobium–legume symbioses : the crucial role of plant immunity. *Trends Plant Sci* 20: 186–194
Google Scholar: [Author Only](#) [Title Only](#) [Author and Title](#)
- Gupta R, Lee SJ, Min CW, Kim SW, Park KH, Bae DW, Lee BW, Agrawal GK, Rakwal R, Kim ST (2016) Coupling of gel-based 2-DE and 1-DE shotgun proteomics approaches to dig deep into the leaf senescence proteome of *Glycine max*. *J Proteomics* 148: 65–74
Google Scholar: [Author Only](#) [Title Only](#) [Author and Title](#)
- Haag AF, Baloban M, Sani M, Kerscher B, Pierre O, Angelo SD, Kondorosi E, Longhi R, Boncompagni E, He D, et al (2011) Protection of *Sinorhizobium* against host Cysteine-Rich Antimicrobial Peptides is critical for symbiosis. *Plos Biol* 9: e1001169
Google Scholar: [Author Only](#) [Title Only](#) [Author and Title](#)
- Hanfrey C, Fife M, Buchanan-Wollaston V (1996) Leaf senescence in *Brassica napus*: expression of genes encoding pathogenesis-related proteins. *Plant Mol Biol* 30: 597–609
Google Scholar: [Author Only](#) [Title Only](#) [Author and Title](#)
- Hayashi M, Shiro S, Kanamori H, Mori-Hosokawa S, Sasaki-Yamagata H, Sayama T, Nishioka M, Takahashi M, Ishimoto M, Katayose Y, et al (2014) A thaumatin-like protein, Rj4, controls nodule symbiotic specificity in soybean. *Plant Cell Physiol* 55: 1679–1689
Google Scholar: [Author Only](#) [Title Only](#) [Author and Title](#)
- Hoffmann B, Trinh TH, Leung J, Kondorosi A, Kondorosi E (1997) A new *Medicago truncatula* line with superior in vitro regeneration, transformation, and symbiotic properties isolated through cell culture selection. *Mol Plant-Microbe Interact* 10: 307–315
Google Scholar: [Author Only](#) [Title Only](#) [Author and Title](#)
- Horváth B, Domonkos Á, Kereszt A, Szűcs A, Ábrahám E, Ayaydin F, Bóka K, Chen Y, Chen R, et al (2015) Loss of the nodule-specific cysteine rich peptide, NCR169, abolishes symbiotic nitrogen fixation in the *Medicago truncatula* dnf7 mutant. *Proc Natl Acad Sci* 112(49): 15232–15237
Google Scholar: [Author Only](#) [Title Only](#) [Author and Title](#)
- Hruz T, Laule O, Szabo G, Wessendorf F, Bleuler S, Oertle L, Widmayer P, Gruissem W, Zimmermann P (2008) Genevestigator V3: A Reference Expression Database for the Meta-Analysis of Transcriptomes. *Adv Bioinformatics* 2008: 420747
Google Scholar: [Author Only](#) [Title Only](#) [Author and Title](#)
- Hu X, Reddy ASN (1997) Cloning and expression of a PR5-like protein from *Arabidopsis*: inhibition of fungal growth by bacterially expressed protein. *Plant Mol Biol* 34: 949–959
Google Scholar: [Author Only](#) [Title Only](#) [Author and Title](#)
- Jakic B, Buszko M, Cappellano G, Wick G (2017) Elevated sodium leads to the increased expression of HSP60 and induces apoptosis in HUVECs. *PloS One* 12(6): e0179383.
Google Scholar: [Author Only](#) [Title Only](#) [Author and Title](#)
- Jaulneau V, Lafitte C, Jacquet C, Fournier S, Salamagne S, Briand X, Esquerré-Tugayé M-T, Dumas B (2010) Ulvan, a sulfated polysaccharide from green algae, activates plant immunity through the jasmonic acid signaling pathway. *J Biomed Biotechnol* 2010: 525291
Google Scholar: [Author Only](#) [Title Only](#) [Author and Title](#)
- John I, Hackett R, Cooper W, Drake R, Farrell A, Grierson D (1997) Cloning and characterization of tomato leaf senescence-related cDNAs. *Plant Mol Biol* 33: 641–651
Google Scholar: [Author Only](#) [Title Only](#) [Author and Title](#)
- Kang Y, Li M, Sinharoy S, Verdier J (2016) A Snapshot of Functional Genetic Studies in *Medicago truncatula*. *Front Plant Sci* 7: 1175
Google Scholar: [Author Only](#) [Title Only](#) [Author and Title](#)
- Koch B, Evans HJ (1966) Reduction of Acetylene to Ethylene by Soybean Root Nodules. *Plant Physiol* 41: 1748–1750
Google Scholar: [Author Only](#) [Title Only](#) [Author and Title](#)
- Krall L, Wiedemann U, Unsin G, Weiss S, Domke N, Baron C (2002) Detergent extraction identifies different VirB protein subassemblies of the type IV secretion machinery in the membranes of *Agrobacterium tumefaciens*. *Proc Natl Acad Sci USA* 99:

11405–11410

Google Scholar: [Author Only](#) [Title Only](#) [Author and Title](#)

Kusch S, Thiery S, Reinstädler A, Gruner K, Zienkiewicz K, Feussner I, Panstruga R (2019) Arabidopsis mlo3 mutant plants exhibit spontaneous callose deposition and signs of early leaf senescence. Plant Mol Biol 101(12): 21–40

Google Scholar: [Author Only](#) [Title Only](#) [Author and Title](#)

Krusell L, Krause K, Ott T, Desbrosses G, Krämer U, Sato S, Nakamura Y, Tabata S, K. James E, Sandal N et al., (2005) The sulfate transporter SST1 is crucial for symbiotic nitrogen fixation in Lotus japonicus root nodules. Plant Cell 17(5): 1625–1636.

Google Scholar: [Author Only](#) [Title Only](#) [Author and Title](#)

Lambert I, Pervent M, Le Queré A, Clément G, Tauzin M, Severac D, Benezech C, Tillard P, Martin-Magniette M-L, Colella S, et al (2020) Responses of mature symbiotic nodules to the whole-plant systemic nitrogen signaling. J Exp Bot 71: 5039–5052

Google Scholar: [Author Only](#) [Title Only](#) [Author and Title](#)

Lee D, Lee G, Kim B, Jang S, Lee Y, Yu Y, Seo J, Kim S, Lee YH, Lee J, et al (2018) Identification of a spotted leaf sheath gene involved in early senescence and defense response in rice. Front Plant Sci 9: 1274

Google Scholar: [Author Only](#) [Title Only](#) [Author and Title](#)

Liu JJ, Ekramoddoullah AKM (2006) The family 10 of plant pathogenesis-related proteins: their structure, regulation, and function in response to biotic and abiotic stresses. Physiol Mol Plant Pathol 68: 3–13

Google Scholar: [Author Only](#) [Title Only](#) [Author and Title](#)

MA H, Ewing J (1986) Acid tolerance in the Rhizobium meliloti – Medicago symbiosis. Aust J Agric. Res 37: 55–64

Google Scholar: [Author Only](#) [Title Only](#) [Author and Title](#)

Ma H, Xiang G, Li Z, Wang Y, Dou M, Su L, Yin X, Liu R, Wang Y, Xu Y (2018) Grapevine 904 VpPR10.1 functions in resistance to Plasmopara viticola through triggering a cell death-like defence response by interacting with VpVDAC3. Plant Biotechnol J 16: 1488–1501

Google Scholar: [Author Only](#) [Title Only](#) [Author and Title](#)

Ma X, Keller B, McDonald BA, Palma-Guerrero J, Wicker T (2018) Comparative transcriptomics reveals how wheat responds to infection by Zymoseptoria tritici. Mol Plant-Microbe Interact 31: 420–431

Google Scholar: [Author Only](#) [Title Only](#) [Author and Title](#)

Malik NSA, Pfeiffer NE, Williams DR, Wagner FW (1981) Peptidohydrolases of soybean root nodules. Plant Physiol 68: 386–392

Google Scholar: [Author Only](#) [Title Only](#) [Author and Title](#)

Martínez M, Cambra I, González-Melendi P, Santamaría ME, Díaz I (2012) C1A cysteine-proteases and their inhibitors in plants. Physiol Plant 145: 85–94

Google Scholar: [Author Only](#) [Title Only](#) [Author and Title](#)

Maunoury N, Redondo-nieto M, Bourcy M, Velde W Van De, Alunni B, Ratet P, Aggerbeck L, Kondorosi E, Mergaert P (2010) Differentiation of symbiotic cells and endosymbionts in Medicago truncatula nodulation are coupled to two transcriptome-switches. PLoS One 5(3): e9519

Google Scholar: [Author Only](#) [Title Only](#) [Author and Title](#)

Mergaert P, Uchiumi T, Alunni B, Evanno G, Cheron A, Catrice O, Mausset A-E, Barloy-Hubler F, Galibert F, Kondorosi A, et al (2006) Eukaryotic control on bacterial cell cycle and differentiation in the Rhizobium–legume symbiosis. Proc Natl Acad Sci USA 103: 5230–5235

Google Scholar: [Author Only](#) [Title Only](#) [Author and Title](#)

Métraux JP, Streit L, Staub T (1988) A pathogenesis-related protein in cucumber is a chitinase. Physiol Mol Plant Pathol 33: 1–9

Google Scholar: [Author Only](#) [Title Only](#) [Author and Title](#)

Oke V, Long SR (1999) Bacteroid formation in the Rhizobium-legume symbiosis. Curr Opin Microbiol 2: 641–646

Google Scholar: [Author Only](#) [Title Only](#) [Author and Title](#)

Oldroyd GED (2013) Speak , friend , and enter : signalling systems that promote beneficial symbiotic associations in plants. Nature 11: 252–263

Google Scholar: [Author Only](#) [Title Only](#) [Author and Title](#)

Paa AS, Bloch CB, Brill WJ (1980) Developmental fate of Rhizobium meliloti bacteroids in alfalfa nodules. J Bacteriol 143: 1480–1490

Google Scholar: [Author Only](#) [Title Only](#) [Author and Title](#)

Patharkar OR, Gassmann W, Walker JC (2017) Leaf shedding as an anti-bacterial defense in Arabidopsis cauline leaves. PLoS Genet 13(12): 849–1584

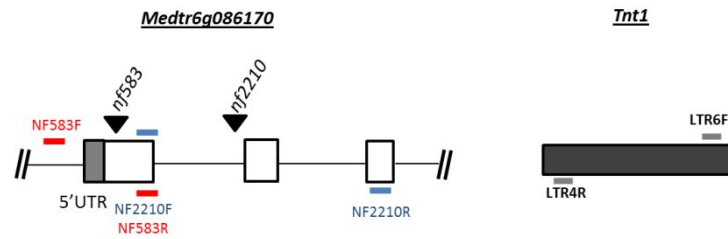
Google Scholar: [Author Only](#) [Title Only](#) [Author and Title](#)

Pérez Guerra JC, Coussens G, De Keyser A, De Rycke R, De Bodt S, Van De Velde W, Goormachtig S, Holsters M (2010)

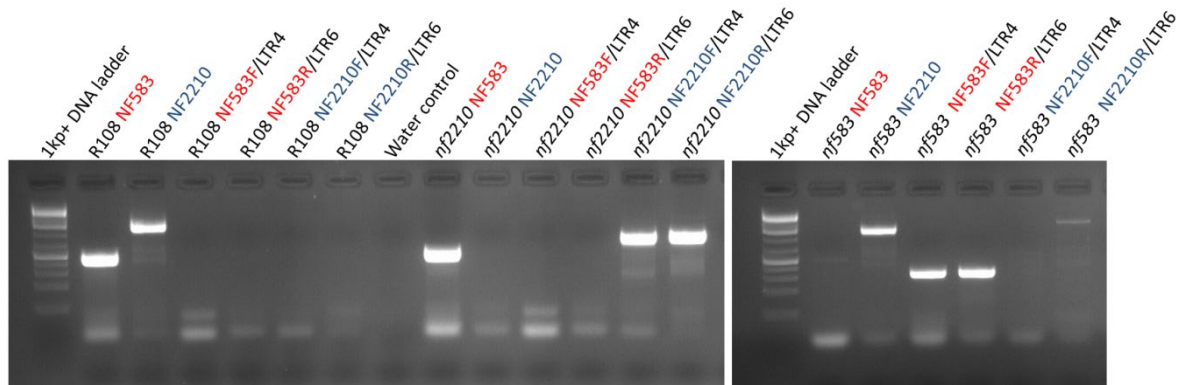
- Comparison of developmental and stress-induced nodule senescence in *Medicago truncatula*.** *Plant Physiol* 152: 1574–1584
Google Scholar: [Author Only](#) [Title Only](#) [Author and Title](#)
- Pierre O, Hopkins J, Combiér M, Baldacci F, Engler G, Brouquisse R, Hérouart D, Boncompagni E (2014) Involvement of papain and legumain proteinase in the senescence process of *Medicago truncatula* nodules.** *New Phytol* 202: 849–863
Google Scholar: [Author Only](#) [Title Only](#) [Author and Title](#)
- Pislariu CI, D. Murray J, Wen J, Cosson V, Muni RRD, Wang M, A. Benedito V, Andriankaja A, Cheng X, Jerez IT, et al (2012) A *Medicago truncatula* tobacco retrotransposon insertion mutant collection with defects in nodule development and symbiotic nitrogen fixation.** *Plant Physiol* 159: 1686–1699
Google Scholar: [Author Only](#) [Title Only](#) [Author and Title](#)
- Pladys D, Vance CP (1993) Proteolysis during development and senescence of effective and plant gene-controlled ineffective alfalfa nodules.** *Plant Physiol* 103: 379–384
Google Scholar: [Author Only](#) [Title Only](#) [Author and Title](#)
- Plet J, Wasson A, Ariel F, Le Signor C, Baker D, Mathesius U, Crespi M, Frugier F (2011) MtCRE1-dependent cytokinin signaling integrates bacterial and plant cues to coordinate symbiotic nodule organogenesis in *Medicago truncatula*.** *Plant J* 65: 622–633
Google Scholar: [Author Only](#) [Title Only](#) [Author and Title](#)
- Schreiber MC, Karlo JC, Kovalick GE (1997) A novel cDNA from *Drosophila* encoding a protein with similarity to mammalian cysteine-rich secretory proteins, wasp venom antigen 5, and plant group 1 pathogenesis-related proteins.** *Gene* 191: 135–141
Google Scholar: [Author Only](#) [Title Only](#) [Author and Title](#)
- Seabra AR, Pereira PA, Becker JD, Carvalho HG (2012) Inhibition of glutamine synthetase by phosphinothricin leads to transcriptome reprogramming in root nodules of *Medicago truncatula*.** *Mol Plant-Microbe Interact* 25: 976–992
Google Scholar: [Author Only](#) [Title Only](#) [Author and Title](#)
- Sels J, Mathys J, De Coninck BMAa, Cammue BPA a, De Bolle MFCC (2008) Plant pathogenesis-related (PR) proteins: a focus on PR peptides.** *Plant Physiol Biochem* 46: 941–50
Google Scholar: [Author Only](#) [Title Only](#) [Author and Title](#)
- Shen Q, Liu L, Wang L, Wang Q (2018) Indole primes plant defense against necrotrophic fungal pathogen infection.** *PLoS One* 13: e0207607
Google Scholar: [Author Only](#) [Title Only](#) [Author and Title](#)
- Sinha M, Singh RP, Kushwaha GS, Iqbal N, Singh A, Kaushik S, Kaur P, Sharma S, Singh TP (2014) Current overview of allergens of plant pathogenesis related protein families.** *Sci World J* 2014: 543195
Google Scholar: [Author Only](#) [Title Only](#) [Author and Title](#)
- Sinharoy S, Torres-Jerez I, Bandyopadhyay K, Kereszt A, Pislariu CI, Nakashima J, Benedito VA, Kondorosi E, Udvardi MK (2013) The C2H2 transcription factor regulator of symbiosome differentiation represses transcription of the secretory pathway gene VAMP721a and promotes symbiosome development in *Medicago truncatula*.** *Plant Cell* 25: 3584–3601
Google Scholar: [Author Only](#) [Title Only](#) [Author and Title](#)
- Stintzi A, Heitz T, Prasad V, Wiedemann-Merdinoglu S, Kauffmann S, Geoffroy P, Legrand M, Fritig B (1993) Plant "pathogenesis-related" proteins and their role in defense against pathogens.** *Biochimie* 75: 687–706
Google Scholar: [Author Only](#) [Title Only](#) [Author and Title](#)
- Tadege M, Wen J, He J, Tu H, Kwak Y, Eschstruth A, Cayrel A, Endre G, Zhao PX, Chabaud M, et al (2008) Large-scale insertional mutagenesis using the Tnt1 retrotransposon in the model legume *Medicago truncatula*.** *Plant J* 54: 335–347
Google Scholar: [Author Only](#) [Title Only](#) [Author and Title](#)
- Tang F, Yang S, Liu J, Zhu H (2016) Rj4, a gene controlling nodulation specificity in soybeans, encodes a thaumatin-like protein but not the one previously reported.** *Plant Physiol* 170: 26–32
Google Scholar: [Author Only](#) [Title Only](#) [Author and Title](#)
- Van de Velde W, Guerra JCP, De Keyser A, De Rycke R, Rombauts S, Maunoury N, Mergaert P, Kondorosi E, Holsters M, Goormachtig S (2006) Aging in legume symbiosis. A molecular view on nodule senescence in *Medicago truncatula*.** *Plant Physiol* 141: 711–720
Google Scholar: [Author Only](#) [Title Only](#) [Author and Title](#)
- Van de Velde W, Zehirov G, Szatmari A, Debreczeny M, Ishihara H, Kevei Z, Farkas A, Mikulass K, Nagy A, Tiricz H, et al (2010) Plant peptides govern terminal differentiation of bacteria in symbiosis.** *Science* 327: 1122–1126
Google Scholar: [Author Only](#) [Title Only](#) [Author and Title](#)
- van Loon LC, Rep M, Pieterse CMJ (2006) Significance of inducible defense-related proteins in infected plants.** *Annu Rev Phytopathol* 44: 135–162
Google Scholar: [Author Only](#) [Title Only](#) [Author and Title](#)

- Walter MH, Liu JW, Wünn J, Hess D (1996) Bean ribonuclease-like pathogenesis-related protein genes (Ypr10) display complex patterns of developmental, dark-induced and exogenous-stimulus-dependent expression. *Eur J Biochem* 239: 281–293
Google Scholar: [Author Only](#) [Title Only](#) [Author and Title](#)
- Walton JH, Kontra-Kováts G, Green RT, Domonkos Á, Horváth B, Brear EM, Franceschetti M, Kaló P, Balk J (2020) The *Medicago truncatula* vacuolar iron transporter-like proteins VTL4 and VTL8 deliver iron to symbiotic bacteria at different stages of the infection process. *New Phytol* 228: 651–666
Google Scholar: [Author Only](#) [Title Only](#) [Author and Title](#)
- Wang C, Yu H, Luo L, Duan L, Cai L, He X, Wen J, Mysore KS, Li G, Xiao A, et al (2016) NODULES WITH ACTIVATED DEFENSE 1 is required for maintenance of rhizobial endosymbiosis in *Medicago truncatula*. *New Phytol* 212: 176–191
Google Scholar: [Author Only](#) [Title Only](#) [Author and Title](#)
- Wang X, Tang C, Deng L, Cai G, Liu X, Liu B, Han Q (2010) Characterization of a pathogenesis-related thaumatin-like protein gene TaPR5 from wheat induced by stripe rust. *Physiol Plant* 139: 27–38
Google Scholar: [Author Only](#) [Title Only](#) [Author and Title](#)
- Wingler A, Brownhill E, Pourtau N (2005) Mechanisms of the light-dependent induction of cell death in tobacco plants with delayed senescence. *J Exp Bot* 56: 2897–2905
Google Scholar: [Author Only](#) [Title Only](#) [Author and Title](#)
- Wyk SG Van, Plessis M Du, Cullis CA, Kunert KJ, Vorster BJ (2014) Cysteine protease and cystatin expression and activity during soybean nodule development and senescence. *BMC Plant Biol* 14: 1–13
Google Scholar: [Author Only](#) [Title Only](#) [Author and Title](#)
- Yarce JCS, Lee HK, Tadege M, Ratet P, Mysore KS (2013) Forward genetics screening of *Medicago truncatula* Tnt1 insertion lines. *Methods Mol Biol* 1069: 93–100
Google Scholar: [Author Only](#) [Title Only](#) [Author and Title](#)
- Yasuda M, Miwa H, Masuda S, Takebayashi Y, Sakakibara H, Okazaki S (2016) Effector-triggered immunity determines host genotype-specific incompatibility in legume-rhizobium symbiosis. *Plant Cell Physiol* 57: 1791–1800
Google Scholar: [Author Only](#) [Title Only](#) [Author and Title](#)
- Yu H, Xiao A, Dong R, Fan Y, Zhang X, Liu C, Wang C, Zhu H, Duanmu D, Cao Y, et al (2018) Suppression of innate immunity mediated by the CDPK-Rboh complex is required for rhizobial colonization in *Medicago truncatula* nodules. *New Phytol* 220: 425–434
Google Scholar: [Author Only](#) [Title Only](#) [Author and Title](#)
- Zhang H, Dugé de Bernonville T, Body M, Glevarec G, Reichelt M, Unsicker S, Bruneau M, Renou JP, Huguet E, Dubreuil G, et al (2016) Leaf-mining by *Phyllonorycter blancardella* reprograms the host-leaf transcriptome to modulate phytohormones associated with nutrient mobilization and plant defense. *J Insect Physiol* 84: 114–127
Google Scholar: [Author Only](#) [Title Only](#) [Author and Title](#)
- Zhang Y, Wang H-L, Li Z, Guo H (2020) Genetic Network between leaf senescence and plant immunity: crucial regulatory nodes and new insights. *Plants(Basel)* 9(4): 495
Google Scholar: [Author Only](#) [Title Only](#) [Author and Title](#)
- Zimmerman JL, Szeto WW, Ausubel FM (1983) Molecular characterization of Tn5-induced symbiotic (Fix-) mutants of *Rhizobium meliloti*. *J Bacteriol* 156: 1025–1034
Google Scholar: [Author Only](#) [Title Only](#) [Author and Title](#)

A

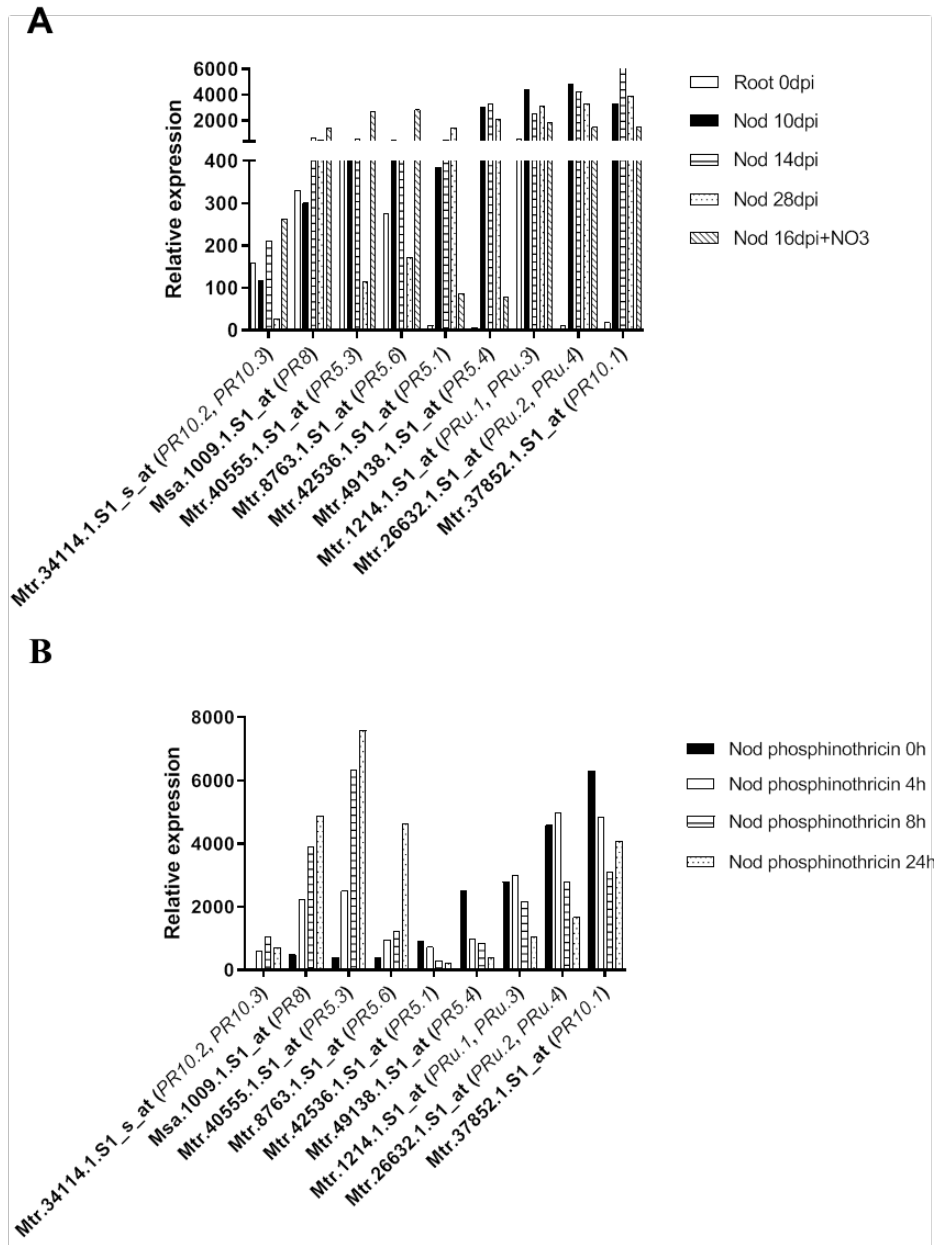


B



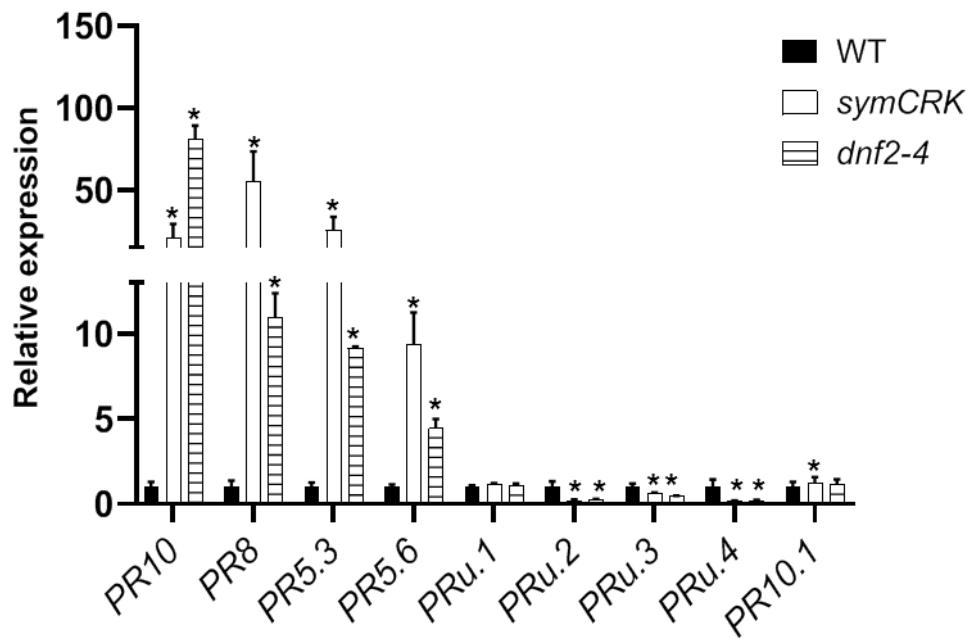
Supplemental Figure S1. PCR genotyping of the *Tnt1* insertion in *nf583* and *nf2210*

(A) Location of the primers used for the genotyping of *Medtr6g086170* and *Tnt1* sequences.
(B) PCR products generated in WT (R108), *nf583*, *nf2210* using different combination of primers. The primers colored in blue and red are respectively used for the genotyping of the *Tnt1* insertion in *nf2210* and *nf583* background. The primers colored in grey recognize the *Tnt1* sequence.



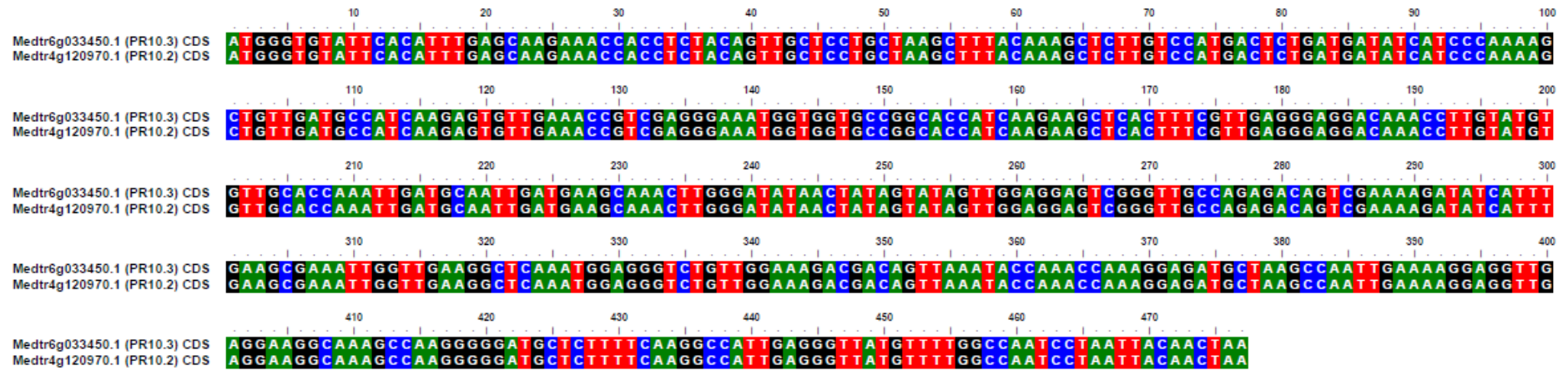
Supplemental Figure S2. Expression patterns of *PR* candidate genes in wild-type nodules in response to nitrate and phosphinothricin.

(A) Expression patterns of *PR* candidate genes for defense studies in *Medicago* roots (0-dpi (day post-inoculation) or nodules (10, 14 or 28-dpi) inoculated with *S. meliloti* or in 16-dpi nodules treated with nitrate (KNO₃, Benedito et al., 2008). (B) Expression of *PR* candidates in nodules of plants at 0, 4, 8 and 24 h after treatment with inhibitor of glutamine synthase, the phosphinothricin [0.25 mM] (Seabra et al., 2012). Expression profiles are based on data available on the *MtGEA* database (<https://medicago.toulouse.inrae.fr/MtExpress>, Noble Research Institute). Relative expression corresponds to mean signal of cDNA hybridization on the microarray for three independent experiments.

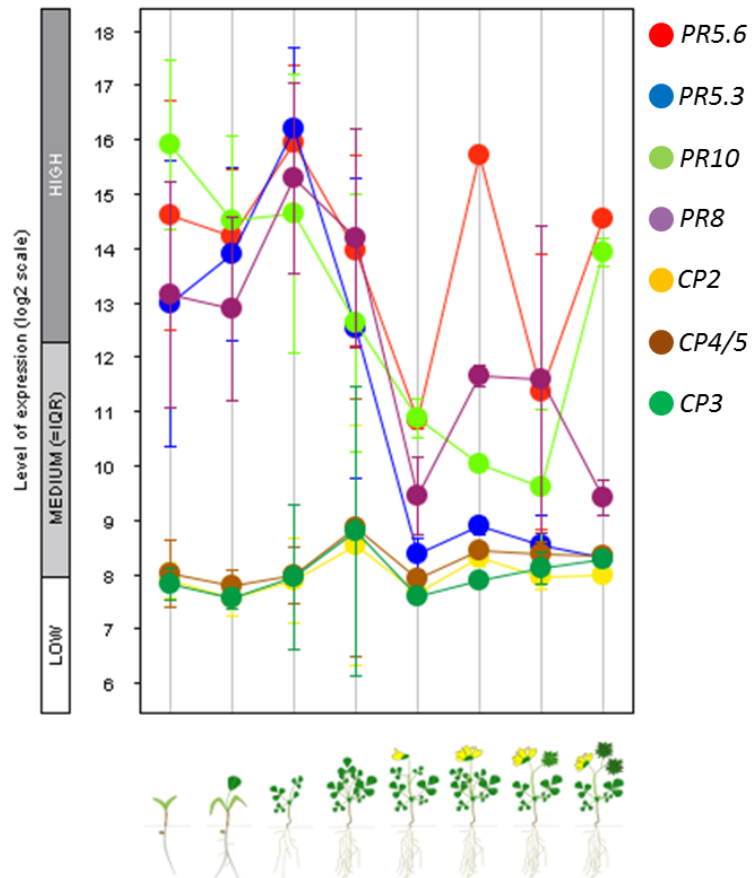


Supplemental Figure S3. Validation by RT-qPCR analysis of 10 *PR* genes selected for defense monitoring in the *Medicago* nodules.

Expression analysis in WT, *symCRK* and *dnf2-4* was done on 21-dpi (day post-inoculation) nodules from plants cultivated *in vitro*. *PRu*: unclassified in a PR group. Error bars show the standard error (SE) and the asterisks represent significant variation (p-value < 2.5%) compared to the WT using Man & Whitney statistical test. The RT-qPCR analyses were made on plants from three biological repetitions (16 plants per repetition) with two technical replicates.

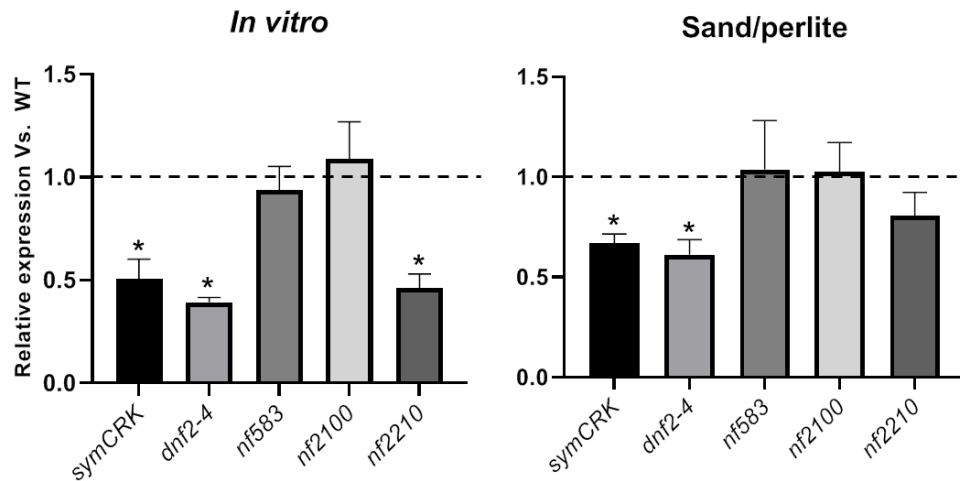


Supplemental Figure S4. Comparison of CDS sequences between *PR10.2* (*Medtr4g120970.1*) and *PR10.3* (*Medtr6g033450.1*).
 Sequence alignment was realized using ClustalW method on Bioedit tool (<https://bioedit.software.informer.com>).



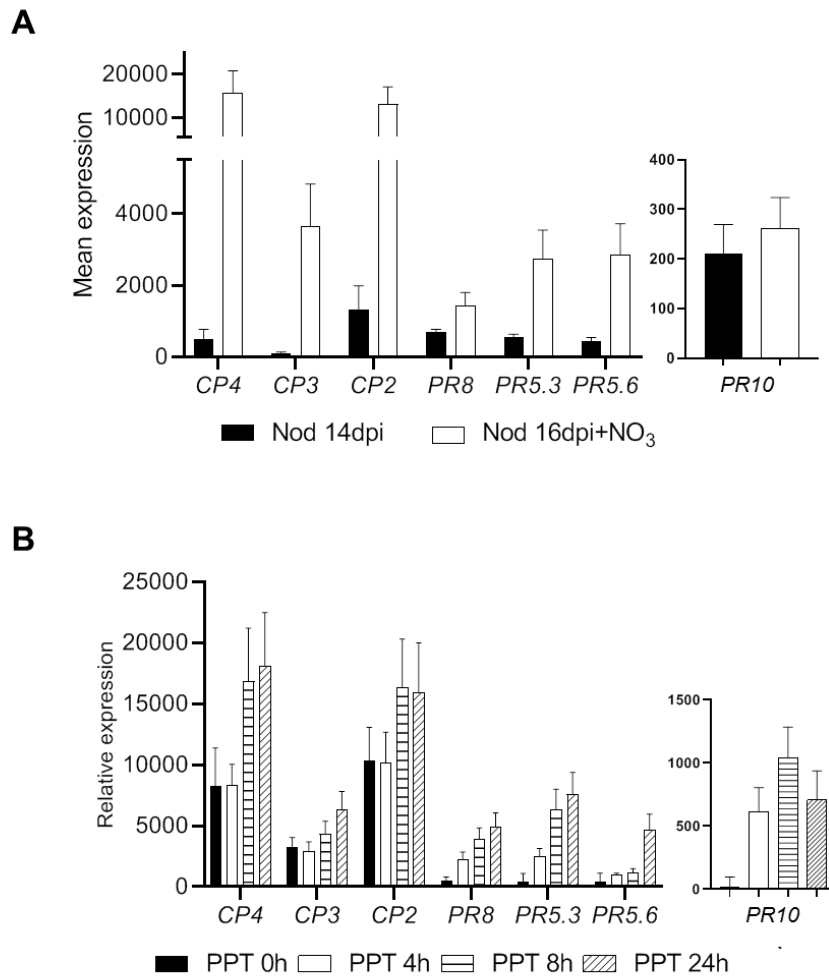
Supplemental Figure S5. Expression analyses of *PRs* and *CPs* during the development of *Medicago*.

The results show log₂ of the expression level in eight developmental stages. The results were generated using the Genevestigator database (<https://genevestigator.com/>). Error bars show the SE of three independent experiments.



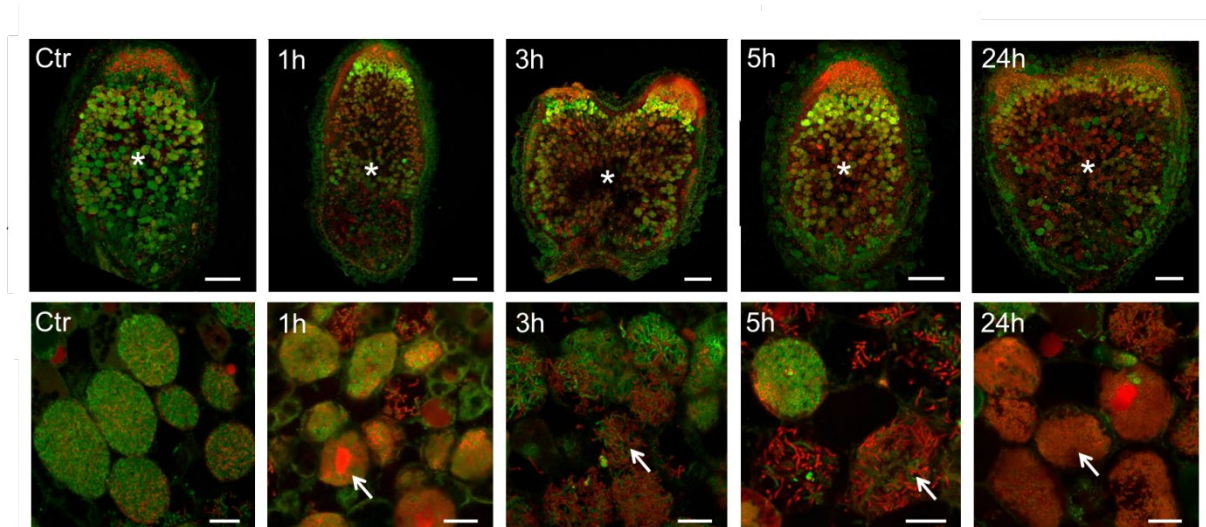
Supplemental Figure S6. Expression pattern of *PHYCYST5* in *Medicago* fix- nodules mutants in response to different environmental conditions.

Expression analysis of the *PHYCYST5* in fix- nodules mutants cultivated *in vitro* and in sand/perlite. The expression was measured using RT-qPCR and the results show mean variation in mutants compared to the WT. The RT-qPCR analyses were made on plants from three biological repetitions (16 plants per repetition) with two technical replicates. Error bars show the SE and the asterisks represent significant variation (p-value < 2.5%) compared to the WT using Man & Whitney statistical test. The dotted lines represent the expression level of the WT.



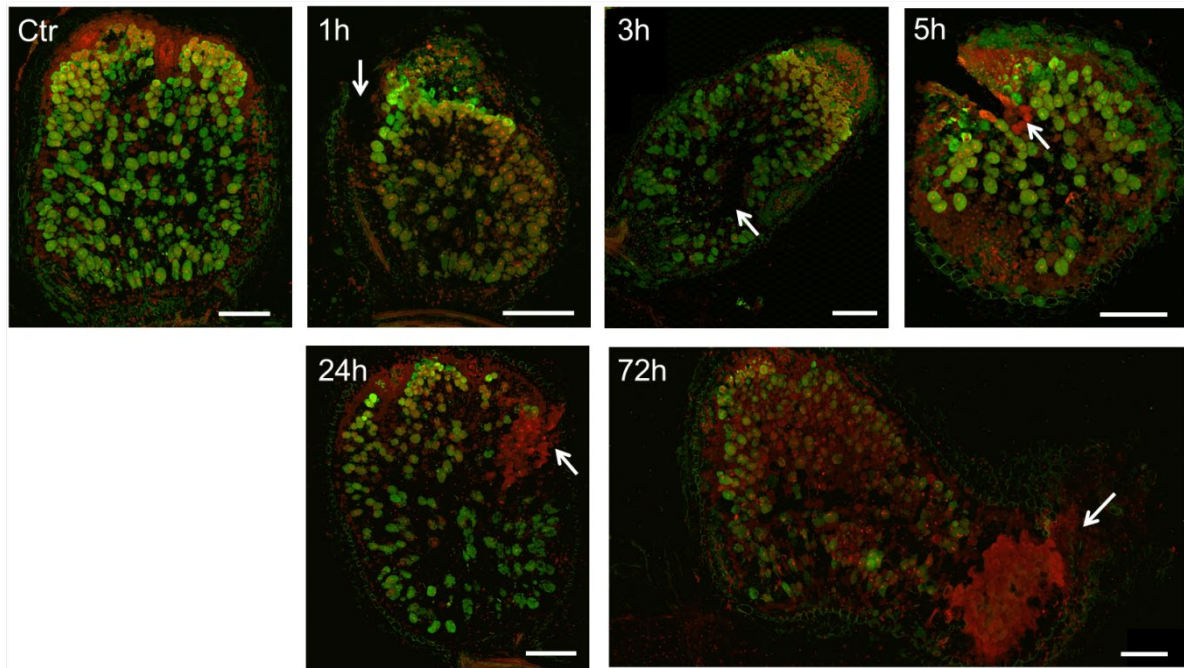
Supplemental Figure S7. Expression pattern of senescence and defense markers in Medicago wild-type nodules in response to nitrate and phosphinothricin treatments.

Expression pattern of senescence (*CP4*, *CP3* and *CP2*) and defense (*PR8*, *PR10*, *PR5.3* and *PR5.6*) markers in untreated (14-dpi) or treated (16-dpi) nodules with nitrate (A, Benedito et al., 2008) or nodules from plants incubated 0, 4, 8, 24h with the inhibitor of glutamine synthase, the phosphinothricin at [0.25 mM] (B, Seabra et al., 2012). Error bars represent SE of three independent experiments. Expression data are provided by *MtGEA* database (<https://medicago.toulouse.inrae.fr/MtExpress>, Noble Research Institute). Relative expression corresponds to mean signal of cDNA hybridization on the microarray.



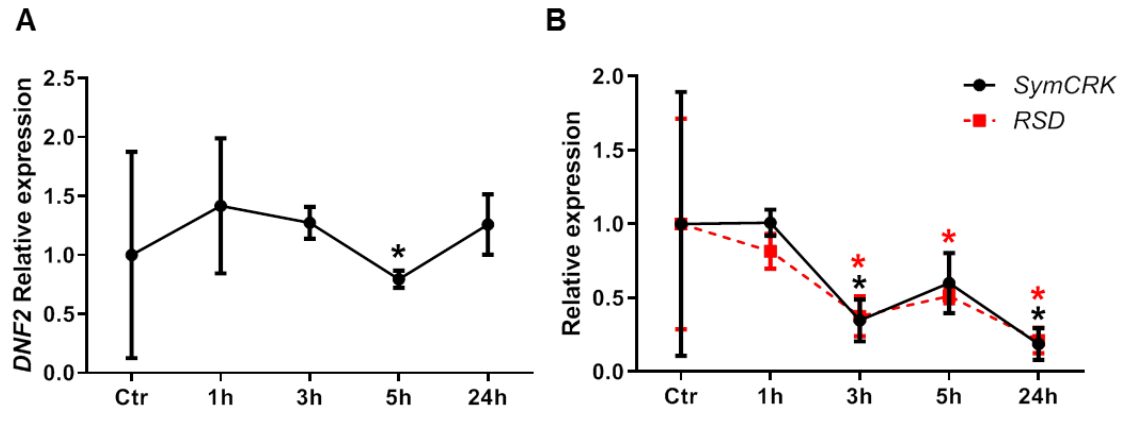
Supplemental Figure S8. Live and dead staining of wild-type inoculated nodules separated from the roots.

Live and dead staining of 21-dpi nodule sections obtained from the WT inoculated with *S. medicae* WSM419. The nodules were separated from the root and incubated 0 (Ctr), 1, 3, 5 and 24h. Top panel displays the nodule sections (scale bars = 200 μ m) and bottom panel shows the bacteroids in the fixation zone III (scale bars = 20 μ m). Asterisk indicates the zone III and the arrows show dead bacteroids. This figure shows the complete image panel corresponding to the experiment of the figure 5D.



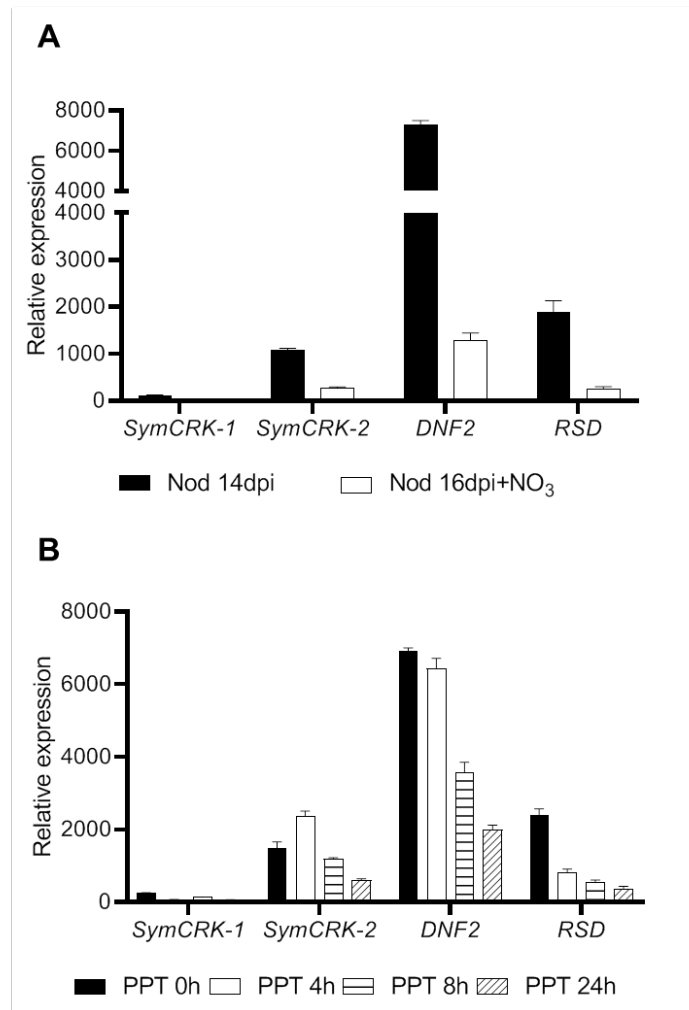
Supplemental Figure S9. Live and dead staining of Medicago wild-type inoculated nodules attached to the roots.

Live and dead staining of 21-dpi nodule sections obtained from the WT inoculated with *S. medicae* WSM419. The nodules tethered to roots were snipped and the nodulated plants were incubated 0 (Ctr), 1, 3, 5 24 and 72h. Scale bars = 250 μ m. The arrows show the snipped zone of the nodules. This figure shows the complete image panel corresponding to the experiment of the figure 5H.



Supplemental Figure S10. Expression pattern of *DNF2*, *SymCRK* and *RSD* in *Medicago* wild-type nodules in response to wounding.

(A) *DNF2*, (B) *SymCRK/RSD* expression 0 (Ctr), 1, 3, 5 and 24h after wounding evaluated using RT-qPCR in 21-dpi WT nodules isolated from plants cultivated *in vitro* and inoculated with *S. medicae* WSM419. The results show mean expression of three independent experiments (16 plants per experiment) with two technical replicates. Error bars show SE and the asterisks represent significant variation using Mann & Whitney statistical test (p-value < 2.5%).



Supplemental Figure S11. Expression pattern of *DNF2*, *SymCRK* and *RSD* in Medicago wild-type nodules in response to nitrate and phosphinothricin treatments.

Expression patterns of *DNF2*, *SymCRK* and *RSD* in 16-dpi nodules treated or not with nitrate (A, Benedito et al., 2008) or from nodulated plants incubated 0, 4, 8 and 24 hours with the inhibitor of glutamine synthase, the phosphinothricin at [0.25 mM] (B, Seabra et al., 2012). Expression data are provided by the *MtGEA* database (<https://medicago.toulouse.inrae.fr/MtExpress>, Noble Research Institute, Benedito et al., 2008). Two probsets annotated *SymCRK-1*, *SymCRK-2* recognized *SymCRK* in the database. Relative expression corresponds to mean signal of cDNA hybridization on the microarray. Error bars show SE for three independent experiments.

Supplemental Table S1. List of *nf583*, *nf2210* and *nf2100* genes showing FSTs.

The genes with high confidence FST located in the ORFs were selected. For each mutant line, the tagged genes, the protein annotation, the probset ID on MtAffymV4 and the expression of the genes in the roots and the nodules of *M. truncatula*, are listed. FSTs and expression data are provided respectively by the Medicago *Tnt1* mutant database and Genevestigator. ND: not determined.

FST NF2210

Data download from Genvestigator		Number of samples	roots 242	nodules 40
GENE ID Mt4.OV1	Protein annotation	Probeset ID	Mean Expression roots	Mean expression nodules
<u>Medtr6g086170</u>	<u>SULFATE TRANSPORTER 3.5-RELATED</u>	<u>Mtr.37708.1.S1_at</u>	<u>15000.42</u>	<u>106081.77</u>
Medtr4g023030	AXI 1 PROTEIN-LIKE PROTEIN	Mtr.14950.1.S1_s_at/ Mtr.10701.1.S1_at	14257.89	14615.44
Medtr5g080390	PUMILIO HOMOLOG 1-RELATED	Mtr.49129.1.S1_s_at	10683.95	13478.64
Medtr5g081960	TRANSFERASE FAMILY (TRANSFERASE)	Mtr.34637.1.S1_at	24149.3	12771
Medtr7g013100	DIHYDROLIPOAMIDE ACETYL/SUCCINYL-TRANSFERASE-RELATED	Mtr.48448.1.S1_at	6924.38	4105.86
Medtr3g079310	BCDNA.GH11111	Mtr.20789.1.S1_at/ Mtr.20787.1.S1_at	4200.64	3629.64
Medtr1g026910	ATP-DEPENDENT PROTEASE CEREBLON	Mtr.39899.1.S1_at	6445.42	2737.87
Medtr1g099290	CHITINASE	Mtr.5384.1.S1_at	3473.9	2621.77
Medtr1g098580	UNKOWN	Mtr.15307.1.S1_at	7399.5	1810.58
Medtr4g066170	PROTEIN C13C4.8	Mtr.37362.1.S1_at/ Msa.1690.1.S1_at	2439.52	1302.47
Medtr1g076720	PANTOTHENATE KINASE	Mtr.6707.1.S1_s_at	1441.21	655.64
Medtr3g080190	ENDOGLUCANASE 11	ND	903.39	594.58
Medtr3g071860	SNF2 DOMAIN-CONTAINING PROTEIN CLASSY 1-RELATED	Mtr.21259.1.S1_at	192.46	234.85
Medtr2g008100	HISTIDINE DECARBOXYLASE / L-HISTIDINE CARBOXY-LYASE	Mtr.22597.1.S1_s_at	204.64	198.11
Medtr1g021520	TRANSCRIPTION REPRESSOR KAN1-RELATED	ND	ND	ND
Medtr1g021965	UNKOWN	ND	ND	ND
Medtr2g015660	UNKOWN	ND	ND	ND
Medtr3g031400	GLUCOSYL/GLUCURONOSYL TRANSFERASES	ND	ND	ND
Medtr3g108080	EMBRYO DEFECTIVE 2410	ND	ND	ND

	PROTEIN			
Medtr3g115650	COILED-COIL DOMAIN-CONTAINING PROTEIN 115	ND	ND	ND
Medtr4g008600	F-BOX/LEUCINE RICH REPEAT PROTEIN	ND	ND	ND
Medtr4g074200	DNA REPAIR PROTEIN XRCC2 HOMOLOG	ND	ND	ND
Medtr5g034370	PLANT PROTEIN OF UNKNOWN FUNCTION (DUF936) (DUF936)	ND	ND	ND
Medtr5g064800	F10B6.4	ND	ND	ND
Medtr5g094810	XENOBIOTIC-TRANSPORTING ATPASE / STEROID-TRANSPORTING ATPASE	ND	ND	ND
Medtr6g035310	UNKOWN	ND	ND	ND
Medtr6g075460	CYCLIC NUCLEOTIDE-GATED ION CHANNEL 19-RELATED	ND	ND	ND
Medtr6g078200	GLUCAN ENDO-1,3-BETA-D-GLUCOSIDASE / LAMINARINASE	ND	ND	ND

FST NF2210

Data download from Genvestigator		Number of samples	roots 242	nodules 40
GENE ID Mt4.0V1	Protein annotation	Probeset ID	Mean Expression roots	Mean expression nodules
<u>Medtr6g086170</u>	<u>SULFATE TRANSPORTER 3.5-RELATED</u>	<u>Mtr.37708.1.S1_at</u>	<u>15000.42</u>	<u>106081.77</u>
Medtr4g050480	PROTEIN IQ-DOMAIN 15-RELATED	Mtr.9374.1.S1_at	34073.8	23460.03
Medtr2g078730	D-AMINO-ACID TRANSAMINASE / D-ASPARTIC AMINOTRANSFERASE	Mtr.37617.1.S1_at	42933.99	22789.97
Medtr2g097670	PUMILIO HOMOLOG 1-RELATED	Mtr.41554.1.S1_at	32940.93	22371.37
Medtr3g074930	ACID PHOSPHATASE RELATED	Mtr.37882.1.S1_at	55444.41	20026.37
Medtr7g029105	UNKOWN	Mtr.45095.1.S1_at	4669.28	4064.76
Medtr6g005390	CBIX (CBIX)	Mtr.5349.1.S1_s_at	4996.46	2072.69
Medtr1g100627	ARM REPEAT SUPERFAMILY PROTEIN-RELATED	Mtr.11503.1.S1_at	28521.97	1712.62
Medtr5g019050	LYSM DOMAIN RECEPTOR-LIKE KINASE 4	Mtr.15787.1.S1_at	3488.11	1449.09
Medtr8g018280	NB-ARC DOMAIN (NB-ARC) // LEUCINE RICH REPEAT	Mtr.46816.1.S1_at	1938.7	981.27
Medtr4g127420	CCT MOTIF (CCT) PROTEIN	Mtr.13254.1.S1_at	882.13	783.93
Medtr5g096200	OLIGOPEPTIDE TRANSPORTER 1-RELATED	Mtr.29264.1.S1_at	694.87	709.75
Medtr5g015170	SF7 - ACR1	Mtr.5494.1.S1_at	428.1	665.88
Medtr8g013610	G-TYPE LECTIN S-RECEPTOR-LIKE SERINE/THREONINE-PROTEIN KINASE SD1-13	Mtr.50504.1.S1_at	2181.7	620.83

Medtr1g069325	KETOHEXOKINASE / HEPATIC FRUCTOKINASE	Mtr.13302.1.S1_at	793.98	477.78
Medtr4g130580	UNKOWN	Mtr.26057.1.S1_at	447.7	463.91
Medtr5g016830	FILAMENT-LIKE PLANT PROTEIN 7	Mtr.11295.1.S1_at	1768.18	431.89
Medtr5g034180	UNKOWN	Mtr.2095.1.S1_at	451.99	401.15
Medtr2g067440	PEROXIDASE / LACTOPEROXIDASE	Mtr.32452.1.S1_at	353.79	289.18
Medtr8g068050	PROTEIN KINASE DOMAIN (PKINASE) // LEGUME LECTIN DOMAIN	Mtr.46816.1.S1_at	1652.28	272.83
Medtr8g018450	LINOLEATE 9S-LIPOXYGENASE / LINOLEATE 9-LIPOXYGENASE	Mtr.24264.1.S1_at	558.91	238.26
Medtr4g102310	CYTOCHROME P450 - LIKE PROTEIN-RELATED	Mtr.38814.1.S1_at	5680.79	209.27
Medtr3g114920	HIGH MOBILITY GROUP B PROTEIN 10-RELATED	Mtr.27853.1.S1_at	207.47	202.83
Medtr5g020900	UNKOWN	Mtr.25509.1.S1_at	193.11	196.59
Medtr4g005270	<u>BETA-AMYRIN SYNTHASE / 2,3-OXIDOSQUALENE BETA-AMYRIN CYCLASE</u>	Mtr.31948.1.S1_at	485.49	195.08
Medtr8g093920	NUCLEAR TRANSCRIPTION FACTOR Y SUBUNIT B-7	Mtr.46490.1.S1_at	187.93	193.04
Medtr1g017790	UNKOWN	ND	ND	ND
Medtr1g017795	UNKOWN	ND	ND	ND
Medtr1g036430	OLYADENYLATE-BINDING PROTEIN (RRM SUPERFAMILY) // SPLICING FACTOR 3B, SUBUNIT 4	ND	ND	ND
Medtr1g106975	PUMILIO HOMOLOG 14-RELATED	ND	ND	ND
Medtr2g062310	DOMAIN OF UNKNOWN FUNCTION (DUF966) (DUF966)	ND	ND	ND
Medtr2g067360	UNKOWN	ND	ND	ND
Medtr2g067450	PEROXIDASE / LACTOPEROXIDASE	ND	ND	ND
Medtr2g083030	OXIDOREDUCTASE, 2OG-FE II OXYGENASE FAMILY	ND	ND	ND
Medtr2g089755	TRANSFERASE FAMILY (TRANSFERASE)	ND	ND	ND
Medtr4g081490	ORGANIC CATION/CARNITINE TRANSPORTER 4	ND	ND	ND
Medtr4g087920	STEROL REGULATORY ELEMENT-BINDING PROTEIN	ND	ND	ND
Medtr4g104690	CDP-GLYCEROL DIPHOSPHATASE / CDP-GLYCEROL PYROPHOSPHATASE	ND	ND	ND
Medtr5g076060	UNCHARACTERIZED CONSERVED PROTEIN	ND	ND	ND
Medtr5g083890	F-BOX DOMAIN (F-BOX) // LEUCINE RICH REPEAT (LRR_2)	ND	ND	ND
Medtr6g015000	UDP-GLUCOSE/GDP-MANNOSE DEHYDROGENASE FAMILY, NAD BINDING DOMAIN	ND	ND	ND

Medtr6g032965	3-KETOACYL-COA SYNTHASE 17-RELATED	ND	ND	ND
Medtr6g043850	SF16 - F14O23.23 PROTEIN	ND	ND	ND
Medtr6g061110	GPI16 SUBUNIT, GPI TRANSAMIDASE COMPONENT (GPI16)	ND	ND	ND
Medtr6g065190	PPR REPEAT (PPR) // PPR REPEAT (PPR_1)	ND	ND	ND
Medtr6g082770	UNKOWN	ND	ND	ND
Medtr6g088240	ELONGATION FACTOR TS	ND	ND	ND
Medtr7g066100	F-BOX DOMAIN (F-BOX) // F-BOX ASSOCIATED (FBA_1)	ND	ND	ND
Medtr7g073980	BTB/POZ DOMAIN (BTB) // NPH3 FAMILY (NPH3)	ND	ND	ND
Medtr8g006470	DUO POLLEN 1	ND	ND	ND
Medtr8g008550	UNKOWN	ND	ND	ND
Medtr8g042520	PEPTIDE EXPORTER, ABC SUPERFAMILY	ND	ND	ND

FST NF2100

Data download from Genvestigator		Number of samples	roots 242	nodules 40
GENE ID Mt4.0V1	Protein annotation	Probeset ID	Mean Expression roots	Mean expression nodules
Medtr7g050980	PECTINESTERASE-RELATED PROTEIN-RELATED	Mtr.8508.1.S1_at	85331,41	11474,21
Medtr4g005730	SERINE/THREONINE-PROTEIN KINASE OSR1	Mtr.31949.1.S1_at/ Mtr.28731.1.S1_at	3003,75	1124,01
Medtr3g014060	14-3-3-Like Protein Gf14 Lambda	Mtr.15400.1.S1_at	350,33	302,48
Medtr4g005270	BETA-AMYRIN SYNTHASE / 2,3-OXIDOSQUALENE BETA-AMYRIN CYCLASE	Mtr.31948.1.S1_at	485,59	195,08
Medtr5g021920	F-BOX DOMAIN (F-BOX)	ND	ND	ND

Supplemental Table S2. List of the identified *PR* genes in the *M. truncatula* genome.

Unclassified *PR* corresponds to PR without defined classes.

V4 Medicago Genome ID	Probeset V4 affymetrix	Predicted domain	Classe
Medtr2g010670.1	Mtr.34477.1.S1_at	CAP, CYSTEINE-RICH SECRETORY PROTEIN, ANTIGEN 5	PR1
Medtr2g435490.1	Mtr.31096.1.S1_at	CAP, CYSTEINE-RICH SECRETORY PROTEIN, ANTIGEN 5	PR1
Medtr2g010600.1	Mtr.8977.1.S1_at	CAP, CYSTEINE-RICH SECRETORY PROTEIN, ANTIGEN 5	PR1
Medtr2g012370.1	Mtr.8977.1.S1_at	CAP, CYSTEINE-RICH SECRETORY PROTEIN, ANTIGEN 5	PR1
Medtr2g010650.1	Msa.3171.1.S1_at	CAP, CYSTEINE-RICH SECRETORY PROTEIN, ANTIGEN 5	PR1
Medtr5g018755.1	Mtr.25125.1.S1_at	CAP, CYSTEINE-RICH SECRETORY PROTEIN, ANTIGEN 5	PR1
Medtr8g078770.1	Mtr.5901.1.S1_at	CAP, CYSTEINE-RICH SECRETORY PROTEIN, ANTIGEN 5	PR1
Medtr5g018770.1	Mtr.82.1.S1_at	CAP, CYSTEINE-RICH SECRETORY PROTEIN, ANTIGEN 5	PR1
Medtr4g050762.1	Mtr.8977.1.S1_at	CAP, CYSTEINE-RICH SECRETORY PROTEIN, ANTIGEN 5	PR1
Medtr2g010610.1	Mtr.8977.1.S1_at	CAP, CYSTEINE-RICH SECRETORY PROTEIN, ANTIGEN 5	PR1
Medtr2g010630.1	Mtr.8977.1.S1_at	CAP, CYSTEINE-RICH SECRETORY PROTEIN, ANTIGEN 5	PR1
Medtr2g010690.1	Mtr.34477.1.S1_at	CAP, CYSTEINE-RICH SECRETORY PROTEIN, ANTIGEN 5	PR1
Medtr2g010700.1	Mtr.34477.1.S1_at	CAP, CYSTEINE-RICH SECRETORY PROTEIN, ANTIGEN 5	PR1
Medtr2g010640.1	Mtr.34477.1.S1_at	CAP, CYSTEINE-RICH SECRETORY PROTEIN, ANTIGEN 5	PR1
Medtr2g010590.1	Msa.3171.1.S1_at	CAP, CYSTEINE-RICH SECRETORY PROTEIN, ANTIGEN 5	PR1
Medtr5g018750.1	Mtr.81.1.S1_at	CAP, CYSTEINE-RICH SECRETORY PROTEIN, ANTIGEN 5	PR1
Medtr8g045490.1	Mtr.10361.1.S1_at	BET_V_1	PR10
Medtr8g045640.1	Mtr.10363.1.S1_x_at	BET_V_1	PR10
Medtr8g045400.1	Mtr.10364.1.S1_at	BET_V_1	PR10
Medtr4g120760.1	Mtr.12615.1.S1_at	BET_V1-LIKE	PR10
Medtr4g120970.1	Mtr.34114.1.S1_s_at	BET_V1-LIKE	PR10
Medtr6g033450.1	Mtr.34114.1.S1_s_	BET_V1-LIKE	PR10

	at		
Medtr1g030810.1	Mtr.3416.1.S1_at	BET_V1-LIKE	PR10
Medtr4g120950.1	Mtr.37852.1.S1_at	BET_V1-LIKE	PR10
Medtr8g045570.1	Mtr.38110.1.S1_at	BET_V1-LIKE	PR10
Medtr8g045665.1	Mtr.40102.1.S1_at	BET_V1-LIKE	PR10
Medtr8g045520.1	Mtr.40106.1.S1_s_ at	BET_V1-LIKE	PR10
Medtr3g055120.1	Mtr.43078.1.S1_at/ Mtr.43078.1.S1_s_ at	BET_V1-LIKE	PR10
Medtr2g435310.1	Mtr.12615.1.S1_at	BET_V1-LIKE	PR10
Medtr8g045560.1	Msa.1635.1.S1_at	BET_V1-LIKE	PR10
Medtr4g120940	Not determined	SRPBCC SUPER FAMILY	PR10
Medtr8g045555	Mtr.40109.1.S1_at	SRPBCC SUPERFAMILY	PR10
Medtr1g031640	Mtr.45999.1.S1_at	SRPBCC SUPERFAMILY	PR10
Medtr8g045555.1	Mtr.40109.1.S1_at	BET_V1-LIKE	PR10
Medtr8g045735.1	Msa.1635.1.S1_at	BET_V1-LIKE	PR10
Medtr8g045300.1	Mtr.45935.1.S1_at	BET_V1-LIKE	PR10
Medtr8g045695.1	Msa.1635.1.S1_at	BET_V1-LIKE	PR10
Medtr4g120940.1	Mtr.34114.1.S1_s_ at	BET_V1-LIKE	PR10
Medtr2g035220.1	Mtr.10317.1.S1_at/ Msa.3122.1.S1_at	BET_V1-LIKE	PR10
Medtr2g035210.1	Msa.3122.1.S1_at	BET_V1-LIKE	PR10
Medtr2g035190.1	Msa.3122.1.S1_at	BET_V1-LIKE	PR10
Medtr2g035320.1	Msa.3122.1.S1_at	BET_V1-LIKE	PR10
Medtr2g035320.2	Msa.3122.1.S1_at	BET_V1-LIKE	PR10
Medtr1g030840.1	Mtr.29236.1.S1_at	BET_V1-LIKE	PR10
Medtr1g030820.1	Mtr.36367.1.S1_at	BET_V1-LIKE	PR10
Medtr2g035150.1	Mtr.42966.1.S1_at	BET_V1-LIKE	PR10
Medtr2g035120.1	Mtr.42968.1.S1_at	BET_V1-LIKE	PR10
Medtr2g035130.1	Mtr.12277.1.S1_at	BET_V1-LIKE	PR10
Medtr2g035100.1	Mtr.40147.1.S1_s_ at/ Msa.2942.1.S1_s_ at	BET_V1-LIKE	PR10
Medtr2g035105.1	Mtr.40147.1.S1_s_ at	BET_V1-LIKE	PR10
Medtr3g055130	Mtr.6516.1.S1_at	BET_V1-LIKE	PR10
Medtr2g034480	Mtr.18650.1.S1_at/ Msa.1736.1.S1_at	GLYCOSYL HYDROLASES FAMILY 17	PR2
Medtr2g034470.1	Mtr.18649.1.S1_s_ at	GLYCOSYL HYDROLASES FAMILY 17	PR2
Medtr2g034440.1	Mtr.18649.1.S1_s_ at	GLYCOSYL HYDROLASES FAMILY 17	PR2

Medtr3g118390	Mtr.331.1.S1_at	GLYCO_HYDRO_19 (CHITINASE CLASSE I)+ CHITIN_BIND_1 (CHITINASE BINDING PROT)	PR3
Medtr7g115220	Mtr.42872.1.S1_at/ Mtr.12237.1.S1_at	BARWIN+CHITIN_BIND_1	PR4
Medtr5g022310.2	Msa.1526.1.S1_at	TLP-PA	PR5
Medtr5g022310.1	Msa.1526.1.S1_at/ Mtr.17914.1.S1_at	G64-TLP-SF	PR5
Medtr8g096900.1	Mtr.10968.1.S1_at	G64-TLP-SF	PR5
Medtr8g088960.1	Mtr.11885.1.S1_at	GH64-TLP-SF	PR5
Medtr8g075550.1	Mtr.15054.1.S1_at	GH64-TLP-SF	PR5
Medtr3g114030.1	Mtr.17199.1.S1_at/ Mtr.33394.1.S1_at	GH64-TLP-SF	PR5
Medtr8g107140.1	Mtr.17268.1.S1_at	TLP-PA	PR5
Medtr8g056820.1	Mtr.19129.1.S1_at	GH64-TLP-SF	PR5
Medtr6g009480.1	Mtr.19465.1.S1_at	TLP-PA	PR5
Medtr2g063160.1	Mtr.19470.1.S1_at	GH64-TLP-SF	PR5
Medtr7g076360.1	Mtr.26405.1.S1_at	GH64-TLP-SF	PR5
Medtr2g069660.1	Mtr.26405.1.S1_at	TLP-PA	PR5
Medtr5g059200.1	Mtr.28302.1.S1_at	TLP-PA	PR5
Medtr2g067980.1	Mtr.29368.1.S1_at	TLP-PA	PR5
Medtr2g068030.1	Mtr.32260.1.S1_at	GH64-TLP-SF	PR5
Medtr7g102380.1	Mtr.33691.1.S1_at	TLP-PA	PR5
Medtr8g075510.1	Mtr.35231.1.S1_at	GH64-TLP-SF	PR5
Medtr8g075510.2	Mtr.35231.1.S1_at	TLP-PA	PR5
Medtr4g063630.1	Mtr.37482.1.S1_at	TLP-PA	PR5
Medtr5g010640.1	Mtr.40555.1.S1_at	GH64-TLP-SF	PR5
Medtr4g073730.1	Mtr.42529.1.S1_at	GH64-TLP-SF	PR5
Medtr2g068655.1	Mtr.42536.1.S1_at	GH64-TLP-SF	PR5
Medtr8g096920.1	Mtr.42775.1.S1_at	TLP-P	PR5
Medtr5g010635.1	Mtr.42989.1.S1_at	GH64-TLP-SF	PR5
Medtr4g073720.1	Mtr.43370.1.S1_at	TLP-PA	PR5
Medtr7g062610.1	Mtr.49138.1.S1_at	GH64-TLP-SF SUPER FAMILY	PR5
Medtr1g062640.1	Mtr.6757.1.S1_at	GH64-TLP-SF SUPER FAMILY	PR5
Medtr5g022350.2	Mtr.7850.1.S1_s_at	TLP-PA	PR5
Medtr5g022350.1	Mtr.7850.1.S1_s_at/ /Mtr.9418.1.S1_s_at/ t/	GH64-TLP-SF SUPER FAMILY	PR5
Medtr8g096910.1	Mtr.8763.1.S1_at	TLP-P	PR5
Medtr1g025420.1	Mtr.9391.1.S1_at	GH64-TLP-SF SUPER FAMILY	PR5
Medtr1g025420.2	Mtr.9391.1.S1_at	TLP-PA	PR5
Medtr1g021945.1	Not determined	GH64-TLP-SF SUPER FAMILY	PR5
Medtr1g062390.1	Not determined	GH64-TLP-SF SUPER FAMILY	PR5
Medtr2g063150.1	Not determined	GH64-TLP-SF SUPER FAMILY	PR5

Medtr3g068015.1	Not determined	GH64-TLP-SF SUPER FAMILY	PR5
Medtr3g081550.1	Not determined	GH64-TLP-SF SUPER FAMILY	PR5
Medtr5g023850.1	Not determined	GH64-TLP-SF SUPER FAMILY	PR5
Medtr5g068670.1	Not determined	GH64-TLP-SF SUPER FAMILY	PR5
Medtr8g037890.1	Not determined	GH64-TLP-SF SUPER FAMILY	PR5
Medtr8g089020.1	Not determined	GH64-TLP-SF SUPER FAMILY	PR5
Medtr3g111620.1	Not determined	TLP-PA	PR5
Medtr6g079580.1	Not determined	TLP-PA	PR5
Medtr8g036215.1	Not determined	TLP-PA	PR5
Medtr1g099310.1	Msa.1009.1.S1_at/ Msa.2848.1.S1_at/ Mtr.12525.1.S1_at	GH18_HEVAMINE_XIPI_CLASS_III+C HITINASE CLASSE III	PR8
Medtr2g076070.1 /Medtr2g076070. 2	Mtr.1214.1.S1_at	PUTATIVE NTF2-LIKE PROTEIN SUPER FAMILY	Unclassified
Medtr2g076010.1 /Medtr2g076010. 2	Mtr.26632.1.S1_at/ Mtr.26632.1.S1_at	PUTATIVE NTF2-LIKE PROTEIN SUPER FAMILY	Unclassified
Medtr8g058350	Mtr.51369.1.S1_at	PUTATIVE NTF2-LIKE PROTEIN SUPER FAMILY	Unclassified
Medtr8g058700	Not determined	NOT DETERMINED	Unclassified
Medtr2g038000	Mtr.15743.1.S1_at/ Mtr.51386.1.S1_at	PHD_PRHA_LIKE+HOX	Unclassified

Supplemental Table S3. List of *PRs* gene validated by RT-qPCR for the study.

Melting curve corresponds to the temperature at which 50% of DNA is denatured. Only primers producing amplification product showing one melting curve were selected for the study. The efficiency corresponds to DNA polymerase efficiency. The primers producing an efficiency less than 80% or superior than 120% were avoided.

Gene ID	Melting curve (specificity)	efficiency =2 (+/- 0,2)	ID Affymetrix	PR classes	PR annotation in the figures
Medtr1g099310.1	Specific	Yes	Msa.1009.1.S1_at	PR8	PR8
Medtr2g076070.1	Specific	Yes	Mtr.1214.1.S1_at	Unkown	PRuk.1
Medtr2g076010.2	Specific	Yes	Mtr.26632.1.S1_at	Unkown	PRuk.2
Medtr2g076070.2	Specific	Yes	Mtr.1214.1.S1_at	Unkown	PRuk.3
Medtr2g076010.1	Specific	Yes	Mtr.26632.1.S1_at	Unkown	PRuk.4
Medtr2g068655.1	Not detected	Not detected	Mtr.42536.1.S1_at	PR5	PR5.1
Medtr4g120950.1	Specific	Yes	Mtr.37852.1.S1_at	PR10	PR10.1
Medtr4g120970.1	Specific	Yes	Mtr.34114.1.S1_s_at	PR10	PR10.2 (PR10)
Medtr5g010640.1	Specific	Yes	Mtr.40555.1.S1_at	PR5	PR5.3
Medtr6g033450.1	Specific	Yes	Mtr.34114.1.S1_s_at	PR10	PR10.3 (PR10)
Medtr7g062610.1	Non specific	No	Mtr.49138.1.S1_at	PR5	PR5.4
Medtr8g096910.1	Specific	Yes	Mtr.8763.1.S1_at	PR5	PR5.6

Supplemental Table S4. Pearson correlation analysis of the *PRs*, *CPs* and *PRs* vs. *CPs* expression.

Expression data of Medicago response to perturbations were downloaded from Genevestigator database (<https://genevestigator.com/>) and Pearson correlation was calculated using Excel software.

Pearson corr	<i>CP5/CP4</i>	<i>CP3</i>	<i>CP2</i>	<i>PR5.6</i>	<i>PR10</i>	<i>PR5.3</i>	<i>PR8</i>
<i>CP5/CP4</i>	1.00	0.93	0.91	-0.10	-0.07	-0.06	-0.10
<i>CP3</i>	0.93	1.00	0.97	-0.08	-0.08	-0.07	-0.10
<i>CP2</i>	0.91	0.97	1.00	-0.09	-0.11	-0.10	-0.10
<i>PR5.6</i>	-0.10	-0.08	-0.09	1.00	0.54	0.64	0.41
<i>PR10</i>	-0.07	-0.08	-0.11	0.54	1.00	0.65	0.37
<i>PR5.3</i>	-0.06	-0.07	-0.10	0.64	0.65	1.00	0.58
<i>PR8</i>	-0.10	-0.10	-0.10	0.41	0.37	0.58	1.00

Supplemental Table S5. Co-expressed *PHYTOCYSTATIN* genes with the studied *PRs*.

PHYTOCYSTATIN co-expressed with one or multiple *PRs* were isolated using the Phytomine tools of the Phytozome database (<https://phytozome.jgi.doe.gov/phytomine/begin.do>). The table shows the two identified *PHYTOCYSTATINS* (*Medtr2g026040*; *PHYTOCYST5* and *Medtr5g088770*; *PHYTOCYST32*) and the corresponding Pearson correlation value.

	<i>PR5.3</i>	<i>PR5.6</i>	<i>PR10.2</i>	<i>PR10.3</i>	<i>PHYTOCYST32</i>
<i>Medtr2g026040 (PHYTOCYST5)</i>	0.909	0.85922	0.9168	0.97454	0.95816
<i>Medtr5g088770 (PHYTOCYST32)</i>	0.92549	X	X	0.93896	X

Supplemental Table S6. List of primers used in this study.

	Gene ID	Gene Name	Primer L	Primer R	Tm	Ref
RT-qPCR primers	<i>Medtr4g107930</i>	<i>CP3</i>	AGTGGATGCCGCTGAAGG	TCAATCACAGTTTGTCTCAAATTAC	60	Pérez Guerra JC et al., 2010
	<i>Medtr4g079770</i>	<i>CP4</i>	TGGAAGCATCTTACCCTACTG	ATATACATAAATCGCAAATCACATTC	60	Pérez Guerra JC et al., 2010
	<i>Medtr5g022560</i>	<i>CP2</i>	CATCTTACCCTACTGCTTAAATGC	AACTAGAAACCATGATGAATGTAGC	60	Pérez Guerra JC et al., 2010
	<i>Medtr4g079470</i>	<i>CP5</i>	GTTGACGGAACCTGCACTGC	CACCCCAATCAGTTCCTCCAT	60	In this study
	<i>TC106667</i>	<i>Actine</i>	TGGCATCACTCAGTACCTTTCAACAG	ACCCAAAGCATCAAATAATAAGTCAACC	60	Berrabah el al., 2015
	<i>Medtr1g099310.1</i>	<i>PR8</i>	CCTCAATGTCTTTCCCTGA	TGGAGCAGCAGCATCATTAG	60	In this study
	<i>Medtr2g076070.1</i>	<i>PR unknown (PRuk.1)</i>	ATGGGAGATGGAGCTGACAC	GCAATTTTCAGGTGGTCCTGT	60	In this study
	<i>Medtr2g076010.2</i>	<i>PR unknown (PRuk.2)</i>	GCAATTTTCAGGTGGTCCTGT	GCAATTTTCAGGTGGTCCTGT	60	In this study
	<i>Medtr2g076070.2</i>	<i>PR unknown (PRuk.3)</i>	GTTAATGGCAGGGAGGGATT	GCAATTTTCAGGTGGTCCTGT	60	In this study
	<i>Medtr2g076010.1</i>	<i>PR unknown (PRuk.4)</i>	CAAGATCCGGTTGCAAGATT	GCAATTTTCAGGTGGTCCTGT	60	In this study
	<i>Medtr4g120950.1</i>	<i>PR10.1</i>	CACGATTCATCGAGAAAGCA	GGGTTGGAACCAATTTGAAC	60	In this study
	<i>Medtr4g120970.1</i>	<i>PR10</i>	TTGAGGGAGGACAAACCTTG	CCTCAATGGCCTTGAAAAGA	60	In this study
	<i>Medtr6g033450.1</i>					
	<i>Medtr2g068655.1</i>	<i>PR5.1</i>	GTTCAAGAGGGCTTGTCTCG	GGGCAGGCCTTACAATTACA	60	In this study
	<i>Medtr5g010640.1</i>	<i>PR5.3</i>	GGCCATCATCATGAAAACAA	GACCCAGATTCTTGCCTTA	60	In this study
	<i>Medtr8g096910.1</i>	<i>PR5.6</i>	TACACAAGCAGCAAGGTTTCG	CTACCGGATACGCTGCAACT	60	In this study
	<i>Medtr5g088770.1</i>	<i>PHYTOCYST32</i>	GGCGGCTCTAGGTGGTAGTA	ACACCTTTTGTCTCCACCA	60	In this study
	<i>Medtr2g026040.1</i>	<i>PHYTOCYST5</i>	AAGGATGCTCTTGTCTGGTGG	CAACTTTCGAGCCAACACA	60	In this study
	<i>Medt3g0119041</i>	<i>SymCRK</i>	GATTTCTGTGTTGAAGCTTGGCT	ACATCAGAAGTGAAGTCTCTGCAA	60	Berrabah et al., 2014
	<i>Medt4g0044681</i>	<i>DNF2</i>	AGGCAATGCGTTCAGAAGGCCT	CGACACCGAAGTGAAGTCTGCAA	60	Bourcy et al., 2013
<i>Medtr7g0239441</i>	<i>RSD</i>	GAAAGATGGAATACACCCAAAACC	AACTTGACCTGGGTCGTCAGA	60	Sinharoy et al., 2013	
Genotyping Primers		NF583F	ACTATTGTGTCAACCACACGTG		65	In this study
		NF583R	GGCATTAGTTATGCCAAACTTGC		65	In this study
		NF2210F	GCAAGTTTGGCATAACTAATGCC		65	In this study
		NF2210R	GGCTTGGGATATTGGTTGATTC		65	In this study
		LTR4F	TACCGTATCTCGGTGCTACA		66	Ratet et al., 2010
		LTR6R	GCTACCAACCAACCAAGTCAA		66	Ratet et al., 2010